Regulation of quiescence by kinase signaling pathways

by

Siyu Sun

A dissertation submitted in partial fulfillment

of the requirements for the degree of

Doctor of Philosophy

Department of Biology

New York University

January 2021

_____

David Gresham, PhD

DEDICATION

To my lovely family.

ACKNOWLEDGMENTS

I would like to thank my advisor, Dr. David Gresham, for his mentorship on every level and his role in inspiring such a great project. I'd like to thank my committee members Dr. Patrick Eichenberger, Dr. Gloria Coruzzi, Dr. Andreas Hochwagen, each has become a unique role model for me. I especially want to thank my external committee Dr. Liam Holt for encouraging a collaboration on studying the biophysical properties in quiescent cells and for welcoming me into his lab. I'd especially like to thank Dr. Pieter Spealman, Dr. Chris Jackson, Dr. Emily Adney, Dr. Darach Miller, for showing me how to be truly passionate about research and for giving me an amazing example of what it means to be a scientist. I'd like to thank Farah Abdul-Rahman and Grace Avecilla for being incredible lab mates -- we've been through a lot together, and I feel lucky to have had their support through it all. I'd like to thank Nathan Brandt for always being cool under pressure because I truly could not have done my P.h.D without his steady presence and guidance. I acknowledge all past and present Gresham lab members, in particular, Stephanie Lauer, Rodoniki Athanasiadou, Angela Hickey, Marissa Knoll, Charles Miller, Carolina Oliveira de Santana and Gunjan Janak Sethia for their support throughout my graduate career -- I'll always remember the board game nights, lab hikes, holiday parties, and beer, ice cream and Ping-Pong outings. I would like to thank the students who worked with me, Yiwen Qin and Fangrui Guo. Working with them for a few years and seeing their dedication and passion for research was inspiring, and they have taught me to be a better mentor. I'd like to thank Christine Vogel and the past and current members of the Vogel lab for being awesome floormates and for their helpful suggestions at lab meetings. I

especially want to thank Funda Mujgan Kar, Kristina Allgoewer, Shuvadeep Maity, Gustavo Monteiro Silva, Songhee Back in the Vogel Lab, who have provided numerous help in my proteomic study from experimental design to data analysis and interpretation. I'd like to thank my entire cohort (especially Shiwei Zheng), for all sanity talks and dancing nights, and fun moments during graduate school. I'd like to thank the NYU Gencore for all their help with sequencing, flow cytometry, and FACS. I would like to thank my husband, Xiang Li, for his unwavering love and support. Finishing up a Ph.D. while taking care of a one-year old baby can easily make me crazy, but I've stayed sane and happy thanks to him. I'd like to thank my son Muchen Li, who has brought so much joy to my life. I'd also like to thank my incredible parents who nurtured my interest in science and encouraged me to pursue graduate school overseas.

ABSTRACT

In eukaryotes, cell growth is tightly controlled by evolutionarily conserved nutrient-sensing signaling pathways including the Tor complex 1 (TORC1), AMP kinase (AMPK) and Ras/Protein kinase A (PKA). A primary function of these signaling pathways is to coordinate protein production with cell proliferation and growth arrest. Misregulation of those pathways can lead to uncontrolled cell growth, which is a hallmark in cancer. Although the role of these pathways has been intensively studied in rapidly proliferating cells, their role in regulating cellular quiescence (a temporary growth arrested state) is poorly understood. The unicellular organism *Saccharomyces cerevisiae (S.cerevisiae)* can exit the mitotic cycle and enter quiescence when starved for one, or more, essential nutrients. However, how cells integrate diverse starvation signals and mount a common cellular state - quiescence is unknown. My thesis aims to characterize quiescence establishment and maintenance in response to natural nutritional starvations, namely carbon, nitrogen and phosphorus at the phenotypic, genetic, and proteome level using a combination of microscopy, high throughput genetics, and mass spectrometry. In chapter 1, I review our current understanding of cellular quiescence across diverse systems and discussed the specific challenges inherent in studying quiescence in yeast. In chapter 2, I describe a genome-wide screen to identify the genetic requirements for maintaining quiescence under three starvations conditions and define the global genetic interaction profiles of key regulatory kinases: TOR1, RIM15 and PHO85 in quiescence. In chapter 3, I quantify the temporal dynamics of the proteome and phosphoproteome during quiescence establishment in three starvation conditions and assess the functional impact

of the serine/threonine kinase Rim15 on regulation of these dynamics. In chapter 4, I characterize the molecular and biophysical properties of quiescent cells with the goal of finding a universal marker for efficiently identifying and isolating quiescent cells. Together, my studies underscore the diversity of processes that underlie quiescence initiation, maintenance, and exit and expand our understanding of the context-specific regulation of cellular quiescence. The future directions and implications of my findings are presented in Chapter 5.

TABLE OF CONTENTS

LIST OF FIGUERS

LIST OF TABLES

Chapter 1 : Cellular quiescence in yeast

This chapter is based on the review paper “Cellular quiescence in budding yeast” by Siyu Sun and David Gresham, which has been accepted for publication to the journal, *Yeast*. I generated all of the figures and wrote the first version of the manuscript with final edits made by David Gresham.

1.1 Abstract

Cellular quiescence, the temporary and reversible exit from proliferative growth, is the predominant state of all cells. However, our understanding of the biological processes and molecular mechanisms that underlie cell quiescence remains incomplete. As with the mitotic cell cycle, budding and fission yeast are preeminent model systems for studying cellular quiescence owing to their rich experimental toolboxes and the evolutionary conservation across eukaryotes of pathways and processes that control quiescence. Here, we review current knowledge of cell quiescence in budding yeast and how it pertains to cellular quiescence in other organisms, including multicellular animals. Quiescence entails large-scale remodeling of virtually every cellular process, organelle, gene expression, and metabolic state that is executed dynamically as cells undergo the initiation, maintenance, and exit from quiescence. We review these major transitions, our current understanding of their molecular bases and highlight unresolved questions. We summarize the primary methods employed for quiescence studies in yeast and discuss their relative merits. Understanding cell quiescence has important consequences for human disease as quiescent single-celled microbes are notoriously difficult to kill and quiescent human cells play important roles in diseases such as cancer. We argue that research on cellular quiescence will be accelerated through the adoption of common

criteria, and methods, for defining cell quiescence. An integrated approach to studying cell quiescence, and a focus on the behavior of individual cells, will yield new insights into the pathways and processes that underlie cell quiescence leading to a more complete understanding of the life cycle of cells.

1.2 Introduction

Living cells exist in one of two distinct states: 1) a proliferative state in which cell size and number increase through growth and the mitotic cell division cycle or 2) a non-proliferative state in which cell growth and division has ceased. Non-proliferative cells can be in either an irreversible state or a reversible state defined by the capacity of the cell to re-initiate the mitotic cell cycle and resume growth and division (Valcourt et al., 2012). Cells that are incapable of re-initiating the cell division cycle include post-mitotic cells that are terminally differentiated in multicellular organisms. Senescent cells are also unable to resume cell growth and division. Cells that have ceased to grow and have temporarily exited the cell cycle, but nonetheless maintain the potential to reinitiate the mitotic cell cycle, are quiescent cells (**Figure 1.1A**) (Cheung & Rando, 2013; Damien Laporte, Gouleme, et al., 2018). Quiescence is the predominant cellular state for all living cells as cells in both single-celled and multi-celled organisms only rarely undergo periods of rapid proliferation and division over the course of their lifespan (O'Farrell, 2011; Valcourt et al., 2012).

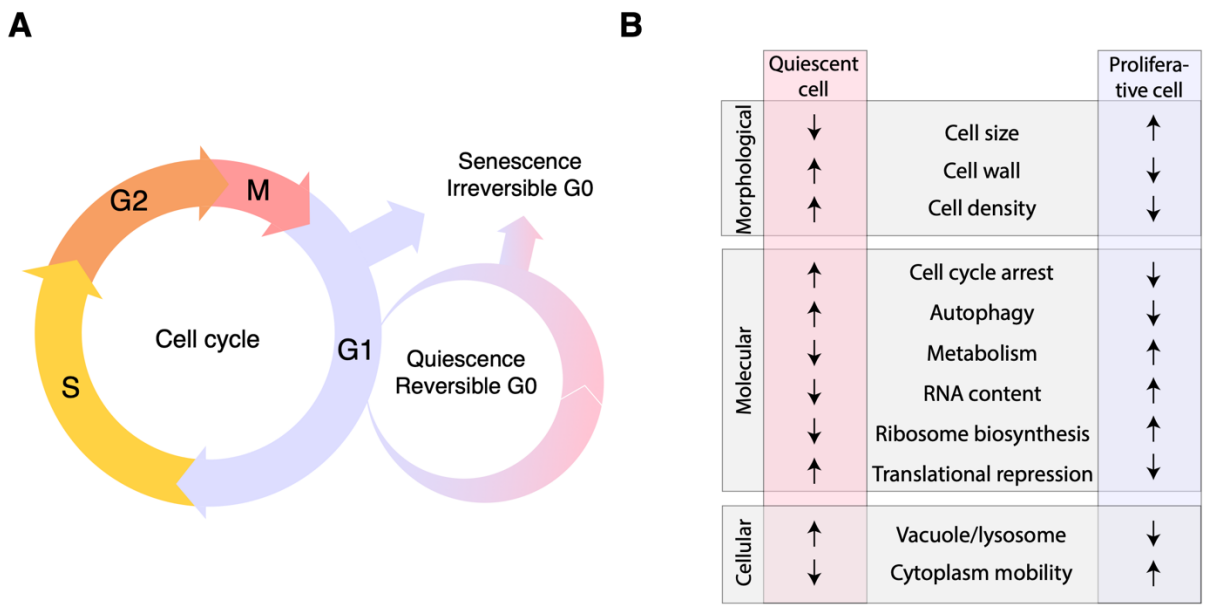

Figure 1.1. Properties for cells at different states: the mitotic cell cycle and quiescence.

A) Quiescent cells have exited the cell division cycle but maintain the capacity to resume growth and re-enter the mitotic cell cycle in response to the appropriate signals. This reversible state is in contrast to terminally differentiated or senescent cells, which cannot recommence the cell division cycle. In budding yeast, most quiescent cells exit the cell cycle in G1 and thus typically present as unbudded cells. However, in some cases, yeast cells can initiate quiescence from other cell cycle stages. **B)** Contrasting properties of quiescent and proliferative cells. Quiescent yeast cells are characterized by a combination of factors including altered cell morphology and remodeling of multiple cellular processes. Key features that distinguish proliferative and quiescent cells, with an indication of whether they are upregulated (up arrow) or downregulated (down arrow), are summarized.

Cell quiescence plays an essential role in organismal development and impacts human disease in a variety of ways (Kim et al., 2005; Lin et al., 2007; Suda et al., 2005). In multicellular organisms, development, tissue renewal, and long-term survival are dependent upon the persistence of quiescent stem cells that maintain the ability to re-enter the cell cycle to self-renew or to produce progeny that can differentiate and re-populate tissues (Cheung & Rando, 2013). The aberrant exit from quiescence, and

initiation of dysregulated proliferative growth is common in cancer (Hanahan & Weinberg, 2011). Conversely, many cancer-related deaths are the result of quiescent tumor cells that are resistant to therapeutics and frequently underlie tumor recurrence (Borst, 2012; Yano et al., 2017). In infectious disease, quiescent prokaryotic and eukaryotic single-celled pathogens are recalcitrant to many drug treatments for diseases including tuberculosis (Parrish et al., 1998), cryptosporosis (Alexander & Perfect, 1997), anthracis (Murray, 1999), candidiasis (Hall, 2015; Traven et al., 2012) and aspergillosis (Latgé & Chamilos, 2019). Thus, understanding the regulation and consequences of cellular quiescence and how cells transition between proliferative and quiescent states is of critical significance to our understanding of development, tissue homeostasis and disease.

Budding (*Saccharomyces cerevisiae*) and fission (*Schizosaccharomyces pombe*) yeasts have been key model organisms for advancing our understanding of eukaryotic cellular quiescence. Given the large evolutionary distance between these two species, identification of shared mechanisms, properties, and consequences of quiescence point to conserved evolutionary consequences. Moreover, many features of quiescence in yeast are found in quiescent human cells, and other animal cells, such as a reduced cell size, cell cycle arrest, condensed chromosomes, reduced rRNA synthesis and protein translation, increased autophagic activity, and increased stress resistance (**Figure 1.1B**) (Dhawan & Laxman, 2015; Ho et al., 2017; Roche et al., 2017; S. S. Su et al., 1996; Valcourt et al., 2012; van Velthoven & Rando, 2019; Yanagida, 2009). Quiescence in multicellular organisms is difficult to study because of the complex interactions between metabolic and hormonal signals that mediate quiescence. By contrast, in budding and

fission yeast, quiescence entry and exit are solely determined by nutrient availability (de Virgilio, 2012; Gray et al., 2004; Yanagida, 2009). Nonetheless, the genes and pathways that control quiescence are conserved from yeast to humans, justifying the use of yeast model systems to make rapid progress in studying the mechanisms that underlie quiescence in human cells.

The study of quiescence in yeast may also be informative about chronological aging - defined as the period of elapsed time in a non-proliferative state (in contrast to replicative aging, which is the total number of divisions a cell has undergone). Historically, quiescence in budding yeast has referred to cells in liquid culture grown to stationary phase (Gray et al., 2004; Herman, 2002). The ability of stationary phase yeast cells to maintain viability, and reinitiate proliferative growth upon addition of nutrients, has also been presented as a model of cellular chronological lifespan (CLS) (Paola Fabrizio & Longo, 2003; Kaeberlein, 2010; N. Zhang & Cao, 2017). Because quiescent cells are defined as those non-proliferative cells that can reenter the cell cycle, CLS is equivalent to the proportion of quiescent cells in stationary phase cultures (Allen et al., 2006; N. Zhang & Cao, 2017). Cells with a shortened CLS have reduced reproductive capacity upon replenishment of nutrients (Garay et al., 2014) and thus are functionally the same as cells that are defective in the regulation of quiescence. Therefore, successful programming into quiescence can extend the CLS of cells (Cao et al., 2016). For example, null mutations in quiescence-regulating genes including TOR1 and SCH9 (a major target of TOR1) are reported to extend the CLS of yeast cells (P. Fabrizio et al., 2001; Paola Fabrizio & Longo, 2003; Powers et al., 2006; M. Wei et al., 2008). Mechanisms linking

chronological aging to cellular quiescence in budding yeast in response to carbon starvation has been discussed in a recent review (Mohammad et al., 2020).

The study of quiescence in the lab is also likely to be informative about the life of yeast cells in non-laboratory and natural environments. As with bacteria, non-pathogenic and pathogenic yeast can form biofilms (Chandra et al., 2001; Lynch & Robertson, 2008; Ramage et al., 2012). The complex structure of biofilms can result in an inadequate supply of nutrients to some individuals, which can lead to initiation of a quiescent state. Antibiotic and antifungal resistance in biofilms can be recapitulated by starvation in non-biofilm conditions (Anderl et al., 2003; Bojsen et al., 2014; Nguyen et al., 2011) indicating that quiescence is an important determinant of drug resistance in biofilms. In this review, we focus on studies of quiescence in the lab.

Despite the central importance of studying quiescence in yeast, several factors have impeded research progress. These include a lack of consensus among researchers on the appropriate strategies for inducing quiescence, the absence of specific molecular or physical markers of quiescence, and insufficient consideration of the role of environmental signals and genotype on quiescence. In this review, we summarize our current understanding of the pathways and processes that underlie quiescence initiation, maintenance, and exit; and the molecular and physical properties of quiescent cells. We highlight key features of quiescence that are evolutionarily conserved, identify key questions in quiescence that await solutions, and propose approaches to their resolution. We conclude that cellular quiescence is a highly dynamic and regulated process that

exhibits significant within population heterogeneity requiring a renewed focus on the behavior of individual cells, rather than population aggregates, to attain a comprehensive understanding of this important cellular state.

1.3 Define quiescence - not all non-proliferative cells are in a quiescent state

Cellular quiescence has been an area of active research for at least 50 years. For many years, there was significant debate about whether quiescent cells are simply in a prolonged G1 phase or whether cellular quiescence is a distinct cell cycle phase (Patt & Quastler, 1963). However, quiescence ultimately came to be understood as a distinct state outside of the replicative cell cycle referred to as G0 (Epifanova & Terskikh, 1969). Evidence for this distinct state came from early studies in human cells that showed that quiescent G0 cells take longer to reinitiate the cell division cycle compared to G1 cells (Zetterberg & Larsson, 1985). Subsequent studies provided further evidence of a clear distinction between G1 and G0 cells; for example, an artificially prolonged G1 arrest (e.g. through inhibition of cyclin-dependent kinases) does not recapitulate the establishment of quiescence in either yeast or mammals (Coller et al., 2006; Damien Laporte et al., 2011).

It is important to note that two additional types of non-proliferative cells, terminally differentiated and senescent cells, are also considered to be in a non-proliferative G0 state but these are not quiescent cells according to the formal definition (**Figure 1.1A**). The key difference is that quiescence is a reversible G0 state and cells can reenter the cell division cycle. Senescent and differentiated cells cannot reenter the cell cycle and

therefore are not quiescent cells. Cellular quiescence can be viewed as a continuum that dynamically changes with time. Quiescent cells may ultimately lose the ability to re-enter the cell cycle and thereby become senescent cells (**Figure 1.1A**), but this fate is not inevitable and most quiescent cells can maintain viability for extremely long periods of time. Thus, it is useful to distinguish a variety of quiescent states that are defined by the time since cell cycle arrest or by the time it takes to re-enter the cell cycle (Kwon et al., 2017; Damien Laporte, Jimenez, et al., 2018). It is worth noting that certain differentiated cells, such as mature hepatocytes, are capable of entering the cell cycle in response to injury or stressful conditions. These cells should also be considered quiescent cells according to the definition (Baserga, 1968) that quiescence is a reversible growth arrest. This definition allows us to distinguish quiescent cells from senescent and most terminally differentiated cells and emphasizes the commonalities (cell cycle arrest) and differences (reversibility) with the broader classification of cells in a G0 state.

1.4 Study quiescence in the lab

1.4.1 Inducing quiescence using nutrient starvation

Quiescence in yeast is initiated in response to nutrient starvation. Haploid yeast cells grow at a constant rate proportional to the population size (i.e. exponentially) when nutrients are abundant and enter stationary phase when nutrients become scarce. Stationary phase is defined at the population level and is characterized by the absence of an increase in detectable population growth. Studies of quiescence in haploid budding yeast

have typically been performed using cells in stationary-phase culture following growth in rich, glucose-containing medium (**Table 1.1**). In this case, most yeast cells have undergone the diauxic shift and exhausted the carbon supply in the media. In this case, carbon starvation is the signal for cell cycle arrest and initiation of quiescence. It has been argued that starvation for glucose is the relevant condition for studying quiescence (Sagot & Laporte, 2019) and indeed the majority of quiescence studies use carbon starvation as the quiescence induction signal (Damien Laporte et al., 2011; Damien Laporte, Gouleme, et al., 2018).

However, early studies of the yeast cell cycle showed that starvation for several different nutrients results in cell cycle arrest (Johnston et al., 1977; Unger & Hartwell, 1976). Subsequent studies have shown that yeast cells respond to a variety of nutrient starvations by exiting the cell cycle and initiating quiescence (Gresham et al., 2011; Klosinska et al., 2011; Lillie & Pringle, 1980; Schulze et al., 1996; Sun et al., 2020; Yanagida, 2009). Starvation for essential nutrients including nitrogen, phosphorus and sulfur results in many of the same characteristics as carbon starved cells including cell cycle arrest as unbudded cells, thickened cell walls, increased stress resistance and an accumulation of storage carbohydrates (Klosinska et al., 2011; Lillie & Pringle, 1980; Schulze et al., 1996). Defining the nutrient starvation signal is a simple process: if all other nutrients are in excess, a single growth limiting nutrient will determine the final population size of a stationary phase culture. A linear relationship between nutrient concentration and population density in stationary phase is indicative of starvation for that nutrient.

An exclusive focus on cellular quiescence in response to carbon starvation is not justified and may impede our understanding of quiescence. Indeed, one of the central questions in studying quiescence is how different starvation signals converge on the same consequence of cell cycle arrest and induction of quiescence. Moreover, many important biological processes are likely to be missed - autophagy being a preeminent example - if carbon starvation is the only condition studied (Kawamata et al., 2017; Lang et al., 2014). Organisms in the natural world experience a range of nutrient limitations and nitrogen and phosphorus appear to be the predominant growth limiting nutrients in most ecologies (Elser et al., 2007). Although fission yeast can also initiate quiescence in response to a variety of starvation signals (Dedo et al., 2015; Ohtsuka et al., 2017; Petrini et al., 2015; Pluskal et al., 2011; S. S. Su et al., 1996), the diauxic-shift is not observed in fission yeast when starved for glucose highlighting key differences in the metabolic states of the two yeast species immediately prior to quiescence. Thus, a comprehensive understanding of cellular quiescence requires explicit consideration of the different nutrient starvation signals that initiate quiescence and determination of the similarities and differences in the inputs and outputs of these signals.

The ability of a cell to initiate quiescence in response to nutrient starvation has evolved over hundreds of millions of years. As a result, cells have mechanisms to sense nutrient starvation signals and mount the appropriate response by initiating quiescence. This is in contrast to laboratory engineered starvations that occur when genetically modified auxotrophs deplete nutritional supplements that complement the auxotrophic mutation. For example, commonly used mutations that function as auxotrophic markers,

such as mutations in ura3 or ade2 in budding yeast, are chemically complemented by the addition of uracil or adenine to the media. If an auxotrophic yeast cell starves for the nutritional supplement, population growth is arrested and the population enters stationary phase; however, these cells do not effectively become quiescent as there is no evolved response to this unnatural starvation signal. As a result, population viability rapidly declines (Boer et al., 2010; Gresham et al., 2011). Even when the supplement is present at high concentrations and cells initially starve for carbon, continued metabolic activity in quiescent cells may result in subsequent starvation for the auxotrophic requirement, resulting in a rapid decline in viability (Mülleder et al., 2012; Santos et al., 2020). The use of auxotrophs and undefined starvation conditions creates considerable ambiguity in the interpretation, and generality, of results and therefore should be avoided.

1.4.2 Quiescence in diploid yeast

Cell ploidy has important consequences for quiescence. *S. cerevisiae* in the wild is usually diploid (Landry et al., 2006; Neiman, 2011); however, quiescence in yeast has most frequently been studied using haploid cells. Diploid yeast cells can either enter quiescence or, typically in response to nitrogen starvation and the presence of a non-fermentable carbon source, undergo meiosis and sporulation to form haploid spores (Honigberg, 2016; Tomova et al., 2019). Both quiescence and sporulation facilitate survival during extended periods of nutritional stress (Esposito & Klapholz, 1981; Freese et al., 1982). Phenotypically, the products of meiosis in yeast - four haploid spores - are in a growth arrested state from which they can exit and resume proliferative growth.

Quiescent budding yeast cells share key features with spores, including increased thermostability, low metabolic activity, reduced transcription and translational activity, and resistance to various environmental stresses. A whole proteome study of quiescent cells and spores in the SK1 strain background showed similar gene expression states in both cell types (Kumar & Srivastava, 2016).

Given the similar properties, haploid spores could be considered a specialized type of quiescent cell. However, quiescent cells and spores do exhibit some differences. Some diploid strains can only enter cellular quiescence, whereas others can only sporulate. For example, W303 haploids can enter quiescence, but their diploid counterparts cannot. However, disabling sporulation or introducing quiescence related genes by genetic manipulation results in diploids entering quiescence in response to sporulation signals (Miles et al., 2019). These results suggest that different genes are involved in regulating quiescence and sporulation and the regulatory mechanisms leading to these two states may be very different (Honigberg, 2016; Miles et al., 2019). Both quiescence (haploid or diploid) and sporulation are strategies that cells utilize to survive long-term under stress environments. However, further studies are required to understand the relationship between these two quiescent states. In this review, we focus on quiescence in haploid yeast cells.

1.4.3 Identification and Isolation of quiescent cells

Although quiescent cells have many distinct features compared to actively proliferating cells (**Figure 1.1B**), no individual feature is unique to quiescent cells. Upon

nutrient starvation, a clonal population of haploid budding yeast differentiates into quiescent and nonquiescent cells (Allen et al., 2006) and populations can exhibit different degrees of heterogeneity depending on genotype and starvation conditions (Damien Laporte et al., 2011; Damien Laporte, Gouleme, et al., 2018; Damien Laporte, Jimenez, et al., 2018; Miles & Breeden, 2017; Palková et al., 2014). A consequence of this heterogeneity is that considering an entire stationary phase culture to be composed of quiescent cells is often inappropriate. Nonetheless, several studies define quiescence as the entire population of cells in a stationary phase culture and do not use methods for isolating or identifying quiescent cells (**Table 1.1**).

Different methods have been used for identifying, enriching, and isolating quiescent cells. From a heterogeneous stationary phase culture, a population-level measure of the fraction of quiescent cells in the population can be determined by plating cells and counting the number of colony forming units (CFUs). The fraction of viable cells in the population, defined as the number of CFUs divided by the number of plated cells, is equivalent to the fraction of quiescent cells. A related approach quantifies the time a starved population takes to reinitiate detectable population growth. In this “outgrowth” approach, a population of cells that contains a small fraction of quiescent cells will take longer to exhibit detectable growth compared with a population comprising a large fraction of quiescent cells. Outgrowth is also a useful approach to enrich for quiescent cells when using complex mixtures of genotypes and analysis using multiplexed methods such as Barcode sequencing (Bar-seq) (Gresham et al., 2011; Sun et al., 2020). Alternative methods for quantifying the fraction of quiescent cells in a population using viability cell

dyes are also widely used, often taking advantage of flow cytometry. Viable cells can be detected using propodium iodine (PI) and Syto9, which make use of the increased membrane permeability of inviable cells to specifically stain non-quiescent cells (Sun et al., 2020). Alternatively, a staining method using SytoxGreen (a DNA intercalating dye) makes use of the fact that quiescent cells have fortified cell walls (**Figure 1.1B**) and therefore are resistant to penetration by the dye. In a heterogeneous population, quiescent cells appear as a discrete peak of reduced fluorescence (Liet al., 2015). These methods are useful to quantify the fraction of quiescent cells in a population, which provides an efficient means of comparing genotypes and conditions. In principle, these methods also enable fractionation of the population using flow cytometry, although there are few examples of this in the literature (Sun et al., 2020).

Fractionation methods have been developed to isolate quiescent cells from heterogeneous cultures based on their physical properties (**Figure 1.1B**). For example, the quiescent cells can be isolated using density centrifugation (Allen et al., 2006). Quiescent cells are denser than non-quiescent cells due to increased storage carbohydrates (e.g. trehalose and glycogen), thickened cell walls and reduced cell volume. The use of a percoll gradient enables isolation of the denser, more rapidly migrating quiescent cells using centrifugation. One limitation of this method is that it requires a large number of cells (2×10^9). Recently, a new separation approach was developed using iodixanol, for which the input cell number can be as low as 3×10^6 (Quasem et al., 2017). An important caveat to these methods is that they enrich the quiescent population that is largely derived from new daughter cells as these cells are the

smallest and most dense. Additionally, the fraction defined as non-quiescent cells actually comprises both quiescent (i.e. viable) and non-quiescent (dead) cells. Thus, a potential limitation of this method is that it isolates a specific subclass of quiescent cells.

A fundamental limitation to fractionation methods is the lack of specific gene expression markers that would make FACS-based fractionation straightforward. The identification of such a marker in yeast would have significant advantages for identifying and isolating quiescent cells in heterogeneous cultures. This would also enable studies of quiescent cells in multicellular eukaryotic model organisms. For example, *Drosophilia melanogaster (D.melanogaster), Caenorhabditis elegans (C.elegans)* have been developed as useful models for studying stem cell quiescence (Baugh & Ryan Baugh, 2013; Cheung & Rando, 2013; Guo et al., 2016; D. Sun & Buttitta, 2015; van Velthoven & Rando, 2019; C. Wang & Spradling, 2020). *C.elegans* and *in vitro* mammalian cell culture (fibroblast cells) are also useful for studying stress-induced quiescence (Baugh & Ryan Baugh, 2013; Coller et al., 2006; Mitra et al., 2018; Salmenperä et al., 2016; Tenen & Greenwald, 2019; Yao, 2014). Cells in structured environments in muti-cellular organisms, such as tissues, also face various micro-environments, including different oxygen supply or physical constraints (Cheung & Rando, 2013; Rumman et al., 2015) resulting in significant heterogeneity. Identification of conserved quiescent-specific gene expression markers for identifying and isolating quiescent cells would be a significant advance. However, finding a universal gene expression marker is challenging as quiescence can be induced by numerous different input signals. More likely, combinatorial markers comprising multiple genes possibly in combination with cellular features, such as

mitochondrial morphology (Damien Laporte, Gouleme, et al., 2018), may be an efficient means of identifying quiescent cells.

Table 1.1. **Methods for studying quiescence in budding yeast.**

A variety of different methods have been used to isolate or identify quiescent cells that rely on their altered properties. The conditions used for inducing quiescence and the method for determining the viability of quiescent cells varies widely among studies.

Isolation/identification methods				Quiescence induction nutrient		Strain genotype		Viability verification		Selected publications
Density	Cell wall	Outgrowth	Imaging	Undefined[a]	Defined[b]	Auxo-troph	Proto-troph	Staining	CFU	
✓				✓		✓		✓	✓	(Allen et al., 2006; Davidson et al., 2011)
✓				✓			✓	✓	✓	(Swygert et al., 2019)
✓	✓			✓			✓		✓	(Liet al., 2015; Lihong Li et al., 2013)
✓						✓		✓	✓	(Damien Laporte, Gouleme, et al., 2018)
		✓					✓	✓		(Gresham et al., 2011; Sun et al., 2020)
		✓				✓	✓		✓	(Bontron et al., 2013)
							✓		✓	(Klosinska et al., 2011)
			✓			✓				(Argüello-Miranda et al., 2018)

Note: A variety of different methods have been used to isolate or identify quiescent cells that rely on their altered properties. The conditions used for inducing quiescence, the genotypes used, and the method for determining the viability of quiescent cells vary widely among studies. [a]Undefined indicates cellular quiescence induced using starvation in nutrient rich (glucose-containing) medium; [b]Defined indicates cellular quiescence induced using chemically defined medium and definition of nutrient starvation signal.

1.5 The three phases in quiescence

Cellular quiescence can be viewed as comprising three distinct phases: initiation, maintenance and exit from quiescence. The ability to effectively initiate, maintain and exit quiescence confers a significant selective advantage across diverse environments resulting in a powerful evolutionary drive for effective cellular quiescence (O'Farrell, 2011). A key challenge of studying cellular quiescence in populations is that individual cells are frequently unsynchronized with respect to these phases resulting in significant temporal heterogeneity. Nonetheless, the processes active during these phases differ making their distinction of practical utility in designing and interpreting quiescent studies.

1.5.1 Quiescence entry

Starving prototrophic yeast strains for various essential nutrients, such as cabron, nitrogen, phosphorus, sulfur or amino acids can result in quiescence entry (Sun et al., 2020). In this case, cells undergo cell cycle arrest in G1 and exit the cell cycle to adopt a G0 state. This is apparent under the microscope as these cells arrest as uniformly unbudded cells. There is some variation in the fraction of unbudded cells depending on the nutrient starvation signal (Saldanha et al., 2004) suggesting that the efficiency of quiescence initiation varies as a function of the starvation signal. A characteristic of unnatural starvations that occur when an auxotroph is starved for its auxotrophic requirement, is that a small fraction of the population arrests as unbudded cells consistent with a failure to effectively initiate quiescence in this scenario (Saldanha et al., 2004).

Quiescence initiated in response to different nutritional starvations results in significant changes in mRNA expression, histone modifications, the proteome and metabolome. Whereas some of the changes are independent of the starvation signal there are specific responses that depend on the exhausted nutrient (Boer et al., 2010; Klosinska et al., 2011; Sun et al., 2020). Quiescence entry is also accompanied by sub-cellular reprogramming, including chromatin reorganization, protein re-localization and cytoskeletal rearrangement (McKnight et al., 2015; Sagot & Laporte, 2019; Swygert & Tsukiyama, 2019). Cells anticipate the exhaustion of essential nutrients well before population growth ceases. This is evident in the accumulation of storage carbohydrates well before cell cycle arrest (Lillie & Pringle, 1980) suggesting that cell quiescence is a regulated process initiated in response to sensing a decline in nutrient availability.

Although regulated establishment of quiescence typically entails cell cycle exit through adoption of a G0 state (**Figure 1.1A**), cells can enter quiescence at different stages of the mitotic cycle. Several yeast species (Costello et al., 1986; Takeo et al., 1995), stem cells (Otsuki & Brand, 2018; Sutcu & Ricchetti, 2018) and cancer cells (Drewinko et al., 1984; Pearl Mizrahi et al., 2016) can enter quiescence in G2. Yeast cells also appear to be able to enter quiescence when arrested in other cell-cycle phases other than G1 or G2 (Daignan-Fornier & Sagot, 2011; W. Wei et al., 1993). The relationship between G0 quiescent cells and quiescent cells that have initiated from other stages of the cell cycle remains largely unknown.

1.5.2 Quiescence maintenance

Once a cell is in a quiescent state it must maintain basal activities to provide protection against long-term cellular stress and environmental insults. Therefore, quiescence is not simply a passive state in which all cellular activities have ceased, but is an actively maintained state (Cheung & Rando, 2013; Coller et al., 2006; Sang et al., 2008). The amount of time that a cell spends in a quiescent state contributes to the underlying changes in cellular and molecular properties. For example, remodeling of cellular machinery in 'early' quiescent cells may not be maintained over time and can change if quiescent cells transition into senescence (**Figure 1.2**) (Damien Laporte, Gouleme, et al., 2018; Sagot & Laporte, 2019).

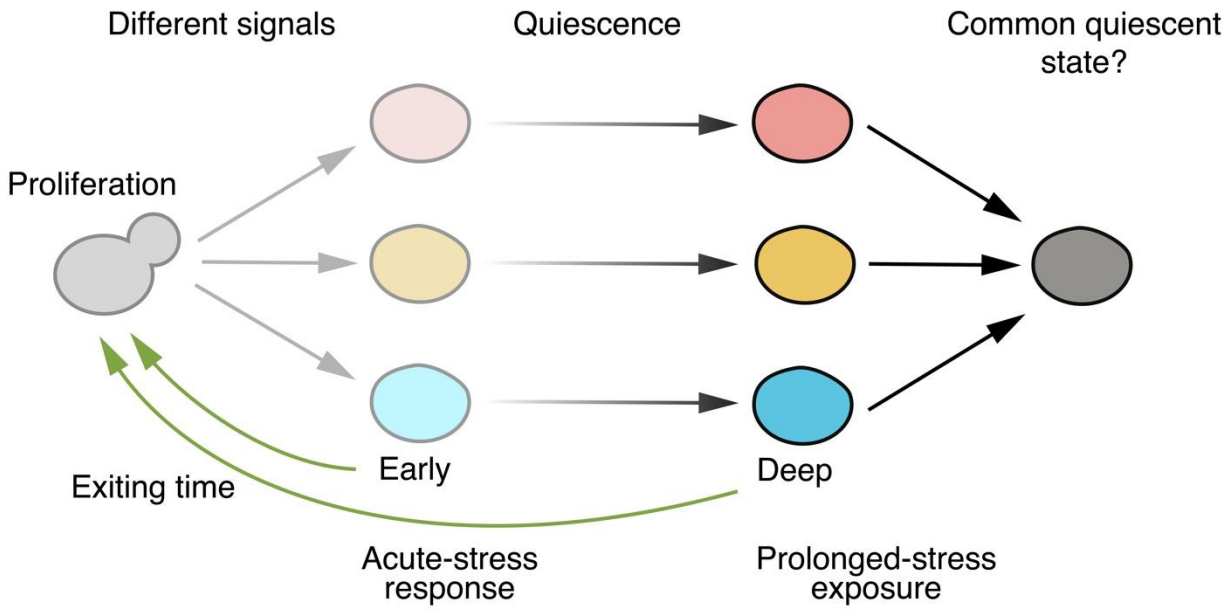

Figure 1.2. Heterogeneity in the initiation, maintenance and exit from quiescence.

The processes that underlie the initiation, maintenance and exit from quiescence are likely distinct, but interrelated.

Genes that have been identified as being important for CLS may be informative for understanding the mechanisms underlying quiescence maintenance. Multiple genome-wide screenings performed in both budding and fission yeast have identified genetic factors that determine CLS using either nitrogen or carbon starvation. In budding yeast, a competitive screening approach revealed that 6.8% of single-gene knockouts had a long-lived phenotype (e.g. chromatin-modification and DNA repair genes), while 7.2% had significantly reduced CLS (e.g. autophagy, mitochondrial, protein trafficking and degradation) under carbon starvation in rich medium (Garay et al., 2014). Similar screening has also been performed in fission yeast under nitrogen starvation (Sideri et al., 2014), which found 48 long-lived mutants although none of their orthologs have been identified in budding yeast screens (Paola Fabrizio et al., 2010; Matecic et al., 2010; Powers et al., 2006), which might indicate differences between the two CLS model systems.

In mammalian systems, quiescent cells can move progressively “deeper” into quiescence and display an elongated pre-DNA-replication phase upon stimulated exit from quiescence (Augenlicht & Baserga, 1974; Kwon et al., 2017; Owen et al., 1989; Yanez & O’Farrell, 1989). Thus, over time the quiescent state deepens and as a result it takes longer for cells to re-enter the mitotic cycle (**Figure 1.2**). Deep quiescent cells also exhibit greater gene expression changes than early quiescent cells (Coller et al., 2006) suggesting that gene expression changes occur during the maintenance of quiescence.

However, little is known about the mechanism that controls the maintenance and

depth of quiescence. A recent study in fibroblast cells identified a Retinoblastoma (Rb)-E2F network switch, whose activation appears to control the depth of cellular quiescence (Kwon et al., 2017). Whether this network switch represents an evolutionary conserved mechanism is unknown, but testing the function of SBF (the yeast homologue of E2F) in regulating the depth of quiescence in budding yeast would be a means of addressing this question.

1.5.3 Quiescence exit

Quiescent yeast cells that are exposed to nutrients, exit from quiescence and reinitiate the cell division cycle. Although little is known of the molecular mechanisms and processes that control exit from quiescence, one prerequisite for quiescence exit is that they maintain mitotic competence (Sajiki et al., 2018). The ability to re-enter the mitotic cycle appears to require the function of multiple processes including the ability to store trehalose and glycogen for use as a future energy source (Shi et al., 2010), the transcriptional repression of specific growth and cell-cycle-related genes (Miles et al., 2013), post-transcriptional regulation of mRNAs (Lihong Li et al., 2013), and transcriptional initiation preparation by maintaining poised RNA Polymerase II upstream of genes (Radonjic et al., 2005). Acetyl-CoA, a metabolite of carbon sources, induces entry into growth. Metabolic activation during exit from quiescence results in the rapid accumulation of acetyl-CoA, which stimulates cell growth by driving the acetylation of histones at specific loci that encode for growth regulatory genes (Cai et al., 2011; Kuang et al., 2017; Shi & Tu, 2013). Whether this metabolic requirement exists for other nutrient

starvation signals in yeast and if it is conserved in quiescent mammalian cells remains unknown.

The efficiency and dynamics of quiescence exit is highly heterogeneous. In a clonal culture of quiescent cells, individual cells exhibit significantly different kinetics in restarting the cell cycle upon stimulated exit (Brooks, 1976; Temin, 1971; Zetterberg & Larsson, 1985). For instance, upon adding serum back to serum-starved cells using a short pulse, some cells re-enter the cell cycle while others remain quiescent (Brooks, 1976; Temin, 1971; Tsuruo, 2008). It has been proposed that this heterogeneity in exiting quiescence is beneficial *in vivo* as it avoids exhausting a pool of quiescent cells with a single stimulus. However, there do appear to be some factors that are predictive of quiescence exit. For example, studies in both yeast and mammalian cells have shown that cell volume and size can affect the efficiency of quiescence exit (Damien Laporte, Jimenez, et al., 2018; X. Wang et al., 2017).

Although there is utility in separating quiescence into three phases, they exist along a continuum and are not mutually independent. A recent study in mammalian cells showed that heterogeneity of quiescence exit reflects a memory of the cell growth and division history immediately prior to quiescence initiation (X. Wang et al., 2017). Understanding the mechanisms that regulate the initiation, maintenance, and exit from quiescence, and the interrelatedness of those mechanisms, is of central importance. Given the heterogeneity among cells at each of these stages of quiescence, studies of

single-cell behavior using quantitative time-lapse microscopy will likely be critical to our understanding of quiescence entry, maintenance and exit.

1.6 The cell biology of quiescence

Cellular quiescence is associated with dramatic reorganization of multiple cellular complexes and organelles. The significance of these large-scale changes has recently gained increased recognition and advances in this area have been summarized in a recent review (Sagot & Laporte, 2019). In brief, multiple organelles and macromolecular structures are remodeled in quiescent cells including accumulation of actin cytoskeleton into actin bodies (Sagot et al., 2006), microtubule stabilization (Danowski, 1998; D. Laporte et al., 2015; Damien Laporte et al., 2013; Pitaval et al., 2017), reorganization of mitochondria (Aulestia et al., 2018; Damien Laporte, Gouleme, et al., 2018), formation of ribonucleoprotein granules (Buchan, 2014; Ramachandran et al., 2011; Sfakianos et al., 2016; Shah et al., 2014), proteasome storage granule (PSG) accumulation out of the nucleus (Damien Laporte et al., 2008; Marshall & Vierstra, 2018), relocalization of enzymes and stress response proteins (Chughtai et al., 2001; Narayanaswamy et al., 2009; O'Connell et al., 2012; Tapia & Morano, 2010), and cytosolic protein aggregation (O'Connell et al., 2014). Many of these phenomena increase the stress resistance of quiescent cells. These large-scale cellular changes may be a means of minimizing the damaging effects of prolonged quiescence and allow the cell to efficiently respond to quiescence exit signals. Organelle-organelle or organelle-cytosol communication and their spatiotemporal dynamics play essential roles in chronological aging of yeast cells

(Dakik & Titorenko, 2016) the proper spatiotemporal dynamics of intercommunication among compartments is likely to be essential for cells to program into quiescent states under different starvation conditions.

The vacuole, the lysosome-like organelle in yeast, appears to be a key organelle for coping with external stimuli (Aufschnaiter & Büttner, 2019; Baba et al., 1994; S. C. Li & Kane, 2009). A recent study in embryonic quiescent fibroblast cells shed light on the role of lysosomes on regulating quiescence depth (Fujimaki et al., 2019). In yeast, many vacuolar or functionally associated genes are essential for quiescence establishment (Liet al., 2015; Sajiki et al., 2009). For example, in *S. pombe* under nitrogen starvation Ypt5 (orthologue of Vpt52/Vpt53/Vps21 in *S. cerevisiae*), Vam6 and Vps11 (orthologue of Pep5 in *S.cerevisiae*) which are involved in vacuole fusion were found to be essential for quiescence entry and maintenance (Sajiki et al., 2009). Genes that function in vacuolar targeting (Gmh1), transportation (Vps20) and biogenesis (Kcs1) are required for quiescence in *S. cerevisiae* under rich medium induced quiescence (Liet al., 2015). Furthermore, a recent genetic study in *S. cerevisiae* found evidence of the functional requirement of vacuole-associated genes in regulating quiescence under multiple environmental conditions (Sun et al., 2020). Vacuoles are important regulators of cellular homeostasis, metabolism and lifespan (Aufschnaiter & Büttner, 2019). Vacuoles are highly dynamic organelles, which can undergo distinct morphological changes in response to different environmental conditions and throughout ageing. For example, nutrient limitation induces vacuolar fusion, resulting in one enlarged vacuole (Baba et al., 1994). Recently, a publication illustrated the importance of vacuoles in coordinating

arginine import and export across vacuole membrane under nitrogen starvation, which suggests that vacuoles can store and transport amino acids during cellular quiescence in multiple conditions (Cools et al., 2020). The significance of morphological dynamics and vacuole reorganization in cell quiescence across different environmental conditions warrants further investigation.

The large-scale reorganization of cellular structures in quiescence is coupled with changes in the biophysical properties of the cytoplasm. Molecular crowding in the cytoplasm is highly dynamic and changes in response to stress conditions such as heat shock, osmotic stress, energy depletion, and nutrient starvation (Delarue et al., 2018; Marini et al., 2020; Mourão et al., 2014; Munder et al., 2016; Riback et al., 2017). Dysregulated homeostasis of cytoplasmic crowding can contribute to cell death (Neurohr et al., 2019). The transition from proliferation to quiescence is coupled with various physicochemical changes, such as lowered cytosolic pH, reduced cell volume, and decreased macromolecule mobility in the cytoplasm (Ashe et al., 2000; Joyner et al., 2016; Munder et al., 2016), as well as physiological changes, such as reduction in protein synthesis, enzymatic activities, and signal transduction (De Virgilio, 2012; Fuge et al., 1994; Gray et al., 2004; Miermont et al., 2013). In yeast, the cytoplasm appears to undergo a transition from a fluid-like material to a glass-like material under glucose starvation, which may be important for long-term survival under stress conditions (**Figure 3**) (Munder et al., 2016). As the majority of metabolic reactions and protein translation take place in the cytoplasm, induced changes in its physicochemical properties of the cytoplasm may be required for the cell to transition into a quiescent state. However, the

extent to which the biophysical properties of the cytoplasm change in response to different pro-quiescence signals and the dynamics, functional consequences, and regulators of these changes are largely unknown.

1.7 Gene expression programs in quiescent cells

1.7.1 Regulation of RNA expression

Quiescent cells maintain basal transcriptional activity consistent with the maintenance of an operational transcriptional machinery. In both yeast and mammalian cells, quiescent cells have distinct transcriptomes compared to actively dividing cells (Coller et al., 2006; Marguerat et al., 2012; Shimanuki et al., 2007). Specifically, the transcription factors responsible for inducing autophagy and stress responses are upregulated in quiescent cells, whereas growth related genes, many of which contribute to protein synthesis, are strongly repressed upon quiescence initiation (Broach, 2012; De Virgilio, 2012; N. Zhang & Cao, 2017).

Cells undergo global downregulation of transcription when entering quiescence. In yeast, the overall mRNA and rRNA levels are reduced in quiescent cells; however, the diversity of transcripts remains high (Marguerat et al., 2012; Shimanuki et al., 2007). An absolute quantification of transcripts in quiescent cells revealed a 30-fold repression of global mRNA levels compared with cells in log phase (McKnight et al., 2015). The global transcriptional repression is correlated with chromatin remodeling during quiescence initiation. Rpd3, a lysine deacetylase, is a key mediator of chromatin remodeling leading

to global repression of gene expression and the activation of quiescence-specific transcription factors, such as Xbp1 and Stb3 (McKnight et al., 2015). The global transcription repression in quiescent cells under carbon starvation also correlates with chromatin condensation (Swygert et al., 2019). This condensin-dependent chromatin compaction is found to be conserved in quiescent human fibroblasts (Swygert et al., 2019) epigenetic mediated chromatin compaction may be a conserved regulatory mechanism for repressing transcription in quiescent cells.

Quiescent cells exhibit a transcriptional profile that has a unique component, reflecting the signal that induced quiescence, and a common component that reflects the quiescent state. The transcriptional state continues to evolve during quiescence. In mammalian cells, the transcriptional profiles of human fibroblasts differ in “early” quiescent cells depending whether the signal is contact inhibition, loss of adhesion or serum starvation, but gradually converge on a common quiescent transcriptome profile as cells enter into “deep” quiescence (Coller et al., 2006). Similarly, budding yeast cells subjected to different starvations exhibit acute signal-specific transcriptional responses initially that become increasingly similar as the period of quiescence increases (Klosinska et al., 2011). One caveat to these findings is that transcriptome studies are not typically performed on fractionated quiescent cells and thus the contribution of senescent cells to the gene expression state is unknown. As characterization of the transcriptome in “early” quiescent cells has allowed identification of several genes essential for quiescence establishment (Shimanuki et al., 2007), an important future direction is to characterize the transcriptome as a function of time spent in quiescence using fractionated samples as

this may lead to identification of factors involved in long-term maintenance and better define the trajectory of quiescence development. Recently developed single-cell RNA sequencing (scRNAseq) approaches in yeast (Jackson et al., 2020) may aid this goal.

1.7.2 Regulation of protein expression

Quiescence results in reduced overall protein production and remodeling of the proteome. On one hand, survival in quiescence requires upregulation of proteins that function as stress protectants such as chaperones or heat shock proteins (Iwama & Ohsumi, 2019; Onodera & Ohsumi, 2005; Tapia & Morano, 2010; Tsukada & Ohsumi, 1993; Verghese et al., 2012). Conversely, protein abundance measurements using GFP-tagged proteins in quiescent cells starved for carbon (Davidson et al., 2011) indicate that several proteins are decreased in abundance, many of which are involved in biosynthetic processes, especially translation. Thus, both degradative and synthetic processes contribute to remodeling the proteome of quiescent cells. However, the relative role of synthetic and degradative processes in regulating proteome homeostasis in quiescent cells and the signaling pathways that regulate these different aspects of proteostasis are largely unknown.

Although both transcription and translation are reduced during quiescence entry, there appears to be a significant discrepancy between the transcriptome and proteome of quiescent cells. An absolute quantitative study in quiescent *S. pombe* cells starved for nitrogen found that the total transcriptome size decreases in proportion to cell size, but the proteome size does not (Marguerat et al., 2012). This highlights the importance of

studying gene expression at both the protein and RNA level to define the roles of post-transcriptional, translational and posttranslational regulation of cellular quiescence. Moreover, the causal connections between proteome homeostasis, cytoplasmic crowding, and changes in organelle morphology during cellular quiescence warrants further investigation.

1.8 Metabolism in quiescent cells

The metabolic activity of quiescent cells is globally suppressed. However, quiescent cells require basal catabolic activity to ensure energy homeostasis and to facilitate effective exit quiescence. Quiescent cells exhibit distinct metabolic profiles compared with proliferative cells. A defining characteristic of quiescent yeast cells is an increase in the storage carbohydrates, glycogen and trehalose (Lillie & Pringle, 1980), which are subsequently degraded upon exit from quiescence (Shi et al., 2010; J. Zhang et al., 2019). These compounds appear to be critical for quiescence as mutants defective in trehalose synthesis are defective in quiescence and adding external trehalose can rescue some diploid mutants that are otherwise not able to establish quiescence (Miles et al., 2019).

Yeast cells starved for different nutrients exhibit different metabolic profiles that reflect the starvation signal. For example, nitrogen starved cells have uniquely reduced levels of amino acids and nucleotide triphosphates are uniquely depleted in phosphorous starved cells (Klosinska et al., 2011). Tri-carboxylic acid (TCA) cycle intermediates accumulate in quiescent cells starved for nitrogen and phosphorus, but not in cells starved

for glucose (Klosinska et al., 2011). Interestingly, the metabolic state of quiescent cells differs from slowly growing cell populations, which are composed of large fractions of cells in G1, consistent with quiescence entailing a distinct metabolic state (Klosinska et al., 2011).

During quiescence initiation, genes required for respiration, fatty acid metabolism, glyoxylate cycle reactions, and antioxidant defenses are turned on to allow scavenging and destruction of reactive oxygen species (ROS) (Ashrafi et al., 1998; Costa & Moradas-Ferreira, 2001; Cyrne et al., 2003; Gasch et al., 2000; Jamieson, 1998). Quiescent cells isolated by density fractionation (Allen et al., 2006; Werner-Washburne et al., 2012) maintain low ROS and maintaining low ROS (e.g. superoxide, hydrogen peroxide, hydroxyl radicals and singlet oxygen) is essential for long term survival as ROS can damage DNA and cellular macromolecules (Gangloff & Arcangioli, 2017). Antioxidants and NADPH, which is used for the recycling of many antioxidants, can protect cells from mitochondrial generated ROS to delay cell aging (Bradshaw, 2019). In addition, transcriptional regulators (e.g. Msn2/Msn4) that accumulate in starved cells under the control of signaling kinases Rim15 (Lee et al., 2013), and upregulate targets including superoxide dismutase 1 (Sod1) and superoxide dismutase 2 (Sod2), which aid in managing stress induced by nutrient deprivation (Auesukaree et al., 2009; Cameroni et al., 2004; P. Fabrizio et al., 2004). Sod1p and Sod2p are upregulated at least two fold in quiescent cells (Davidson et al., 2011) and Sod1 or Sod2 deletion results in increased loss of viability when stationary cells are aerated (Longo et al., 1996).

Metabolism is closely related to protein production (Litsios et al., 2018) as ribosome biogenesis requires most of the cellular biosynthetic capacity of a cell and protein translation is by far the most expensive biosynthetic process in the cell. Central metabolism is essential for amino acid production and therefore determines the rate of protein synthesis and degradation (Ljungdahl & Daignan-Fornier, 2012). Given these premises, understanding the regulatory connections between metabolism and protein production is central to understanding the role of metabolism in quiescence. In addition, dissecting metabolic regulation during different stages of quiescence is required for understanding how metabolism drives maintenance of quiescence and exit from quiescence (Kaplon et al., 2015). Identifying the causal relationships between regulatory mechanisms, gene expression and metabolism in quiescence represents a major challenge in the field.

1.9 Signaling pathways in regulating quiescence

The transition from a proliferative to quiescent state requires signaling pathways that sense environmental signals and transmit that information within the cell. Multiple evolutionary conserved pathways are known to regulate cell quiescence including the Ras/protein kinase A (PKA), SNF1 (AMPK in humans), TORC1 (the target of rapamycin complex I) and PHO80-PHO85 (cyclin dependent kinase 5 in humans) pathways. These pathways are conserved from yeast to humans (De Virgilio, 2012). As central regulators of quiescence and cell growth these pathways are frequently dysregulated in human diseases including cancer and diabetes (Beristain et al., 2015; Broach, 2012; Faubert et

al., 2015; L. C. Kim et al., 2017; Mathieu Laplante & Sabatini, 2012).

In yeast, these pathways respond to specific nutrients. The quiescence entry program relies on information transmitted by three nutrient signaling pathways: TORC1 pathway, regulated by nitrogen sources, the glucose-responsive Ras/PKA pathway and the phosphorus-responsive PHO pathway (**Figure 1.3**) (Bontron et al., 2013; De Virgilio, 2012). When nutrient availability declines, decreased activity of these pathways results in reduction of growth-related processes and derepression of growth-repressed processes. Similarly, PKA, PHO85, or TORC1 inhibition causes growth arrest and promotion of a G0-like state (De Virgilio & Loewith, 2006; Menoyo et al., 2013; Tatchell, 1986; Thevelein & de Winde, 1999; Wullschleger et al., 2006). These pathways are essential for quiescence as cells mutant for these pathways rapidly lose viability when starved for specific nutrients (Gresham et al., 2011; Sun et al., 2020). Conversely, cells with uncontrolled, elevated PKA activity typically fail to acquire many physiological characteristics of quiescence in stationary phase.

Quiescence regulating pathways converge on common targets. In yeast, there is evidence of interactions between signaling pathways (Jorgensen et al., 2004; Mathieu Laplante & Sabatini, 2012; M. Laplante & Sabatini, 2009; Marion et al., 2004; Oliveira et al., 2015) and convergence on a common regulatory kinase, RIM15 (Pedruzzi et al., 2003; Sun et al., 2020; Swinnen et al., 2006). Systematic approaches are needed to study the coordination between signaling pathways in quiescent cells. One efficient approach to define functional relationships between genes and pathways is through quantitative

genetic interaction mapping (Billmann et al., 2016, 2018; Costanzo et al., 2016; Ryan et al., 2012). Quantitative maps of genetic interactions between signaling pathways in multiple environmental conditions allows identification of context specific functional relationships between signaling pathways. We recently developed an approach to quantifying genetic interactions in quiescent cells (Sun et al., 2020) using Bar-seq and found that *TOR1*, *RIM15* and *PHO85* exhibit signal-dependent genetic interaction profiles in quiescence, but that *RIM15* genetically interacts with protein degradation and synthesis genes in different quiescent conditions consistent with its function as a master regulator of quiescence via modulation of protein homeostasis (**Figure 1.3**). How *RIM15* regulates protein homeostasis and whether *RIM15* phosphorylates the same set of targets under different starvation conditions is unknown.

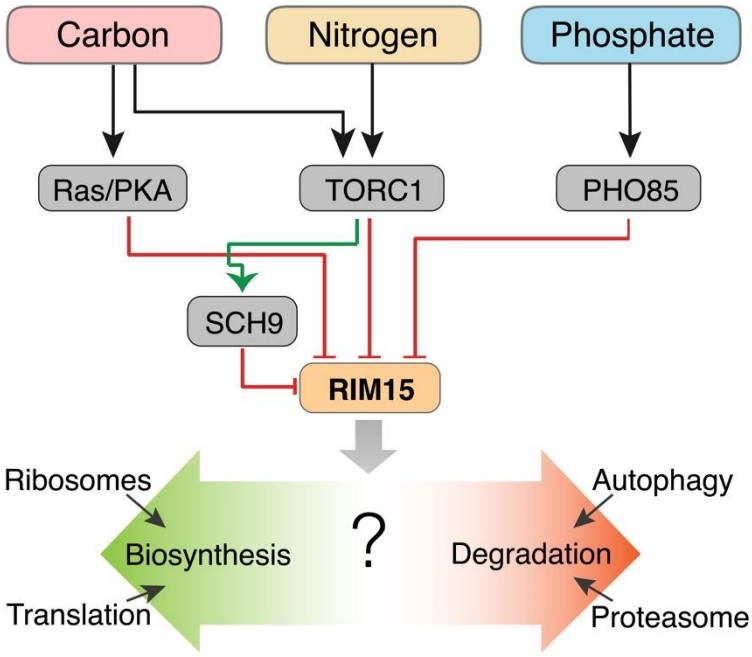

Figure 1.3. Conserved signaling pathways regulating cellular quiescence in budding yeast.

Different nutritional starvation signals (carbon, nitrogen, and phosphorus) are sensed and transmitted via distinct signaling pathways. These pathways converge on regulation of the protein kinase, RIM15, which is considered the master regulator of quiescence. Regulation of protein homeostasis is a major downstream target of these pathways. Red arrow indicates global upregulation, and green arrow indicates an overall downregulation of major activities that contribute to protein degradation (autophagy and proteasome activity) and biosynthesis (ribosome and translation)

1.10 Clinical relevance

Understanding the regulation of quiescence is of significant clinical relevance as many pathogenic microbes exist in a quiescent state that makes them difficult to kill. Although mutation and selection frequently underlie drug resistance, there is growing appreciation of the role of non-genetic variation in drug resistance (Balaban et al., 2004). Many microbes form complex community structures, such as biofilms, which are an increasing problem in hospitals and in invasive therapeutic devices such as catheters and stents (Lynch & Robertson, 2008; Ramage et al., 2012). The complex structure of biofilms can result in the inadequate supply of nutrients to some cells leading to initiation of a quiescent state.

Understanding quiescence in pathogenic fungi such as *Candida albicans (C. albicans)* and *Candida aureus* is likely to be useful for developing new antifungal drugs and strategies that target non-proliferative cells. *C. albicans* typically undergoes morphological changes in response to different nutritional starvation signals (Kadosh & Mundodi, 2020; Sudbery, 2011). Recently, studies from several groups have shown that signaling pathways essential in regulating cellular quiescence in yeast, such as the TORC1 and Ras/PKA pathways, play similar roles in regulating morphological changes

in *C. albicans*, conferring drug-resistance (Chen et al., 2018; Flanagan et al., 2017; C. Su et al., 2013). Therefore, extending studies to other eukaryotic microorganisms will be beneficial for devising therapeutic strategies and informing our understanding of the conservation of quiescence in different species.

Quiescence also has a significant role in human cancers. Recent studies have shown that quiescent cancer stem cells (CSCs) are able to evade immune surveillance and promote tumor development (Agudo et al., 2018; Bruschini et al., 2020; Laughney et al., 2020). Studies have also shown that stem cells, such as those in hair follicles and muscle, are resistant to T-cell killing (Agudo et al., 2018). Furthermore, in ex-vivo experiments, quiescent stem cells appear to be protected from natural killer (NK) cells (Laughney et al., 2020). These results suggest that the immune privileged status is not an intrinsic property of CSCs, but is linked to the ability to enter a quiescent state. Understanding the interaction between quiescent CSC and the microenvironment will potentially contribute to more effective cancer treatments. Studies in yeast have the potential to rapidly develop and test hypotheses regarding therapeutic strategies that leverage an enhanced understanding of cellular quiescence.

Chapter 2 : Understanding functional relationships between protein kinases using quantitative genetic interaction mapping

This chapter is based on the research paper “Genetic interaction profiles of regulatory kinases differ between environmental conditions and cellular states” by Siyu Sun, Anastasia Baryshnikova, Nathan Brandt and David Gresham, which appeared in *Molecular and Systems Biology* in May 2020. I generated all of the data for all figures and tables, wrote the first version of the text, and generated all of the supplementary figures presented here.

2.1 Abstract

Cell growth and quiescence in eukaryotic cells is controlled by an evolutionarily conserved network of signaling pathways. Signal transduction networks operate to modulate a wide range of cellular processes and physiological properties when cells exit proliferative growth and initiate a quiescent state. How signaling networks function to respond to diverse signals that result in cell cycle exit and establishment of a quiescent state is poorly understood. Here, we studied the function of signaling pathways in quiescent cells using global genetic interaction mapping in the model eukaryotic cell, *Saccharomyces cerevisiae* (budding yeast). We performed pooled analysis of genotypes using molecular barcode sequencing (Bar-seq) to test the role of ~4,000 gene deletion mutants and ~12,000 pairwise interactions between all non-essential genes and the protein kinase genes *TOR1*, *RIM15*, *PHO85* in three different nutrient-restricted conditions in both proliferative and quiescent cells. We detect up to ten-fold more genetic interactions in quiescent cells compared to proliferative cells. We find that both individual gene effects

and genetic interaction profiles vary depending on the specific pro-quiescence signal. The master regulator of quiescence, *RIM15* shows distinct genetic interaction profiles in response to different starvation signals. However, vacuole-related functions show consistent genetic interactions with *RIM15* in response to different starvation signals suggesting that *RIM15* integrates diverse signals to maintain protein homeostasis in quiescent cells. Our study expands genome-wide genetic interaction profiling to additional conditions, and phenotypes, and highlights the conditional dependence of epistasis.

2.2 Introduction

Most cells spend the majority of their lifetime in a quiescent state defined as the temporary and reversible absence of proliferation (O'Farrell 2011; Lemons et al. 2010; Valcourt et al. 2012). Quiescence requires exit from the mitotic cell division cycle and initiation of a distinct G0 cell cycle phase, during which cells remain viable and maintain the capacity to re-initiate the cell cycle and proliferative growth (Valcourt et al. 2012). In multicellular organisms development, tissue renewal and long term survival is dependent upon the persistence of stem cells that are quiescent, but retain the ability to re-enter the cell cycle to self-renew, or to produce progeny that can differentiate and re-populate the tissue (Miles and Breeden 2017). Exit from quiescence, and initiation of aberrant proliferation, is a hallmark of cancer (Hanahan and Weinberg 2011; Miles and Breeden 2017). Conversely, many cancer-related deaths are the result of quiescent tumor cells that are resistant to therapeutics and underlie tumor recurrence (Yano et al. 2017; Borst 2012). Thus, understanding cellular quiescence and how cells regulate the transition between

proliferative and quiescent states is of fundamental importance to our understanding of cellular homeostasis and disease.

Cells exit the cell cycle and enter quiescence when they are deprived of essential nutrients or growth factors (Valcourt et al. 2012; Daignan-Fornier and Sagot 2011; Klosinska et al. 2011). Quiescence in the model eukaryotic organism, *Saccharomyces cerevisiae* (budding yeast) shares many important features with that of higher organisms, including cell cycle arrest, condensed chromosomes, reduced rRNA synthesis and protein translation, and increased resistance to stress (Valcourt et al. 2012; Dhawan and Laxman 2015). Therefore, the mechanisms that regulate cell cycle arrest and the establishment, maintenance and exit from a quiescent state, as well as the physiological processes associated with this state, are likely to be shared across eukaryotic cells.

Studies of quiescence in yeast typically examine stationary-phase cells, namely cells grown to saturation in rich, glucose-containing medium (Joseph V. Gray et al. 2004; Young et al. 2017). In this case, cells typically first exhaust glucose through fermentative metabolism and then, following the diauxic shift, switch to respiration using ethanol as the carbon source. Upon exhaustion of ethanol, cells enter quiescence. However, in addition to carbon starvation, yeast cells can respond to a variety of nutrient starvations by exiting the cell cycle and initiating quiescence (Lillie and Pringle 1980; Gresham et al. 2011; Klosinska et al. 2011). Starvation for essential nutrients including nitrogen, phosphorus and sulfur result in many of the same characteristics as carbon-starved cells including arrest as unbudded cells, thickened cell walls, increased stress resistance and an

accumulation of storage carbohydrates (Lillie and Pringle 1980; Klosinska et al. 2011; Schulze et al. 1996). Although in laboratory conditions yeast primarily experience carbon starvation, in the wild, yeast is likely to experience a diversity of nutrient deprivations. How the cell integrates these diverse signals to mount the same physiological response, and establish cellular quiescence, remains poorly understood.

The ability of stationary phase yeast cells to maintain viability has also been used as a model for chronological aging. Chronological lifespan (CLS) has been defined as the time a yeast cell can survive in a non-dividing, quiescent state (Fabrizio and Longo 2003; Kaeberlein 2010; Walter, Matter, and Fahrenkrog 2014). Therefore, CLS is closely related to the proportion of quiescent cells in stationary phase cultures because non-quiescent cells have a reduced ability to reenter the cell cycle (Allen et al. 2006; Walter, Matter, and Fahrenkrog 2014). Cells with a shortened CLS have reduced reproductive capacity upon replenishment of nutrients (Garay et al. 2014). Identification of genes that mediate CLS in yeast under different nutrient restrictions is potentially informative about the regulation of aging in higher organisms.

The genotype of a yeast cell has a profound impact on the regulation of quiescence. Many studies of survival in stationary-phase cells, and their application to the study of CLS, have been conducted using auxotrophic strains. However, starvation for an engineered auxotrophic requirement is an unnatural starvation that results in a failure to effectively initiate a quiescent state and therefore leads to a rapid loss of viability (Boer, Amini, and Botstein 2008; Gresham et al. 2011). This is likely due to the fact that yeast

cells have not evolved a mechanism for sensing and responding to lab engineered auxotrophic requirements. The use of undefined media and auxotrophic strains for studying CLS can be confounded by inadvertent starvation for auxotrophic requirements. Thus, the identification of mutants that suppress the rapid loss of viability upon undefined starvation in auxotrophic strains may be of limited relevance for understanding the regulation of quiescence and CLS. Previous studies of quiescence using prototrophic yeast cells, and defined starvation for nutrients that are essential for growth in wildtype cells (i.e. natural starvation), have shown that the genetic requirements for quiescence differ depending on the nutrients for which the cell is starved (Gresham et al. 2011; Klosinska et al. 2011). However, whether the genes required for proliferation in different nutritional conditions are the same set of genes that are required for programming quiescence is not known.

Multiple evolutionarily conserved nutrient sensing and signal transduction pathways, including the target of rapamycin complex I (TORC1), protein kinase A (PKA), adenosine monophosphate kinase (AMPK) and PHO85 pathways have been shown to regulate quiescence. The integrator of these diverse signaling pathways is thought to be the protein kinase RIM15, a great wall kinase that is a homologue of the mammalian gene, microtubule associated serine/threonine like kinase (MASTL) (Castro and Lorca 2018). RIM15 appears to be downstream of multiple signaling pathways and is required for the establishment of quiescence. However, how different starvation signals are coordinately transduced via these pathways, and how RIM15 orchestrates the establishment of cellular quiescence is not known (de Virgilio 2012; Broach 2012).

The relationship between different cellular processes and pathways can be investigated using a variety of methods that identify physical and functional interactions. One efficient approach to define interactions between genes and pathways is through quantitative genetic interaction mapping (Billmann et al. 2016, 2018; M. Costanzo et al. 2016). A genetic interaction is a relationship between two genes in which the phenotype of the double mutant diverges from that expected on the basis of the phenotype of each single mutant (A. H. Y. Tong et al. 2004; Boone, Bussey, and Andrews 2007; Mani et al. 2008; Beltrao, Cagney, and Krogan 2010; Michael Costanzo et al. 2010). Genetic interactions can be informative of the functional relationship between the encoded products. Positive genetic interactions may be indicative of genes that exist within pathways or complexes whereas negative genetic interactions often reflect genes that function in parallel pathways or processes that converge on the same function (van Leeuwen, Boone, and Andrews 2017). Extension of genetic interaction mapping to test genome-wide interactions between defined alleles results in a genetic interaction profile, comprising the set of negative and positive genetic interactions for a given gene. The systematic application of this approach has demonstrated that genes that share similar functions, or operate in the same pathway, often share similar genetic interaction profiles. As such, the similarity in quantitative genetic interaction profiles between two genes (typically quantified as a correlation coefficient) is informative about the similarity between the two genes' functions. The culmination of genome-wide genetic interaction mapping in budding yeast has been the construction of a global genetic interaction similarity network that serves as a functionally informative reference map (Michael Costanzo et al. 2010; M.

Costanzo et al. 2016). The recent completion of this comprehensive genetic interaction map leads to two related questions: 1) to what extent are genetic interactions dependent on environmental conditions?, and 2) can genome-wide genetic interaction mapping be expanded to other phenotypes? Quantitative genetic interaction mapping is increasingly being applied in other organisms, including Drosophila melanogaster and mammalian cells using RNAi or CRISPR (Fischer et al. 2015; Billmann et al. 2016, 2018; Du et al. 2017) making these questions of broad significance.

To date, genome-wide genetic interaction mapping in yeast has primarily been performed in a single condition and assayed using a single phenotype - colony growth in optimal nutritional conditions (Roguev et al. 2008; A. H. Tong et al. 2001; Michael Costanzo et al. 2010). Some studies have extended genetic-interaction mapping to different stress conditions (Martin et al. 2015; Gutin et al. 2015; St Onge et al. 2007; Díaz-Mejía et al. 2018), but not on a genome-wide scale. Therefore, the extent to which genetic interactions depend on environmental conditions and the feasibility of using additional phenotypes beyond colony growth phenotypes in genetic interaction mapping remains largely unexplored. Targeted studies of specific genotypes suggest that functional relationships between genes are environmentally dependent (Díaz-Mejía et al. 2018; Bandyopadhyay et al. 2010; St Onge et al. 2007; Jaffe et al. 2019) suggesting that a complete understanding of global genetic interaction networks requires identification of genetic interactions in multiple conditions and using multiple phenotypes.

Here, we have developed a new method for quantifying phenotypes of pooled

single and double mutants in different conditions using Bar-seq. We applied this approach to quantify the genetic requirements, and identify genetic interactions, in two different cellular states and three different nutritional conditions. Our experimental design entailed quantification of both fitness during proliferative growth and survival during prolonged defined starvation for each genotype. We find that the genetic requirements for quiescence differ depending on the nutrient starvation signal. Using genome-wide genetic interaction mapping for three key regulatory kinases, we find that these genes exhibit different interaction profiles in different growth conditions and in different cellular states. Finally, we find that the master regulator of quiescence, *RIM15* shows distinct genetic interaction profiles and regulates different functional groups in response to different starvation signals. However, vacuole-related functions show consistent negative genetic interactions with *RIM15* in response to different starvation signals consistent with *RIM15* controlling quiescence by integrating diverse signals to regulate protein degradation processes (Cameroni et al. 2004; Swinnen et al. 2006). *RIM15* also interacts positively with ERAD genes specifically in nitrogen starvation conditions pointing to a previously unappreciated role for this quality control pathway in quiescence. Our study points to a rich spectrum of condition-specific genetic interactions that underlie cellular fitness and survival across a diversity of conditions and introduces a generalizable framework for extending genome-wide genetic interaction mapping to diverse conditions and phenotypes.

2.3 Results

2.3.1 Quantifying mutant fitness using pooled screens in diverse conditions

Cellular quiescence in yeast can be induced through a variety of nutrient deprivations, but whether establishment of a quiescent state in response to different starvation signals requires the same genetic factors and interactions is poorly understood. Therefore, we sought to test the specificity of gene functions and genetic interactions in quiescent cells in response to three natural nutrient starvations: carbon, nitrogen and phosphorus. The use of prototrophic yeast strains is essential for the study of quiescence as unnatural (starvation of an auxotroph for its auxotrophic requirement), or unknown starvations can confound results and their interpretation (Boer, Amini, and Botstein 2008; Gresham et al. 2011). Therefore, we constructed haploid prototrophic double mutant libraries using a modified synthetic genetic array (SGA) mating and selection method (**Figure 2.S1A**). Briefly, double mutant libraries were constructed using genetic crosses between the ~4,000 non-essential gene deletion strains (Giaever et al. 2002) and query strains deleted for one of three genes encoding the catalytic subunit of different regulatory protein kinases: *TOR1*, *RIM15*, and *PHO85* (**Table 2.1 & Methods**). In addition, we constructed a single mutant library using the same method by mating the gene deletion collection with a strain deleted for *HO*, which has no fitness defects in haploids. We confirmed the genotype and ploidy of the resulting three haploid double gene deletion libraries and the single mutant (*HO*) library using selective media and flow cytometry (**Figure 2.S1B**).

Table 2.1. List of strains used and constructed in this study.

Strain ID	Gene/Alias	Genotype	Notes
Background Strain	NA	MATα can1Δ::STE2pr-Sp_his5 lyp1Δ his3Δ1	Prototrophic strain background
YJR066W_y13791	TOR1	MAT α tor1ΔNatR can1Δ::STE2pr-Sp_his5 lyp1Δ his3Δ1 LYS2+ URA3+ MET3+ LEU2+	Prototrophic SGA query strain
YFL033C_y13792	RIM15	MAT α rim15ΔNatR can1Δ::STE2pr-Sp_his5 lyp1Δ his3Δ1 LYS2+ URA3+ MET3+ LEU2 +	Prototrophic SGA query strain
YDL227C_y13819	HO	MAT α hoΔ::NatR can1Δ::STE2pr-Sp_his5 lyp1Δ his3Δ1 LEU2+ URA3+ MET15+ LYS2+	Prototrophic SGA control strain
YPL031C_y13820	PHO85	MAT α pho85Δ::NatR can1Δ::STE2pr-Sp_his5 lyp1Δ0his3-1 LEU2+ URA3+ MET15+ LYS2+	Prototrophic SGA query strain

Previously, genome-wide genetic interaction mapping in yeast has been performed using colony growth phenotype as a measurement of genotype fitness (Michael Costanzo et al. 2010; M. Costanzo et al. 2016). In liquid cultures, the growth cycle of a population of microbial cells comprises a lag period, an exponential growth phase, and a subsequent period in which growth is no longer observed, known as stationary phase. Stationary phase is indicative of cell growth and cell cycle arrest due to starvation for an essential nutrient (de Virgilio 2012). To study each genotype over the complete growth cycle in liquid cultures, we first analyzed the four libraries (**Figure 2.1A**) in three different defined nutrient-restricted media: carbon-restricted (minimal media containing 4.4mM carbon), nitrogen-restricted (minimal media containing 0.8mM nitrogen), and phosphorus-restricted (minimal media containing 0.04 mM phosphorus)

(**Methods and materials**). The composition of these media ensures that, following an exponential growth phase, cells experience either carbon, nitrogen or phosphorus starvation, respectively. In each of the three conditions media, 1.5×10^8 cells from each of the four libraries (**Figure 2.1A**) of pooled mutants were used to inoculate cultures (t = 0). In nitrogen- and phosphorus-restricted media, we observed that the starvation period commenced 24 hours after inoculation (**Figure 2.S1C**). Cells in carbon-restricted media underwent the diauxic shift after 24 hours and reached stationary phase approximately 48 hours post inoculation (**Figure 2.S1C**). Beyond these time points we did not observe additional cell division or population expansion consistent with defined nutrient starvation and the initiation of quiescence.

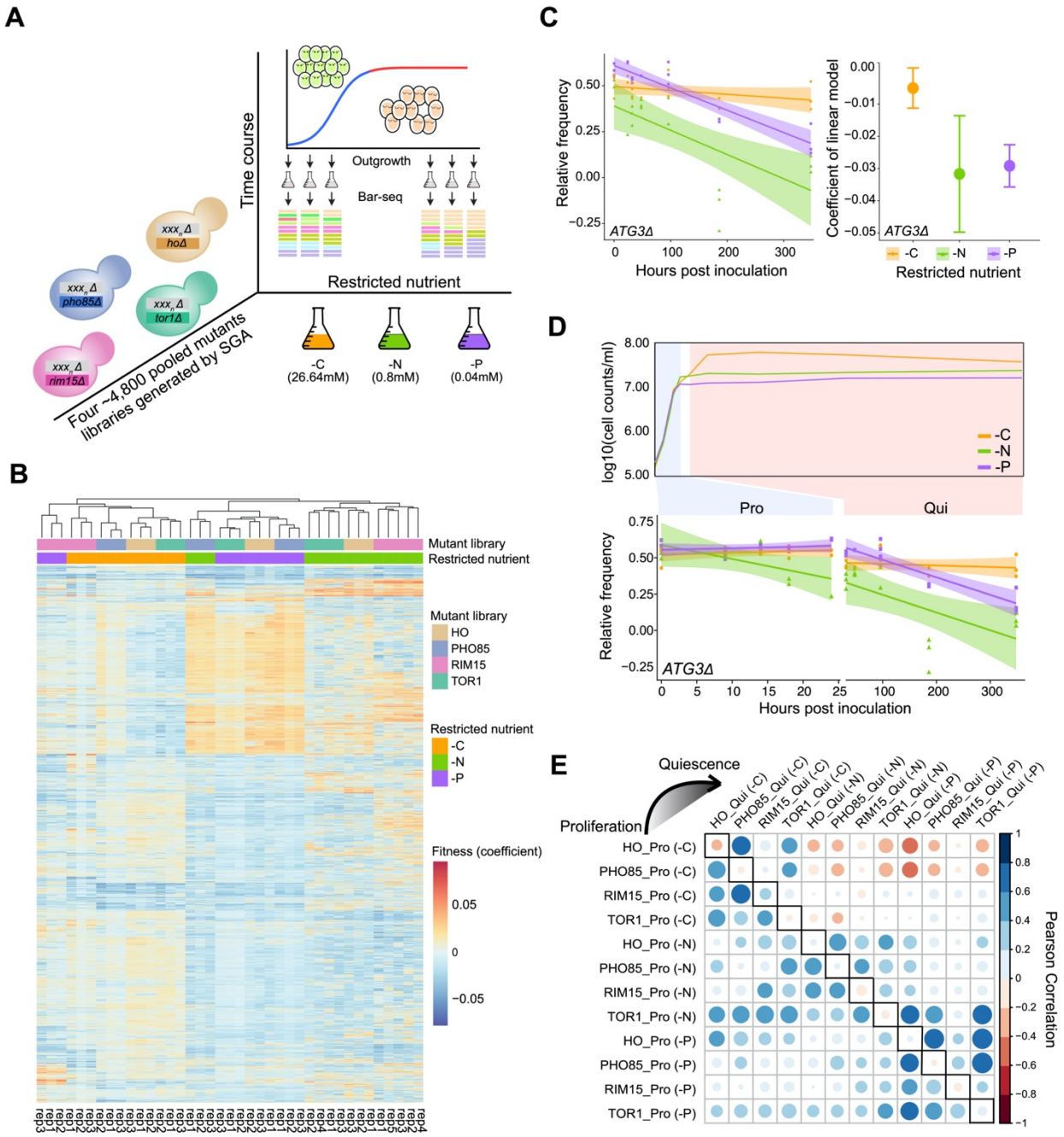

Figure 2.1. Fitness and survival rate estimation over the entire growth cycle using pooled mutant libraries and Bar-seq.

A) Experimental design for multiplexed mutant survival assay using Bar-seq. The synthetic genetic array (SGA) method was used to construct four genome-wide double-mutant prototrophic libraries (**Figure 2.S1A**). The yeast deletion collection (*xxx$_n$Δ*::natMX) was mated with query strains deleted for one of three genes that encode regulatory kinases important in quiescence: TOR1(*tor1Δ*::kanMX), RIM15 (*rim15Δ*::kanMX), and PHO85 (*pho85Δ*::kanMX). A

control library was made by mating the deletion collection to a neutral gene deletion of HO (*hoΔ*::kanMX). To maintain library complexity, 1.5×10^8 cells from each library was used to inoculate (t=0) cultures restricted for glucose (-C, 4.4mM), ammonium sulfate (-N, 0.8mM), and potassium phosphate (-P, 0.04mM) in 300mL cultures. The starvation period for -N and -P conditions commenced after 24 hours and after 48 hours for -C condition (**Figure 2.S1C**). At different time points we removed a ~1×10^6 cell sample from the culture and expanded the viable subpopulation using outgrowth in supplemented minimal media (Table 2.2). DNA was isolated from the resulting outgrowth culture and the library composition was analyzed using Bar-seq. **B)** Hierarchical clustering of mutant fitness profiles computed for each replicate separately across the entire culturing period. White indicates that the strain has not changed in fitness compared to wild-type, blue represents increased fitness and red represents decreased fitness. Culture conditions are indicated by color (orange: carbon restricted; green: nitrogen restricted; purple: phosphorus restricted). Three kinase mutant libraries (TOR1, RIM15, PHO85) and one control library (HO) are shown. **C)** Representative gene (ATG3) for relative fitness estimation across the entire culturing period. The abundance of the *atg3Δ0* strain was determined at multiple timepoints on the basis of counts of its unique DNA barcode and fitness was determined using linear regression. Linear models (predicted value +/- 95% CI) fit to the data are shown on the left, colored by condition. The coefficient (slope) of each model is shown in the dot plot on the right, with a 95% confidence interval indicated as an error bar. **D)** Cells exist in two distinct states depending on nutrient availability. An example of fitness determined during proliferation, and survival, determined during quiescence, in the three different nutrient restricted conditions is shown for *atg3Δ0*. **E)** Relationship of fitness profiles and survival profiles between mutant libraries. Heatmap of correlation coefficients between fitness profiles (left bottom) and between survival profiles (top right) for four different mutant libraries (HO, TOR1, RIM15, PHO85) in three nutrient-restricted conditions (cabron -C, nitrogen -N, phosphorus -P) and two cellular states (Pro and Qui). The dots on diagonal (solid box) indicate the correlation between fitness and survival profiles for the same mutant library under the same condition.

To compare the fitness of each genotype over the complete growth cycle in each condition, a 1mL sample (1 x 10^6 cells) was removed from the culture at sequential time points and the subpopulation of viable cells was expanded using 24-48 hours of outgrowth in supplemented minimal media (**Figure 2.1A, methods**). This step is required to enrich for mutants that survive proliferation and starvation and to deplete those that have undergone senescence. Sampling 1 x 10^6 cells from the cultures minimized the probability ($P < 0.018$) that a genotype was not measured due to sampling error (**Figure 2.S1D** and **methods**). We also quantified population viability throughout this period and observed no

substantial change in any of the conditions (**Figure 2.S1E**). Using an identical outgrowth step at every time point, and determining the rate of change in the relative abundance of viable mutants in the outgrown population, accounts for growth rate differences between mutants during the outgrowth (Gresham et al. 2011). The abundance of each mutant in the heterogenous pool was estimated by sequencing DNA barcodes that uniquely mark each genotype using Bar-seq (Smith et al. 2009; Robinson et al. 2013). In total, we studied the four libraries in the three conditions with between 3-5 independent experiments to account for biological and technical variability (i.e. total of 39 genetic screens).

To determine the fitness of each strain during the complete growth cycle, we initially applied linear regression modeling of the relative frequency of each mutant against time (t = 0, 24, 48, 96, 186, 368 hours) (**Figure 2.S1C**). To test the reproducibility of our fitness assay, we first estimated fitness for each biological replicate separately and used PCA analysis to identify and exclude poorly behaved libraries (**Figure 2.S1F**). Hierarchical clustering of the filtered libraries shows that, for all 39 experiments, biological replicates cluster as nearest neighbors (**Figure 2.1B**). Different libraries cultured in the same medium tend to cluster together, indicating that environmental conditions are a major determinant of fitness effects (**Figure 2.1B**). However, the *PHO85* library in nitrogen-restricted media and the *RIM15* library in phosphorus-restricted media were exceptions to this general trend (**Figure 2.1B**), which indicates that genotype also plays a key role in determining fitness. In general, mutants in carbon-restricted media show less similarity to that observed in nitrogen and phosphorus-restricted conditions, particularly

for *HO* and *PHO85* libraries.

To quantify fitness, and the associated uncertainty (expressed as a 95% confidence interval), for each estimate we performed model fitting for each library in each condition using all biological replicates. We identified numerous cases in which the fitness of a single mutant significantly differs between conditions. For example, deletion of the autophagy gene *ATG3* (*atg3Δ0 hoΔ0)*, results in reduced fitness in nitrogen- and phosphorus-restricted media, but not in carbon-restricted media (**Figure 2.1C**).

2.3.2 Nutrient starvation signal is the primary determinant of mutant survival in quiescent cells

The fitness of a genotype during proliferative growth in different media may differ from the survival of the genotype in response to a specific starvation signal. To test this, we separately modeled the relative abundance of each genotype during the growth phase (i.e. from t = 0 to t = 24 hours) and during the starvation period (i.e. from t = 32 to t = 368 hours) for all mutant libraries using all replicates. This analysis distinguishes the effect of each gene deletion in two distinct physiological states: proliferation and quiescence. As cells do not generate progeny when starved we refer to the phenotype during the starvation phase as “survival” and phenotype during proliferation as “fitness” (**Figure 2.1D**). To identify the primary determinant of these two phenotypes we quantified the similarity between fitness and survival for each mutant library in each condition (C, N, P restricted conditions) (**Figure 2.1E**). We find a clear distinction between proliferative and quiescent cells. During proliferation, mutant libraries starved for different nutrients tend to

share similar fitness profiles regardless of the nutrient signals (**Figure 2.1E - lower left**). By contrast, in quiescent cells, different mutant libraries starved for the same nutrient are more prone to have similar survival profiles than those starved for different nutrients (**Figure 2.1E - upper right**). Consistent with the fitness estimation over the entire growth cycle, libraries starved for carbon have negative correlation with the other libraries starved for nitrogen and phosphorus (**Figure 2.1E**).

2.3.3 Distinct cellular functions are required for quiescence in response to different nutrient starvation signals

Previous genome-wide genetic analyses of quiescence quantified the survival of each mutant in the absence of specific essential nutrients but did not assess the effect of each gene deletion on cellular proliferation prior to starvation (Klosinska et al. 2011). To test whether the genetic requirements for proliferation in nutrient-restricted media and quiescence in response to starvation for the same nutrient are distinct, we investigated the fitness and survival of each genotype in the single mutant library (i.e. the *HO* library). We find that fitness in proliferation and survival in quiescence are poorly correlated for all three nutrient-restricted media: pearson $r = -0.033$ in carbon restricted condition, 0.052 in nitrogen restricted conditions, and 0.064 in phosphorus restricted conditions (**Figure 2.S2A**). The fitness of the single gene deletion mutants (**methods**) is distributed around 0 in each of the three proliferative conditions (**Figure 2.2A**), and the majority of mutants do not show significant fitness defects compared to wild-type cells during proliferation (**Figure 2.2A & Figure 2.S2B**). By contrast, we find that many mutants show a survival defect in quiescent cells when starved for specific nutrients (**Figure 2.S2B**) resulting in

increased variance in the distributions of survival compared to the distributions of fitness (**Figure 2.2A**). Critically, many of the genes that are dispensable for proliferative growth in each of the three media conditions are required for quiescence. For example, deletion of genes involved in the cAMP-PKA signaling pathway, GPB1/2, RGT2, GPR1 results in a profound survival defect in response to carbon starvation, but deletion of these genes does not lower the fitness of carbon-restricted proliferating cells and actually appear to result in a fitness increase, suggestive of a trade-off (**Figure 2.2A left-panel**). This observation is consistent with the fact that mutations in cAMP-PKA pathway have increased fitness in carbon-limiting conditions (Venkataram et al. 2016). Similarly, the autophagy genes *ATG4, ATG5, ATG7,* and *ATG12* have poor survival when starved for nitrogen, but do not have a fitness defect during proliferation in nitrogen-restricted media relative to wild type (**Figure 2.2A, mid-panel**). In response to phosphorus starvation, genes involved in response to pH have poor survival, but those same mutants show profound fitness increase in phosphorus-restricted proliferating cells (**Figure 2.2A right-panel**). Thus, the genetic requirements for growth in a specific nutrient-restricted media and quiescence in response to starvation for that nutrient are distinct.

To further investigate the functional relationship between proliferating and quiescent cells, we applied GSEA to the fitness and survival profiles of the single mutant library in each nutrient-restricted condition. We find no functional overlap between different cellular states under the same nutrient-restricted condition (**Figure 2.S2C**). Moreover, in many cases the same set of genes has the opposite behavior in fitness and survival. For example, deletion of genes involved in protein deacetylase activity shows no

significant impact on survival in quiescent cells but results in reduced fitness during proliferation in nitrogen-restricted conditions (**Figure 2.S2C**).

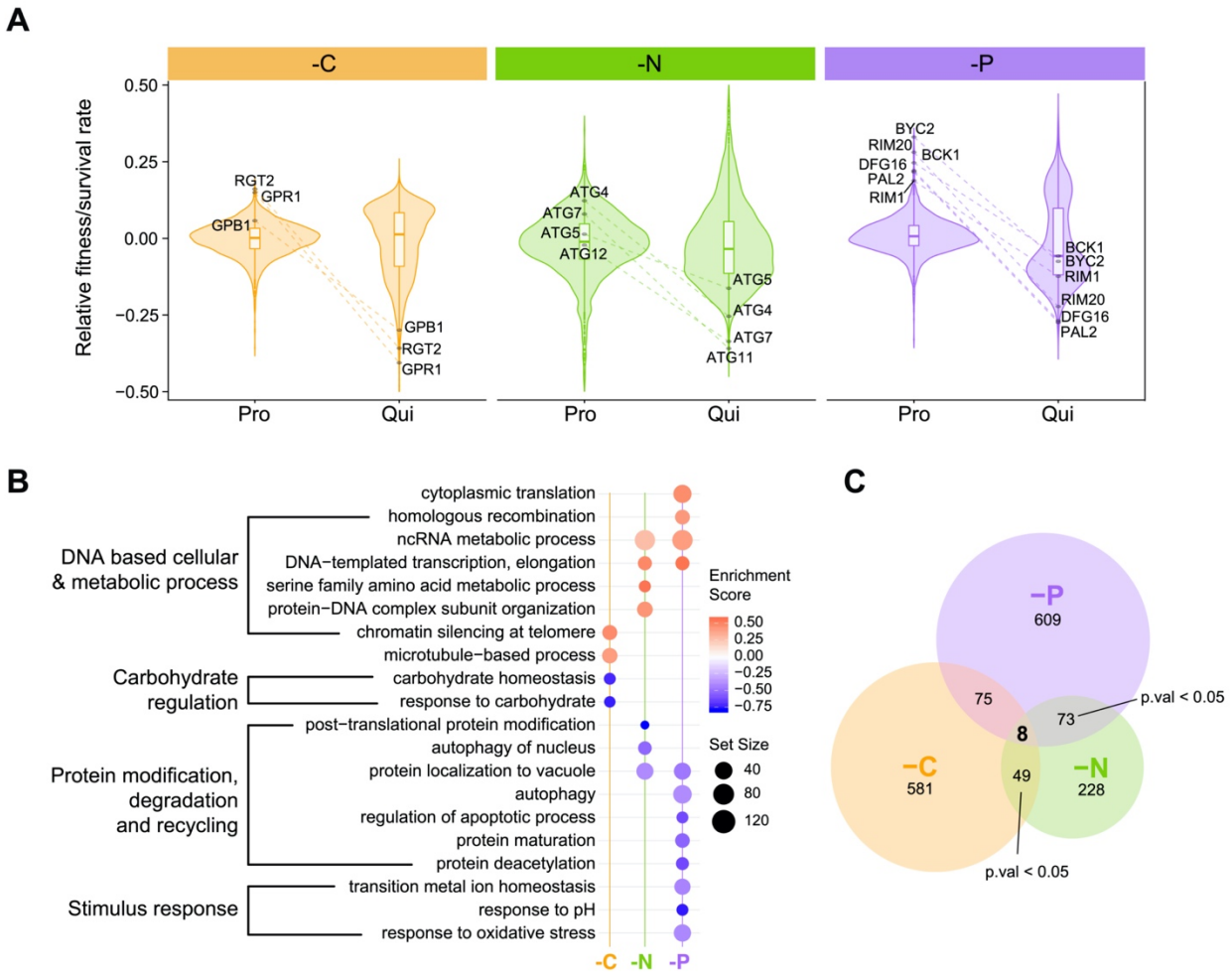

Figure 2.2. Distinct functional requirements for quiescence in response to different starvation signals.

A) Violin plots of the distribution of fitness and survival for all mutants during proliferation and quiescence in response to different nutrient restrictions. The indicated genes are examples of genes that are dispensable for proliferative growth (increased fitness or no significant fitness defects) in each of the three conditions but required for quiescence (decreased survival). **B)** Enriched GO terms identified using Gene Set Enrichment Analysis (GSEA). GSEA was applied to a ranked gene list based on the difference in survival during starvation and fitness during proliferation (S_{Qui} - F_{Pro}) estimated using ANCOVA. The false discovery rate (FDR) was set at 0.05. Positive enrichment scores (red) indicate functions that have increased survival when starved (S_{Qui} - $F_{Pro} > 0$). Negative enrichment scores (blue) indicate functions that when impaired result in decreased survival (S_{Qui} - $F_{Pro} < 0$) during nutrient starvation. Set size indicates the

gene number in each enriched term. **C)** Genes that are required for survival of starvation but dispensable for proliferation. We found 8 genes that are commonly required for survival of all three nutrient starvations (**Figure 2.S2D**); however, the overlap between conditions is not significant (Fisher's exact test, $p > 0.05$).

Genes may be required specifically for proliferation, specifically for quiescence, or necessary for both. To identify gene functions that have a critical role uniquely in quiescence we performed Gene Set Enrichment Analysis (GSEA) (Guangchuang Yu et al. 2012; Subramanian et al. 2005) using gene lists ranked by the phenotypic difference between survival in quiescent conditions and fitness in proliferative conditions ($S_{Qui} - F_{Pro}$) (**methods**). We identified significantly enriched GO terms ($p.adj < 0.05$) and found that functions involved in responding to the specific starvation signal are required for survival. For example, trehalose accumulation provides a reserve of fermentable sugar to reinitiate the cell cycle and provides protection against stress in quiescence (Joseph V. Gray et al. 2004; Shi et al. 2010b; Klosinska et al. 2011). Therefore, we expect to see mutants defective in trehalose storage should fail to survive when starved for carbon. Indeed, this is the case, but the impairment of this function does not impact survival when starved for nitrogen or phosphorus (**Figure 2.2B**). Autophagy has previously been found to affect survival during phosphorus starvation (Gresham et al. 2011), which we recapitulate in our assay (**Figure 2.2B**). Similarly, our observation that genes required for survival of nitrogen starvation are uniquely enriched for selective autophagy of nucleus related amino acid trafficking and recycling is consistent with protein degradation involving autophagy playing a major role in nitrogen recycling (Tesnière, Brice, and Blondin 2015). Some functional groups show similar requirements in response to both nitrogen and phosphorus

starvation, such as autophagy and protein localization by the cytoplasm-to-vacuole targeting (CVT) pathway. By contrast, response to carbon starvation requires an entirely unique set of gene functions. Thus, the biological pathways and functions that are specifically required for cellular quiescence differ depending on the nutrient starvation.

2.3.4 No evidence for common quiescence-specific genes

We sought to determine whether a common set of genes are required for quiescence in all starvation conditions. We identified a comparable number of quiescent-specific (hereafter: QS) genes detected in carbon (538) and phosphorus (707) restriction media. In nitrogen-restricted media, we identified about 2.5 times fewer QS genes: 314 (**Figure 2.2C**). To define a common set of QS genes, we applied three independent filtering criteria. We identified mutants that 1) are dispensable for proliferation in all three nutrient-restricted conditions ($F_{Pro} >= 0$, p.adj < 0.05), 2) show significant defects in quiescence in all three conditions ($S_{qui} < 0$, p.adj < 0.05), and 3) for which there is a significant negative difference between fitness and survival in all three conditions ($S_{qui} - F_{Pro} < 0$, p.adj < 0.05) (**methods**). Using these criteria, we found 8 genes that are commonly required for quiescence regardless of the type of nutrient starvation (**Figure 2.2C & Figure 2.S2D**). However, this does not differ from what would be expected by chance (Fisher's exact test, $p > 0.05$). Thus, we find no evidence for the existence of a common set of QS genes that are required for establishing quiescence in response to carbon, nitrogen and phosphorus starvations.

2.3.5 Detection of genetic interactions using pooled assays

We aimed to identify the set of genetic interactions between all non-essential genes and the three query kinase genes in three different nutritional conditions (carbon, nitrogen and phosphorus restricted media) and two different cellular states (proliferation and quiescence). As there have been limited studies using pooled fitness assays and time course data for quantifying genetic interactions, we considered two possible approaches for data analysis. First, we used analysis of covariance (ANCOVA) to compute the genetic interaction score (GIS) defined as the fitness (in proliferation) or survival (in quiescence) difference between the double (*queryΔ::kanMX xxx$_n$Δ::natMX*) and single mutant (*hoΔ::kanMX xxx$_n$Δ::natMX)* (**methods**). In this case, the two different genotypes (single and double mutant) are treated as independent variables in the model, scaled time is the covariate, and the normalized frequency at different timepoints is the dependent variable.

In a second approach, the GIS was calculated using the approach employed in previous genome-wide SGA studies which defines a null model based on a multiplicative hypothesis and defines a genetic interaction as a significant difference (ε) between the observed and expected double mutant fitness: $\varepsilon = f_{ab} - f_a \cdot f_b$ (Michael Costanzo et al. 2010). We computed the expected fitness for each double mutant by first computing the two single mutant fitness from the single deletion library (*HO*) and then computing ε by determining the difference between the expected and measured fitness of double mutants. A limitation of this approach is that both single gene deletion mutants must be well measured whereas the ANCOVA approach does not require quantifying the query mutant

in the single mutant library and therefore only requires the measurement of one single mutant phenotype.

We find that the agreement between the two approaches is high (pearson's R > 0.9) when applied to both fitness in proliferative cells and survival in quiescent cells. The genetic interaction profiles calculated by ANCOVA or the multiplicative model for both *TOR1* and *RIM15* (**Figure 2.S3A & Figure 2.S3B**) are highly correlated across all nutrient-restricted conditions. As the *PHO85* deletion allele was not identified in the single mutant library (possibly due to an erroneous barcode) we could not perform this comparison for its genetic interactions. To further compare the two approaches, we applied GSEA to genetic interaction profiles calculated using each model and compared the similarity of generated GO terms using GoSemSim (G. Yu et al. 2010). The significant GO terms for a given condition identified using the different models are very similar, indicating that ANCOVA identifies the same genetic interactions and functional groups as the classic multiplicative model. As ANCOVA has a well-developed statistical framework for error estimation and significance testing, we elected to use ANCOVA to compute GIS for all subsequent analyses. As has been previously observed ((M. Costanzo et al. 2016), genes with larger phenotypic effects (either fitness or survival) tend to have strong interactions.

2.3.6 Genetic interactions are condition dependent and common in quiescence

To date, genome-wide genetic interaction mapping in yeast has primarily been performed

in a single condition - rich media - and assayed using a single phenotypic readout - colony size. To investigate the utility of using additional phenotypes in genetic interaction mapping, we compared both fitness estimates and genetic interactions identified in our study with the global reference set (M. Costanzo et al. 2016). As our conditions (nutrient limitation and nutrient starvation) differ substantially from those used in the global reference set (rich undefined medium) the genetic requirements are likely to be distinct. As expected, no significant correlation was detected for fitness measurements in all conditions (three proliferative and three quiescent conditions) or kinases (**Figure 2.S4**), supporting the notion that fitness effects are highly conditionally dependent. Similarly, no significant correlation was detected between the genetic interaction profiles quantified in both studies (**Figure 2.S5**).

We find that genetic interactions between genes are also frequently condition dependent and differ both as a function of cellular state and environmental conditions. For example, in quiescent cells, the autophagy gene *ATG7* positively interacts with *TOR1* in carbon starvation, but negatively interacts with *TOR1* in phosphorus starvation (**Figure 2.3A & 3B**). *ATG7* interacts negatively with *PHO85* and *RIM15* in phosphorus starvation but these interactions are not found in carbon or nitrogen starvation conditions (**Figure 2.3A & 3B**). This example is illustrative of the conditional dependence of genetic interactions, which we find is the case for the vast majority of genotypes (data and model fitting for all genetic interactions can be explored in the associated web application).

Single mutants show stronger phenotypic defects in starvation conditions

compared with growth conditions (**Figure 2.2A**). We found a weaker correlation between phenotypes of single and double mutants in quiescent cells compared to proliferative cells (**Figure 2.3C**, **Figure 2.S3C**) suggesting that the introduction of a second mutation affects many of the gene deletion phenotypes in quiescent cells. More genetic interactions are detected in quiescent cells compared to proliferative cells regardless of the starvation signal (**Figure 2.3D**). For example, at an FDR of 5%, 55 genes (~1.4% of mutant pairs tested) show significant interactions with *TOR1* in proliferative cells growing in carbon-restricted media (**Figure 2.S3D**). The fraction of genes that significantly interact with *TOR1* is similar to the proportion of significant interactions in (M. Costanzo et al. 2016). By contrast, we identified 228 negative and 381 positive (15% or ~10 times more) genetic interactions with *TOR1* in carbon-starved quiescent cells (**Figure 2.S3D**). This trend is observed for all three kinases (*TOR1*, *RIM15*, *PHO85*) in all starvation conditions (**Figure 2.S3D**). We detected both positive and negative interactions for each of the three kinases and an increase in total interactions for a given kinase as more conditions are assayed (**Figure 2.3D & Figure 2.S3E**) indicating that each additional assay reveals unique genetic interactions. We did not detect a bias in the number of positive or negative interactions in either cellular state.

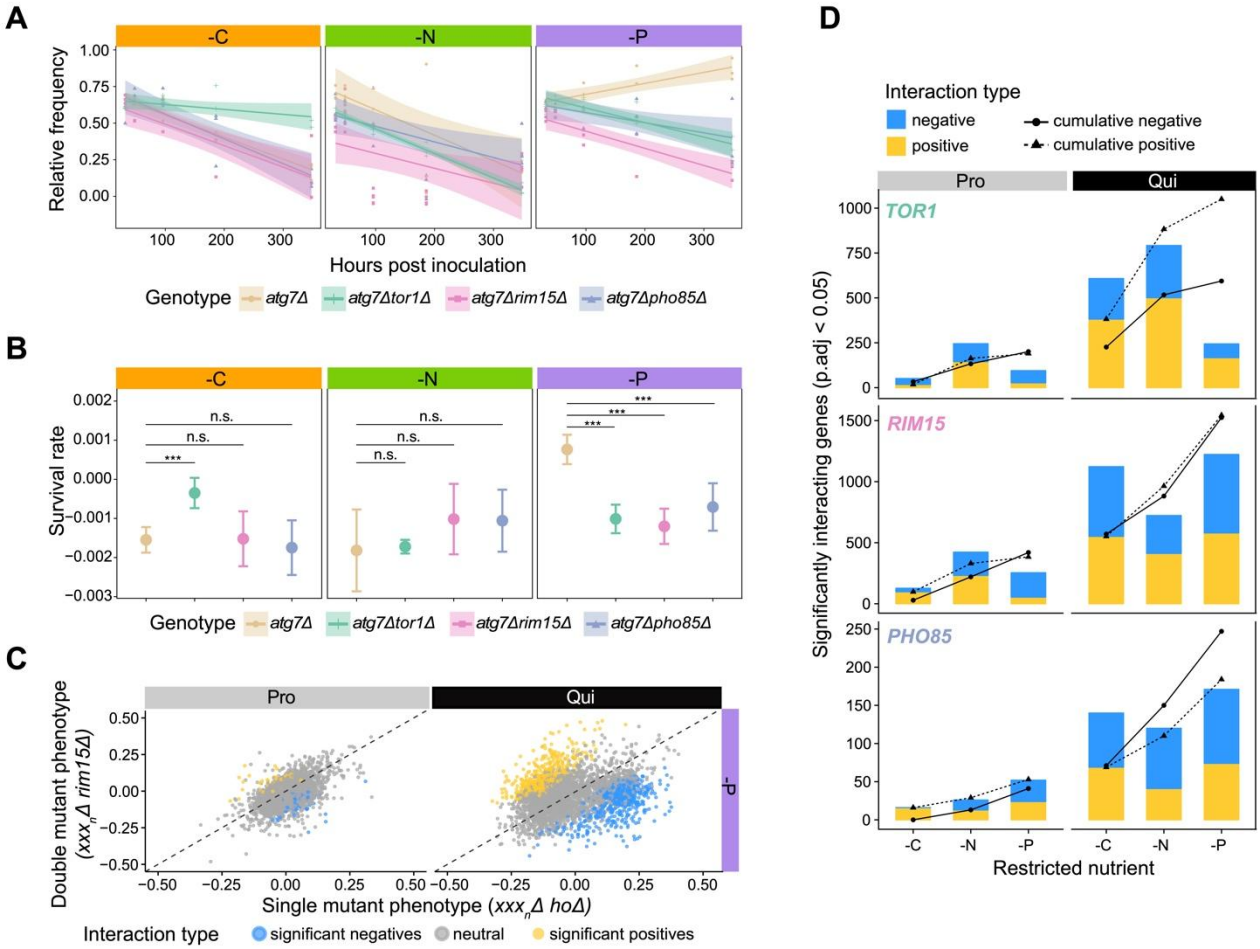

Figure 2.3. Identification of condition specific genetic interactions using pooled double mutant analysis.

A) Genetic interactions for each gene were determined for three different query genes (*TOR1*, *RIM15*, and *PHO85*) in three different conditions and two different cellular states: quiescence (shown) and proliferation (not shown) using pooled mutant time series analysis. **B)** Survival rate for each genotype indicated in A) and the statistical significance estimated using ANCOVA (*** p.adj<0.05). **C)** Relationship between single mutant phenotype (*xxx$_n$Δ::natMX*) and the corresponding phenotype of the mutant in the background of a *RIM15* deletion (*rim15Δ::KanMX xxx$_n$Δ::natMX*) in two different cellular states (Pro - proliferation, Qui - quiescence). The dashed line is the line of equality. Blue dots are genes that show a significant negative interaction with *RIM15* and yellow dots depict significant positive interactions. **D)** At a false discovery rate (FDR) of 5%, different numbers of significant genetic interactions are detected for three regulatory kinases in the three nutrient restrictions and two cellular states. Solid lines with circles indicate the cumulative total number of unique negative interactions and dashed lines with triangles indicate the cumulative total number of unique positive interactions.

2.3.7 Genetic interaction profiles of kinases differ between cellular states

Genes that are functionally related tend to share a common set of genetic interactions that define a genetic interaction profile (Michael Costanzo et al. 2010; M. Costanzo et al. 2016). As the activity of regulatory kinases depends on environmental signals, the functional consequences of deleting kinases is likely to be conditionally dependent, which may result in condition-dependent genetic interaction profiles. To identify the primary determinant of genetic interaction profiles in our study we quantified the similarity between all pairs of genetic interaction profiles for each kinase in each condition and cellular state. Clustering of genetic interaction profiles reveals a clear distinction between proliferative and quiescent cells (**Figure 2.S6A**).

In quiescent cells, genetic interaction profiles of the different kinases cluster as a function of the starvation signal (**Figure 2.S6A**). By contrast, in proliferative conditions *TOR1*, *RIM15*, and *PHO85* genetic interactions profiles do not exclusively cluster by nutritional condition (**Figure 2.S6A**). These results indicate that genetic interaction profiles differ as a function of cellular state and that the impact of the environmental conditions on genetic interactions is variable.

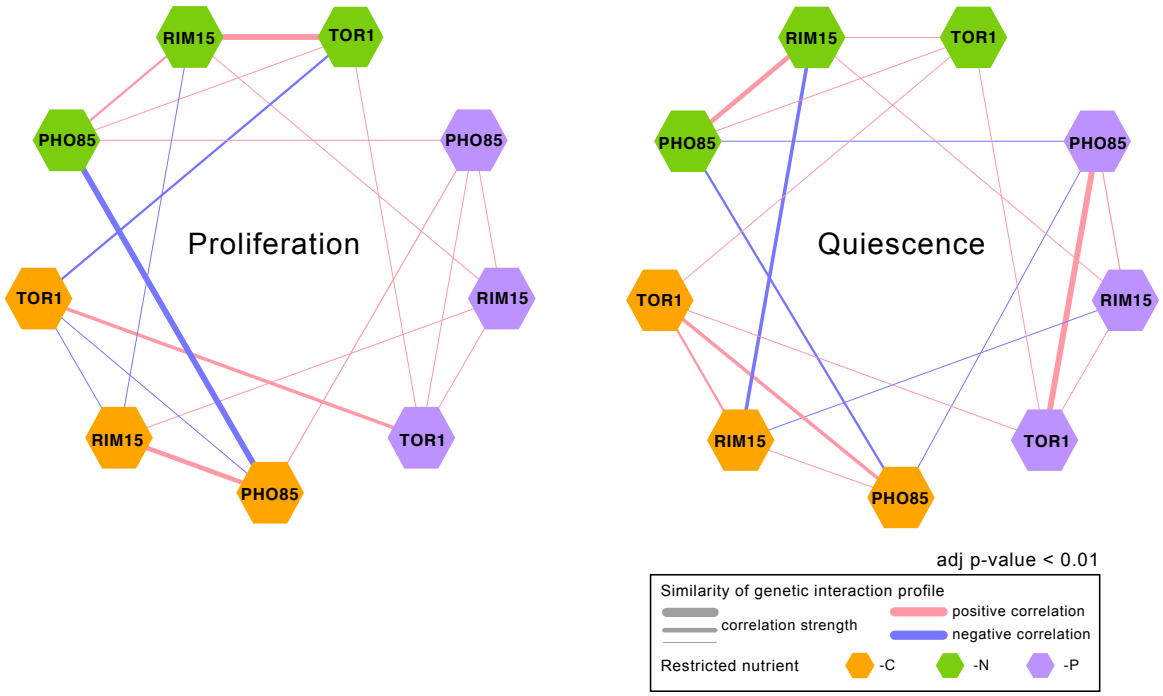

Figure 2.4 Genetic interaction profile similarities are condition dependent.

Correlation networks based on genetic interaction profiles for *TOR1*, *RIM15*, and *PHO85* in proliferating cells (Pro) and quiescent cells (Qui) in three different nutrient restricted media: carbon (-C), nitrogen (-N), and phosphorus (-P). Kinases with positive pearson correlation are connected with pink edges and kinases with negative pearson correlation scores are connected with blue edges. The thickness of the edge indicates the strength of the correlation (i.e. a larger absolute correlation is represented by thicker edge).

To visualize the correlation between genetic interaction profiles for each kinase in each condition, we constructed correlation networks for both proliferative and quiescent cells (**Figure 2.4**). These correlation networks emphasize the importance of cellular state in determining the similarity of genetic interaction profiles as the genetic interaction profile similarity network is drastically remodeled in quiescence (**Figure 2.4B**) compared to proliferation (**Figure 2.4A**). For example, a negative correlation is detected for *TOR1* and *PHO85* in proliferative cells growing in carbon-restricted condition, but their genetic

interaction profiles are positively correlated in carbon-starved quiescent cells (**Figure 2.4B & Figure 2.S6B**). For cells in the same physiological state, the environmental conditions can also alter the functional relationship between the same pair of kinases. For example, *RIM15* and *PHO85* genetic interaction profiles are highly correlated during growth in carbon-restricted media, but this similarity is greatly reduced during proliferation in phosphorus-restricted conditions (**Figure 2.4A & Figure 2.S6C**). These results suggest that environmental conditions alter the regulatory relationships among signaling pathways both in quiescent and proliferative cells.

2.3.8 Genetic interaction profiles are functionally coherent

To functionally annotate genetic interaction profiles for each kinase in each condition we used spatial analysis of functional enrichment (SAFE) (Baryshnikova 2016). We used SAFE to map quantitative attributes onto the reference network, defined by the correlation network of genome-wide genetic interaction profiles of 3,971 essential and non-essential genes (M. Costanzo et al. 2016), and test for functional enrichment within densely connected regions, which define domains . Each of the 17 domains within this map comprises genes that share similar genetic interaction profiles and functional annotations (**Figure 2.S6A**). Importantly, SAFE uses the entire set of genetic interactions for a given query gene, including those interactions that do not reach statistical significance, which allows identification of coherent trends that may exist despite a lack of significance associated with each individual genetic interaction. This analysis tests specifically for coherence in attributes such that strong positive and negative genetic interaction scores

that are randomly distributed throughout the network will produce no enrichment, whereas weak scores that tend to cluster as either positive or negative scores within domains will have significant enrichment. We superimposed genetic interaction profiles of each kinase in each of the three nutrient-restricted media and both cellular states onto the reference network using SAFE. We find that kinases that show higher similarity in genetic interaction profiles (**Figure 2.4**) also show more similar enrichment patterns using SAFE analysis (**Figure 2.5**). In general, genetic interactions in proliferative conditions tend to show increased enrichment when superimposed on this reference map indicating greater similarity among positive or negative interactions within each domain despite the relative paucity of significant interactions (**Figure 2.5 & Figure 2.S7B**). This difference may reflect the fact that genetic interactions in quiescent cells reflect novel regulatory relationships compared with those identified using fitness measurements in rich media that were used to construct the reference map.

The functional annotation of genetic interactions for each kinase differs as a function of the cellular state. For example, functional domains related to respiration, oxidative phosphorylation, mitochondrial targeting, transcription, and chromatin organization are enriched for negative genetic interactions with *TOR1* and *PHO85* in carbon restricted proliferative cells (**Figure 2.5**), but we find no evidence for enrichment of these functions in quiescent cells starved for carbon (**Figure 2.5**). Similarly, in nitrogen restricted conditions, *TOR1, RIM15* and *PHO85* share similar coherent functional interactions in proliferative cells, which are not observed in quiescent cells starved for nitrogen.

In addition, the functional enrichment of genetic interactions for each kinase differs between the three different nutrient restricted conditions. For example, ribosome biogenesis genes are enriched for negative interactions with *TOR1* in nitrogen restricted proliferative cells (**Figure 2.5**), but in phosphorus restricted proliferative cells ribosome biogenesis genes positively interact with *TOR1* (**Figure 2.S7B**). We find multiple additional cases of enrichment within functional domains, in which the sign of the genetic interactions is opposite between nitrogen and phosphorus restrictions in *TOR1* (**Figure 2.5 & Figure 2.S7B**), suggesting that *TOR1* may play different regulatory roles in responding to nitrogen and phosphorus restriction.

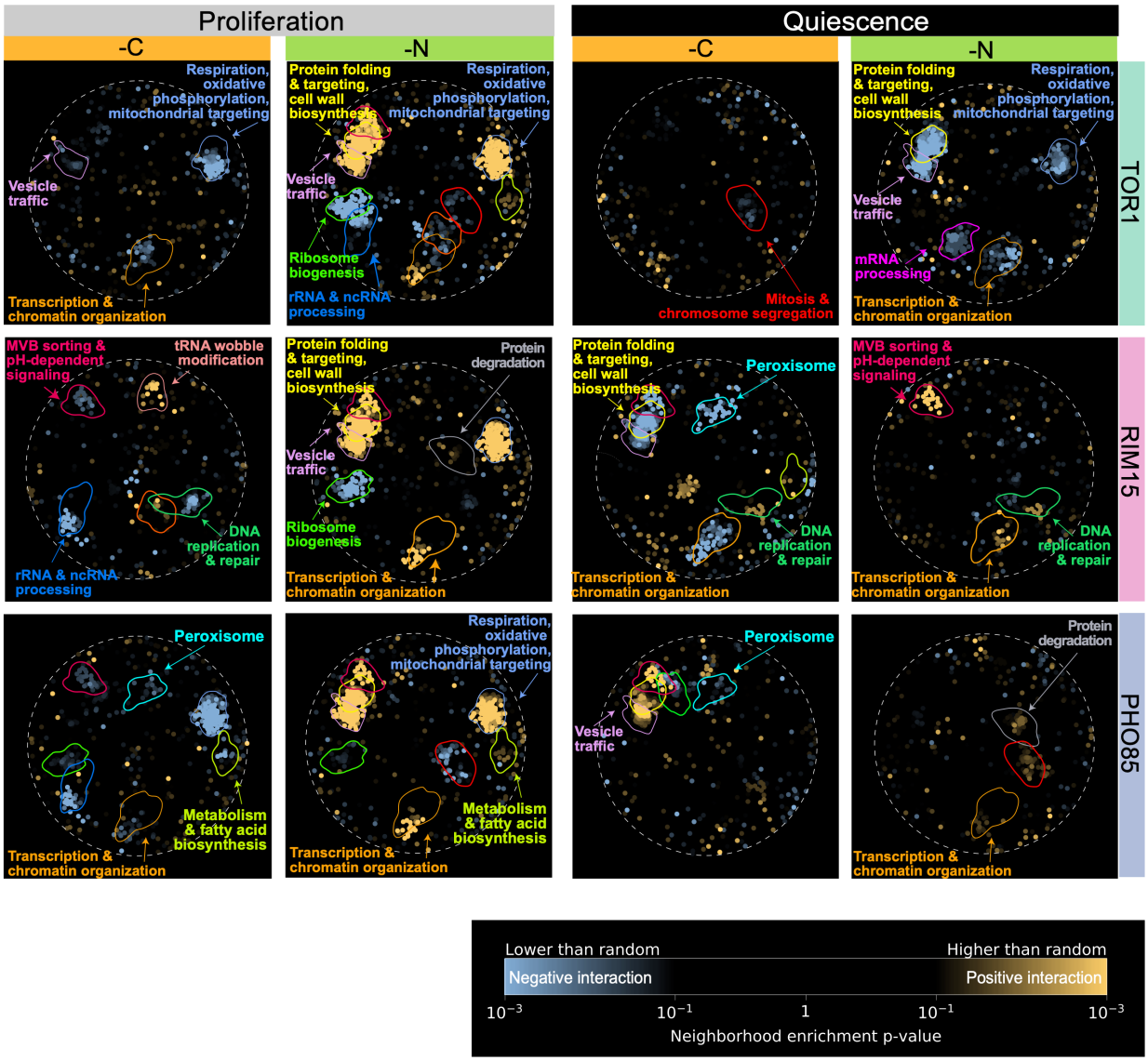

Figure 2.5. Functional mapping of kinase genetic interaction profiles in proliferating and quiescent cells.

Genetic interaction enrichment landscape of *TOR1, RIM15, PHO85* in proliferating and quiescent cells under different nutrient restrictions: carbon (-C), nitrogen (-N). Each dot represents one gene. Blue dots represent genes that have negative interactions with corresponding kinase (row-wise) in each condition (column-wise), and yellow dots represent genes with positive interactions.

We also found cases of functional enrichment that are maintained in the two different cellular states. For example, genes involved in peroxisome functions are enriched for negative interactions with *PHO85* in carbon restricted proliferative cells and carbon starved quiescent cells (**Figure 2.5**, cyan arrow/circle). This is consistent with the known role of *PHO85* in regulating long-chain based kinase during stationary phase (Iwaki et al. 2005) suggesting that *PHO85* may play a role in maintaining long-chain fatty acid recycling and provide energy for cells in calorie-restricted conditions.

2.3.9 Common and specific genetic interactions with RIM15 support its role as a central mediator of quiescence

RIM15 has previously been identified as an integrator of quiescence signals that is downstream of TOR1, PHO85 and PKA (Ivo Pedruzzi et al. 2003; Wanke et al. 2005; Olivares-Marin et al. 2018). Therefore, we expect that the genetic interaction profiles for *RIM15* should show more functional coherence in response to different quiescence signals compared to *TOR1* and *PHO85*, which are upstream of *RIM15*. Using SAFE analysis, we find that *RIM15* consistently interacts with genes functioning in multivesicular bodies (MVB) sorting and pH-dependent signaling under all starvation conditions in both cell types (**Figure 2.5**). This suggests that *RIM15* plays an essential role in regulating protein homeostasis via MVB sorting. As the reference genetic interaction map used for SAFE does not include all genes in our genetic interaction dataset (only ~2,900 non-essential genes are present in the reference) and tests only for coherence of both statistically significant and non-significant interactions, we performed over-representation analysis on the sets of genes that significantly interact with each kinase (**Methods and**

materials). Due to the limited number of significant interactions detected in proliferative cells (**Figure 2.3D**), we did not find any enriched GO terms for kinases in proliferative cells. However, we identified multiple significantly enriched functional categories in quiescent cells. As with SAFE analysis, the functional enrichment of the significant interacting genes for a given kinase depends on the starvation signal (**Figure 2.6A & Figure 2.S8A**).

Consistent with its role*, RIM15* genetic interactions show more common functional enrichments in response to different starvation signals in comparison with *TOR1* and *PHO85*. Three functional groups are shared among genes interacting with *RIM15* in response to carbon/nitrogen or nitrogen/phosphorus starvations (**Figure 2.6A,** lower panel) whereas there is limited, or no functional overlap detected for *TOR1* or *PHO85* genetic interaction profiles under the same conditions (**Figure 2.S8A**). This is consistent with a model in which *RIM15* regulates quiescence through integration of diverse signals and execution of similar regulatory interactions. In quiescent cells, *RIM15* shows consistent negative genetic interactions with genes involved in vacuolar functions regardless of the starvation signals perhaps reflecting a role for *RIM15* in regulating autophagy and protein recycling in response to different starvations.

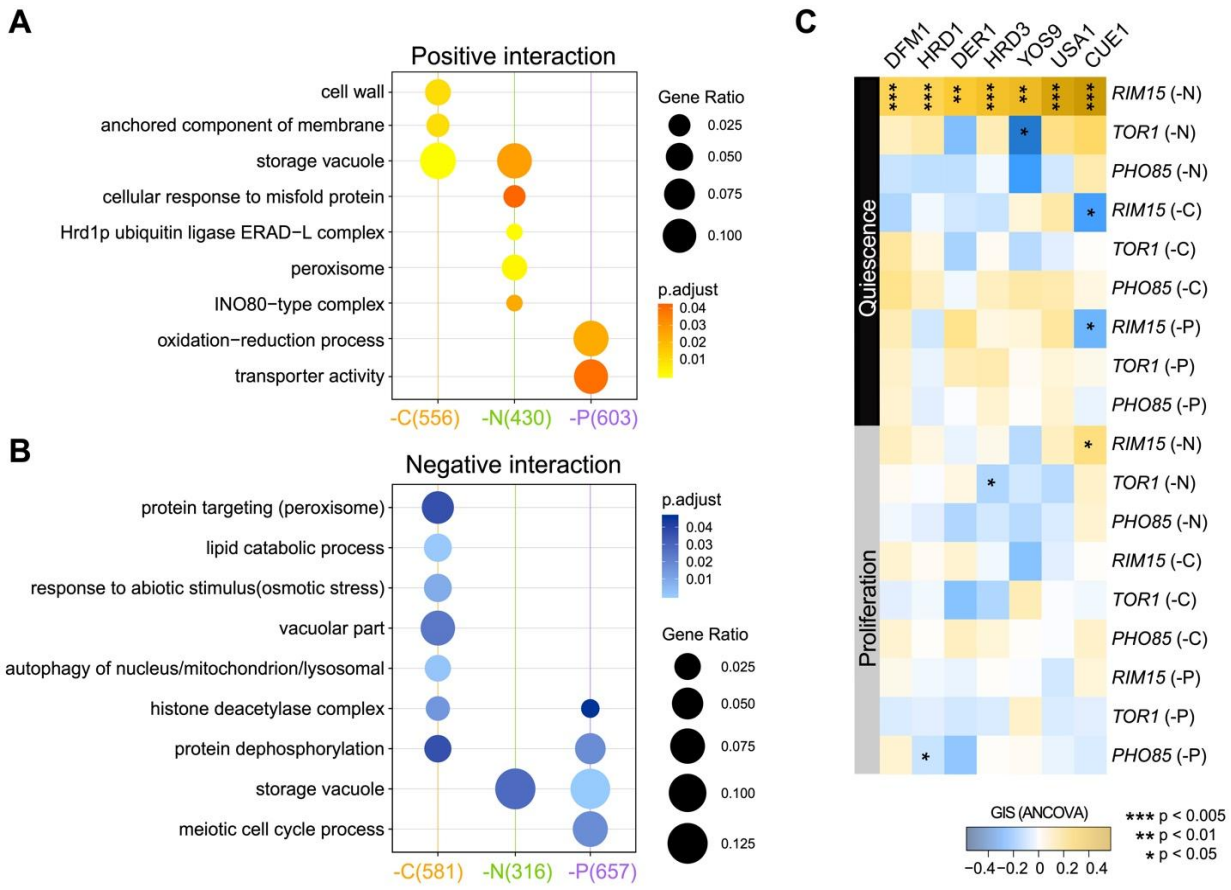

Figure 2.6. *RIM15* genetic interactions profiles indicate it is an integrator of quiescence signals with nutrient-specific functions.

A) GO term enrichment analysis for genes that significantly interact with *RIM15* in all nutrient starvation conditions. Only significantly enriched GO terms are shown (p.adj < 0.05). (yellow - positive interaction, blue - negative interaction). **B)** Genetic interaction profile of the genes encoding the ERAD-L complex. ERAD-L genes show a unique cohesive set of positive genetic interactions with *RIM15* in nitrogen starvation-induced quiescent cells. Each column is the genetic interaction score between ERAD-L genes and *RIM15* quantified using ANCOVA, and each row is the genetic interaction score between ERAD-L genes and each of the other kinases in each nutrient restricted condition.

Interestingly, we find that genes that function in the Endoplasmic-reticulum-associated protein degradation, luminal domain monitored (ERAD-L) pathway show coherent positive interactions with *RIM15* specifically in nitrogen-starved quiescent cells

(**Figure 2.6A**). This includes each of the genes that is known to function in ERAD-L: *USA1, YOS9, DFM1, HRD1, HRD3, CUE1, and DER1* (**Figure 2.6B** and **Figure 2.S8B**). ERAD-L genes present in the genetic interaction reference data used for SAFE analysis; *HRD1, HRD3, CUE1, and USA1* are found in the domain enriched for ubiquitin-dependent protein catabolic process (**Figure 2.S8C,** red arrow). Those results point to a specific function for *RIM15* in proteostasis regulation in response to nitrogen starvation.

2.4 Discussion

Cellular quiescence is the predominant state of eukaryotic cells. To study the genetic requirements of cellular quiescence in yeast cells we quantified the effect of each gene deletion in response to three distinct nutrient starvation signals (carbon, nitrogen, phosphorus). To study how these signals are coordinated within quiescent cells we quantified genetic interactions with three regulatory kinases in each of the three starvation conditions. To undertake this study, we quantified phenotypic differences in different cellular states (proliferation versus quiescence) and genotypes (single versus double mutational background) using multiplexed barcoded analysis to track thousands of different genotypes using time course analysis. By testing the contribution of ~4,000 yeast non-essential genes to fitness in proliferating cells and survival in quiescent cells in three different nutrient-restricted conditions we find no evidence for genes that are commonly required for quiescence. We extended our method for multiplexed analysis of genotypes to study ~14,400 double mutants encompassing three core kinase genes: *TOR1*, *RIM15* and *PHO85*, which allowed us for the first time to test genome-wide for genetic

interactions with regulatory kinases that mediate quiescence.

2.4.1 Distinct gene functions are required for quiescence in response to different nutrient starvation signals

The functional requirements for maintaining and exiting quiescence differ depending on starvation signals. Time course analysis of fitness during proliferation and survival during starvation support previous findings that yeast cells have distinct functional requirements for maintaining viability of quiescent cells in response to different nutritional starvations (Klosinska et al. 2011). In addition, our results show that a substantial fraction of the non-essential yeast genome is required for survival during quiescence independent of their requirements for growth. For example, in carbon-restricted conditions, deletion of 713 (~15%) of the non-essential genes results in a significant defect in quiescence (**Figure 2.2C**). Clearly, the definition of an "essential gene" is dependent on the condition in which essentiality is assessed.

Across all starvation conditions, we found that only 8 genes are commonly required for quiescence, a result that is not significantly different from chance (**Figure 2.S2D**). The absence of a common set of genetic requirements for quiescence in response to different natural nutrient starvation signals is consistent with earlier work (Klosinska et al. 2011). Although there appears to be no common set of genetic requirements for quiescence, different nutrient starvations do share some genetic requirements. Nitrogen- and phosphorus- starved quiescent cells tend to have more overlapping features compared to carbon-starvation induced quiescence: 81 genes are required for maintaining

quiescence in response to both nitrogen and phosphorus starvation, whereas only 57 genes are commonly required for quiescence in nitrogen and carbon starvation (**Figure 2.2C**). Results from functional enrichment analysis are consistent with the trend of greater overlap in genetic requirements in nitrogen and phosphorus starvation. For example, genes involved in protein localization by CVT pathway are required in response to nitrogen or phosphorus starvation. The patterns of functional overlap in genetic interactions in response to nitrogen, phosphorus, and carbon starvation may reflect their different primary biological uses: carbon is the major energy source, whereas both nitrogen and phosphorus are primarily utilized for macromolecular synthesis (de Virgilio 2012; Broach 2012)(Alberts et al. 2013; Wilson and Roach 2002); (de Virgilio 2012; Broach 2012); (Alberts et al. 2013; Wilson and Roach 2002).

2.4.2 Expanding phenotypic space to identify novel genetic interactions

To date, genome-wide genetic interaction mapping in yeast has primarily been assayed using a single phenotype in a single condition - colony growth in rich media. Our genome-wide genetic interaction mapping in different conditions and cellular states indicates that: 1) genetic interactions with regulatory kinases vary between conditions; 2) genome-wide genetic interaction mapping is extensible to additional phenotypes and analyzing condition-specific phenotypes may increase the sensitivity for identifying novel regulatory relationships; 3) less favorable conditions result in an increased number of significant interactions; and 4) for a given physiological state (e.g. proliferation or quiescence), increasing the number of environmental conditions results in an increase in the number

of significant genetic interactions. The points are consistent with, and extend, the limited number of studies that have investigated genetic interactions in different growth and stress conditions (Gutin et al. 2015; Martin et al. 2015; St Onge et al. 2007). Despite the fact that our genetic interaction data set is limited in its scale and is focused on regulatory kinase genes, we anticipate that our methodology can be broadly applied to define genetic interactions in different conditions and cellular states.

2.4.3 Novel function of RIM15 in autophagy and ERAD-L

Endoplasmic-reticulum-associated protein degradation (ERAD) is a quality control mechanism that ensures only properly folded proteins leave the ER. Autophagy has been proposed to be a backup mechanism for ERAD. Previous studies have shown that *RIM15* plays a role in regulating autophagy and protein homeostasis (Waliullah et al. 2017; Huang et al. 2018). In our study we find that genes that function in ERAD show coherent positive interactions with *RIM15* in nitrogen starvation conditions, suggesting that *RIM15* regulation of ERAD activity in response to nitrogen starvation is essential for quiescence. It is possible that *RIM15* functions to regulate clearance of stress-induced misfolded proteins during nitrogen starvation by mediating the balance between autophagy and ERAD.

2.4.4 Implications for quantitative genetics

Our study has important implications for our understanding of the genotype to phenotype map. The prevailing result from our study is that the effect of a given gene deletion on a

phenotype (either fitness or survival) is highly dependent on the specific environmental conditions of the cell. Although nitrogen, carbon and phosphorus starvation all lead to cell cycle arrest and the initiation of quiescence, the genetic requirements for this behavior are distinct. We find that the conditional dependence extends to genetic interactions as we detect different sets of genetic interactions in different growth and starvation conditions. These results are consistent with our previous study of natural genetic variation in which we found that the effect sizes of QTL underlying fitness differences, and genetic interactions between QTL, are acutely sensitive to the composition of the growth media (Ziv et al. 2017). Identifying quantitative genetic effects and interactions that are insensitive to environmental variation appears challenging and may, in fact, be extremely rare.

2.4.5 Implications for the study of cellular quiescence in yeast

It has been argued that starvation for glucose is the relevant condition for studying quiescence (Sagot and Laporte 2019) and indeed the vast majority of quiescence studies are performed in conditions in which carbon starvation is the pro-quiescence signal (Laporte et al. 2011; Laporte, Gouleme, et al. 2018). However, it has been appreciated for many decades that yeast cells can initiate a quiescent state in response to different starvation signals (Lillie and Pringle 1980). Our study reiterates the importance of studying quiescence in response to different nutrient starvation conditions. Many important biological processes are likely to be missed - autophagy being a preeminent example - if carbon starvation is the only condition studied (Kawamata et al. 2017).

Organisms in the natural world experience a range of nutrient limitations and nitrogen and phosphorus appears to be the predominant limiting nutrients in most ecologies (Elser et al. 2007). Thus, a complete understanding of cellular quiescence requires the study of different nutrient starvation signals.

2.4.6 Relevance to aging and cancer

The study of cellular quiescence may inform our understanding of cellular aging and provide insight into the therapeutic challenge of dormant cancer cells. Our study supports previous findings that quiescence establishment does not follow the same route depending on the nature of the inducing signal (H. A. Coller, Sang, and Roberts 2006; Klosinska et al. 2011). In addition, different 'degrees' of quiescence may exist (H. A. Coller, Sang, and Roberts 2006; Gookin et al. 2017; Laporte, Gouleme, et al. 2018) as we find that cells maintained longer in quiescence need more time to return to growth. Thus, quiescence may be viewed as a continuum that ultimately leads to senescence (even if that may take thousands of years) unless conditions favorable for proliferation are met.

Overall, our data highlights the fact that quiescence does not imply uniformity (O'Farrell 2011). The idea that quiescence establishment is the result of a universal program is clearly an over-simplification. Our study points to a rich spectrum of condition-specific genetic interactions that underlie cellular fitness and survival across a diversity of conditions and introduces a generalizable framework for extending genome-wide genetic interaction mapping to diverse conditions and phenotypes. Deciphering the underlying regulatory rationale and the hierarchical relationships between these signaling pathways

in different conditions is critical for understanding cellular quiescence.

2.5 Methods and materials

Table 2.2. Reagents and Tools Table

Reagent/Resource	Reference or Source	Identifier or Catalog Number
Chemicals, enzymes and other reagents		
SYBRGreen	invitrogen	Cat # S7563
LIVE/DEAD™ FungaLight™ Yeast Viability Kit, for flow cytometry	invitrogen	Cat # L34952
Software		
Cytoscape v3.7.1	http://www.cytoscape.org	NA
metScape 3 Correlation Calculator v1.0.1	http://metscape.ncibi.org/calculator.html	NA
Revigo	http://revigo.irb.hr/	NA
Other		
Kits, instrumentation, laboratory equipment		
Illumina NexSeq 500	Illumina	NA
PureLink™ Pro 96 Genomic DNA Purification Kit	invitrogen	K182104A
Tecan Freedom Evo and Infinite Microplate Reader	Tecan	NA

Culter counter	Backman Culter	NA
Flow cytometry	BD Accuri^{TM} C6	NA
QIAquick PCR purification columns	QIAGEN	28104
Chemostats (Bioreactor)		NA

2.5.1 SGA Library construction

The haploid prototrophic double deletion collections were constructed using the synthetic genetic array method (Tong et al, 2001). The genotype and ploidy of double mutants are prototrophic haploid (**Figure 2.S1B**). For the single deletion collection (array mutants), gene deletion alleles are marked with the kanMX4 cassette conferring G418 resistance, which is flanked by two unique molecular barcodes (the UPTAG and DNTAG). For double deletion collection, an additional query allele is marked with NatR cassette conferring nourseothricin resistance. To construct the *RIM15* and *TOR1* SGA query strains we mated a MATa *xxx$_n$Δ0*::NATr strain (transformed from FY4 with a NATr PCR product targeting the xxx$_n$ allele) with the Y7092 strain. A haploid prototrophic strain was identified following tetrad dissection and genotyping using selective media with G418 and nourseothricin. To construct the *HO*, and *PHO85* SGA query strains we transformed a prototrophic strain containing the SGA marker with a NATr PCR product targeting the *xxx* allele. Insertion of NATr was confirmed via PCR and the genotype of the strain was checked via replica plating onto selective media resulting in strains listed in **Table 2.1**.

2.5.2 Growth conditions

After the growth of individual selected mutants on YPD agar plates, all mutants were pooled to a final density around 1.7 × 10^9 cells/ml. Each agar plate contained single colonies of individual genotypes and replicated colonies of the control *hoΔ* strain. We inoculated 1.5 × 10^8 cells into 300ml of nutrient limited medium: for glucose- (C, 4.4mM carbon), ammonia- (N, 0.8mM nitrogen), and phosphorus- (P, 0.04mM phosphorus) at 300ml. To define the fitness of ~ 4,000 mutants within each nutrient limiting conditions and growing stage, we performed three independent experiments for each mutant per nutrient limiting conditions. In total, we had 4 mutant collections × 3 biological replicates × 3 nutrient limiting conditions in bioreactors used to maintain the temperature at 30 degrees and pH at 5. To model the fitness of each genotype at different states spanning both proliferative and quiescence stages, we collected five time points in each stage (based on growth curve **Figure 2.S1C**). The duration of the experiment was 15~16 days, and populations were sampled at 0, 9, 14, 18, 24, 32, 48, 96, 187, 368 hours for outgrowth and barcode sequencing. To isolate viable cells from the stationary phase culture, we transferred 1mL (i.e., 1 × 10^6 cells) from the pooled library at each time point into 5 mL minimal cultures. Cells were grown for 24~32 hr to a final density of 3 × 10^8 cells/mL in all conditions. Cells were then washed with water once, and then resuspended in 1mL sorbitol buffer for genomic DNA purification.

2.5.3 Viability quantification using propidium iodide & SYTO® 9

For viability quantification at each time point, 1 × 10^7 cells were collected and

subsequently washed once with sterilized DI water and one more time with PBS. The washed cell pellet was resuspended with 1mL 1 x PBS and stained with 3.34μM of SYTO® 9 and 20μM of propidium iodide for 20 minutes. The stained samples were then analyzed by flow cytometry (BD Accuri™ C6).

2.5.4 DNA extraction and library preparation for Bar-seq

Genomic DNA was isolated from 1 × 10^8 cells for each sample (3 nutrient-restricted × 3 biological replicates × 4 deletion collections × 10 times points) using invitrogen PureLink™ Pro 96 Genomic DNA Purification Kit. We adapted the two-step PCR protocol for efficient multiplexing of Bar-seq libraries (Robinson et al, 2013). Briefly, UPTAGs and DNTAGs were amplified separately from the same genomic DNA template. In the first PCR step, unique sample indices are added to each sample. For each biological replicate, we used 120 unique sample indices that differed by at least two nucleotides to label each sample from 3 nutrient limiting conditions × 4 deletion collections × 10 timepoints. We normalized genomic DNA concentrations to 10 ng/ml and used 100 ng template amplified barcodes using the following PCR program: 2 min at 98°C followed by 20 cycles of 10 sec at 98°C, 10 sec at 50°C,10 sec at 72°C, and a final extension step of 2 min at 72°C. PCR products were confirmed on 2% agarose gels and quantified the concentration using a SYBRGreen staining followed by Tecan Freedom Evo and Infinite Microplate Reader. We combined 35 ng from each of the 120 different UPTAG libraries and, in a separate tube, 35 ng from each of the 120 different DNTAG libraries for each condition/deletion collection. The multiplexed UPTAG libraries were then amplified using the primers P5

(59-A ATG ATA CGG CGA CCA CCG AGA TCT ACA CTC TTT CCC TAC ACG ACG CTC TTC CGA TCT-39) and Illumina_UPkanMX, and the combined DNTAG libraries were amplified using the P5 and Illumina_DNkanMX primers using the identical PCR program as the first step with 75 ng template. The 140-bp UPTAG and DNTAG libraries were purified using QIAquick PCR purification columns, quantified using a Qubit fluorometer for qPCR quantification, combined in equimolar amounts after qPCR, and adjusted to a final concentration of 4 nM mixture of pooled UPTAG and DNTAG. In total, each sequencing library contained 120 UPTAG and 120 DNTAG libraries from 120 different samples. The library was sequenced on a single lane of an Illumina NextSeq 500 with HighOutput 1 x 75bp read configuration. 20% PhiX was spiked into each library for increasing the complexity of two-color base calling on the Illumina NextSeq500 platform.

2.5.5 Data analysis, filtering and normalization

Sequence reads were matched to the yeast deletion collection barcodes using re-annotated by Smith *et al*. (2009). Inexact matching was performed by identifying barcode sequences that were within a Levenshtein distance of 2 from each read (Levenshtein 1966). Sample indices were similarly matched using a maximum Levenshtein distance of 1. 52 libraries with total read depth less than 1×10^5 reads were removed from the 720 libraries. We merged the UPtag and DOWNtag counts representing the same gene within each condition resulting in 311 libraries in total. A set of outliers was identified that had fewer than 3,000 total reads across all 311 samples. These low-count matches (=< 4)

were likely due to sequencing errors and were removed. 1,996 mutants were removed with a coverage less than 3,000 or missing in either tag counts. After filtering, a matrix containing 3,931 mutants consistent with high quality counts data across 311 conditions was generated corresponding to 692,755,604 sequence reads. This counts table was normalized using the function varianceStabilizingTransformation in the DESeq2 package (Love et al, 2014) (version 1.8.1) with arguments blind = FALSE and fitType = “local”.

2.5.6 Fitness, survival, and phenotypic difference quantification

The normalized frequency of each mutant within each library were used for linear regression modeling. For example, in *HO* library, the count for each mutant (*ho::kanMX xxx$_n$::natMX*) is normalized by the count for the wild type control (*hoΔ::kanMX his3Δ1 can1Δ::STE2pr-Sp_his5)* at corresponding time points. In the other double mutant libraries, the counts for each double mutant (*query::kanMX xxx$_n$::natMX*) is normalized by the counts of the query mutant (*queryΔ::kanMX his3Δ1 can1Δ::STE2pr-Sp_his5)* at corresponding time points. For each mutant strain N, fitness f_n was calculated as the coefficients of linear regression model using R:

$$lm(\frac{F^n}{F^{wt}} \sim T),$$

therefore,

$$f_n = \frac{\frac{F^n}{F^{wt}} - \delta}{T}$$

with F^n being the normalized counts of strain N at each time point and F^{wt} is the normalized count of query mutant strain at each time point. T refers to timepoints, which was measured in days for quantifying the fitness in prolonged starvation. δ is the error term.

In order to compare the phenotypic difference for a given mutants between different cellular states, before linear regression modeling at different cellular states, we scaled the independent variable, time (hours) for each stage into the same unit but maintaining the natural interval using $scale()$ function in R with $center = FALSE$. For example, the time point (independent variable) in proliferative stage were scaled from 0h, 9h, 14h, 18h, 24h into 0, 0.5246676, 0.8161497, 1.0493353, 1.3991137, and the time point for sample collected during quiescence were scaled from 32h, 48h, 96h, 187h, 368h into 0.1553874, 0.2330811, 0.4661622, 0.9031894, 1.6995499. Then, we quantified the phenotypic difference between fitness in proliferation and survival in quiescence using ANCOVA:

$$lm(\frac{F^n}{F^{wt}} \sim T * GS)$$

where T is the scaled time and GS is the Growing Stage (e.g. proliferation or quiescence). The different growth stages in this function is the interaction term, which was used to test for statistical significance.

After quantifying the fitness difference between quiescence and proliferation for a

given mutant, we ranked the mutants by fitness difference in a descending order and then applied gene set enrichment analysis (GSEA) using clusterprofiler (Guangchuang Yu et al. 2012).

To understand whether the common genes that required in response to different quiescent signals are statistically significant or not, we implemented the multi-set intersection test algorithm in an R software package $SuperExactTest$ (M. Wang, Zhao, and Zhang 2015). This framework is used to compute the statistical distributions of multi-set intersections based upon combinatorial theory and accordingly designed a procedure to calculate the exact probability of multi-set intersections. The inputs for $SuperExactTest$ include three lists of genes that are essential in quiescence. The three lists correspond to three conditions (-carbon, -nitrogen, -phosphorus) and the size of the background population from which the sets are sampled is 5,000.

2.5.7 Comparison of SGA genetic interaction quantification with ANCOVA

2.5.7.1 SGA genetic interactions scoring method

We first computed genetic interactions using a method analogous to estimation of epsilon (ε) as defined in classical SGA screens from the Boone lab. The SGA-like score was quantified by testing the null hypothesis based on a multiplicative model from single mutant fitness:

$\varepsilon = f_{aq} - f_a * f_q$ (a - array mutant; q - query mutant)

In our case, ε is calculated as the difference between the coefficients of linear modeling:

where

f_{aq} is the coefficients generated by $lm\ (\frac{F^{aq}}{Fq}\ \sim\ T)$,

f_a is the coefficients generated by $lm\ (\frac{F^{a}}{F^{wt}}\ \sim\ T)$,

f_q is the coefficients generated by $lm\ (\frac{F^{q}}{F^{wt}}\ \sim\ T)$,

Therefore, f_{aq}, f_a, f_q should be normally distributed around 0 with positive (better than WT) and negative (worse than WT) fitness. To estimate the expected fitness in double mutant based on multiplicative model, we take the $exp()$ of the coefficients for each model to eliminate the discordance of the signs in fitness. Then we calculated the expected fitness using multiplicative model:

$$f_{aq}^{exp} = exp\ (f_q)\ \times exp\ (f_a)$$

Therefore

$$\varepsilon = exp\ (f_{aq})\ - f_{aq}^{exp}$$

The standard error S_a & S_q are the standard error of each linear model. The standard error in expected fitness is calculated by propagating standard error from each individual model:

$$S_{a+q}^2 = S_a^2 + S_q^2$$

Then, the statistical significance between expected (multiplicative model) and observed model was calculated by *Welch's t-test*:

$$t = \frac{f_{aq} - f_{a+q}}{\sqrt{\frac{S_{aq}^2}{N_{aq}} + \frac{S_{a+q}^2}{N_{a+q}}}}$$

where the degrees of freedom associated with this variance estimate is approximated using the Welch-Satterthwaite equation:

$$\upsilon \approx \frac{\left(\frac{s_{aq}^2}{N_{aq}} + \frac{s_{a+q}^2}{N_{a+q}}\right)^2}{\frac{s_{aq}^4}{{N_{aq}}^2 \ (N_{aq} - 1)} + \frac{s_{a+q}^4}{{N_{a+q}}^2 \ (N_{a+q} - 1)}}$$

2.5.7.2 Genetic interactions quantification by ANCOVA

All libraries were normalized by the common query deletion. Therefore, our GIS can be calculated by looking at the difference between normalized fitness/survival without worrying about the query mutant phenotype,

$$GIS = f_{aq} - f_a,$$

Where

$$f_{aq} = lm(\frac{F^{aq}}{F^{q}} \sim T) \quad \& \quad f_{a} = lm(\frac{F^{a}}{F^{wt}} \sim T) \quad ,$$

In this case, the genetic interaction is calculated directly by testing whether the query mutation significantly changes the relationship between time and relative fitness for a given mutant. We applied ANCOVA using:

$$lm\,(\frac{F^{n}}{F^{wt}} \sim T * GT)$$

where T is the scaled time and GT is the GenoType (e.g. $\frac{F^{aq}}{F^{q}}$ or $\frac{F^{a}}{F^{wt}}$). The significance of the interaction term was determined using a standard *t test*.

2.5.8 Functional annotation and network construction

Gene Set Enrichment Analysis (GSEA) was applied on the ranked gene list based on phenotypic difference using clusterProfiler (Guangchuang Yu et al. 2012). The GO overrepresentation test was applied to significantly interacting genes and quiescent specific gene lists. The correlation among genetic interaction profiles were calculated by metScape 3 Correlation Calculator v1.0.1 using the DSPC method and then visualized in Cytoscape 3.7.1.

2.5.9 Spatial Analysis of Functional Enrichment (SAFE)

The systematic functional annotation and visualization of interaction profile for all kinases under different conditions and cellular states was applied without any filtering on the interaction list. In this enrichment analysis we used all genes without filtering based on statistical interaction significance (from ANCOVA). This is because isolated false positives are scattered throughout the entire network, which do not typically result in significant enrichment anywhere in the network. Meanwhile, weak but consistent effects, e.g. genes having weaker or less significant GIs but clustering together in the network are very interesting. The visualization and local enrichment annotation was performed using SAFE (Baryshnikova 2016).

2.6 Supplementary figures

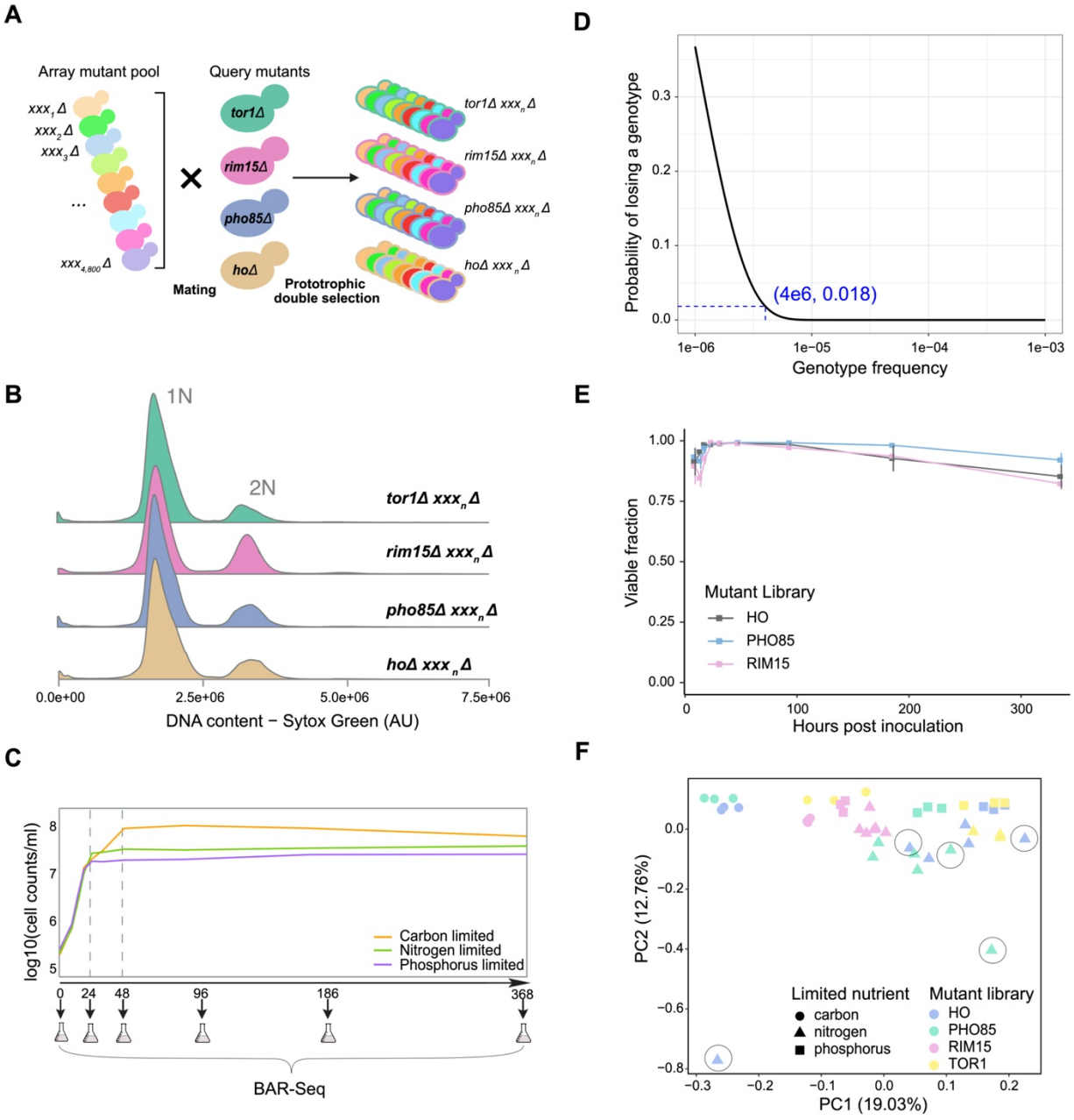

Figure 2.S1. Ploidy confirmation, growth tracking, data cleaning.

A) Ploidy confirmation for double mutant libraries assayed using Sytox Green staining. **B)** Bar-seq data pre-processing pipeline for each library/sample. **C)** Growth curve of 12 mutant libraries, 4 different mutant libraries (HO, RIM15, TOR1, PHO85) x 3 replicates, in different

media (orange - carbon restriction, green - nitrogen restriction, purple - phosphorus restriction). **D)** Population viability for mutant library HO, PHO85, and RIM15. Viable fraction was quantified by PI/Syto9 staining followed by flow cytometry. **E)** PCA analysis for identifying poorly correlated replicates. Circle libraries have been removed for later analysis. **F)** Probability of missing a genotype with given frequency. The probability is estimated based on binomial distribution.

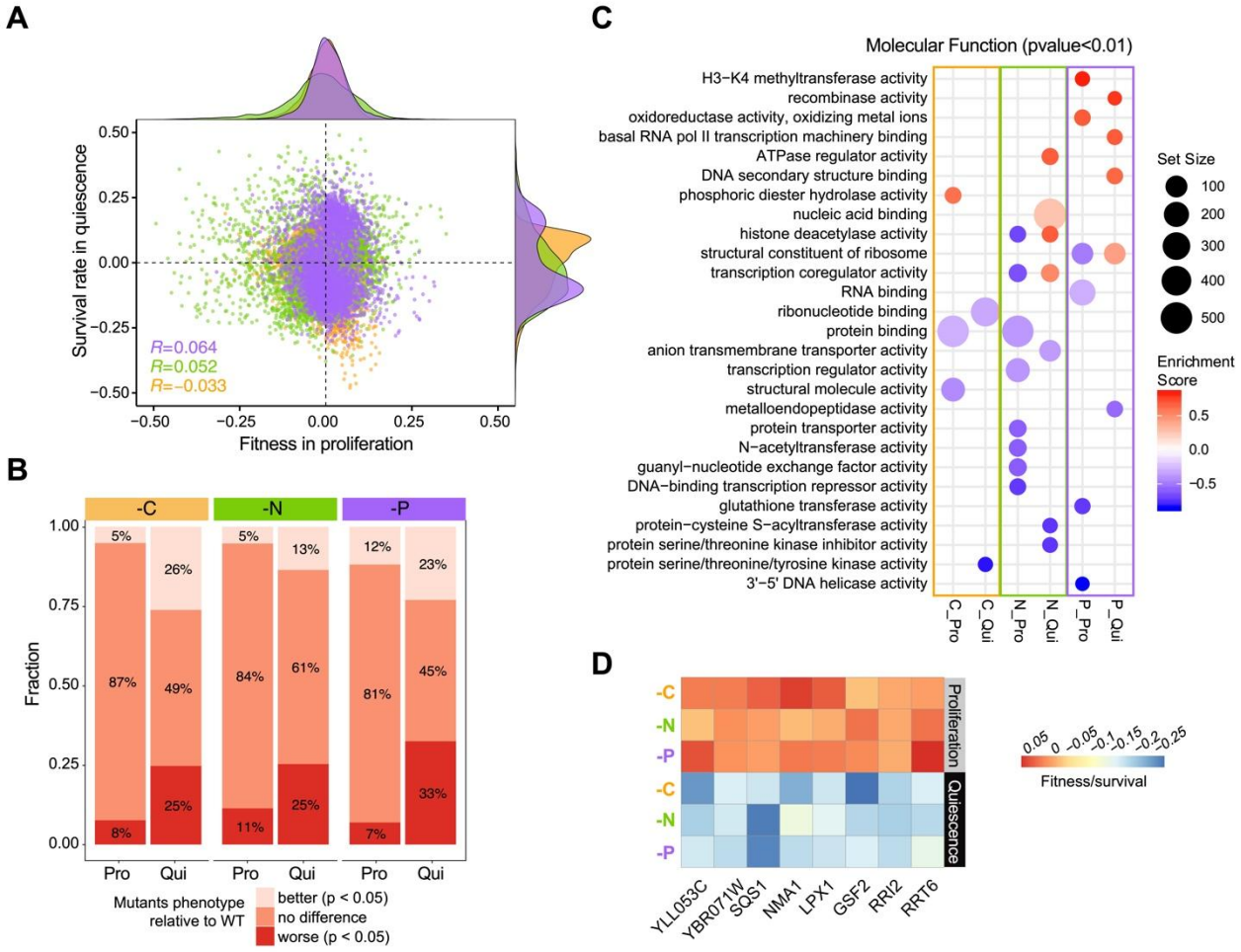

Figure 2.S2. Correlation between single mutant (*HO*) fitness in proliferation and survival in quiescence.

A) The distributions of fitness and survival for thousands of mutants in different conditions are shown on the top (fitness) and right (survival). Pearson correlation score is labeled on the bottom left of the plot with p-value < 0.05. All scatter plots, frequency plots and labels are colored based on media types. **B)** The proportion of mutants with different fitness and survival compared to wild type in proliferation and quiescence across three nutrient restrictions. Proportions were calculated based on the statistics summarized from linear regression

modeling. Better than wild type - regression coefficients of those mutants are larger than 0 (p.adj < 0.05); no difference compared to wild type are the mutants with corrected p.adj > 0.05; worse than wild type are the mutants whose regression coefficient is less than 0 (p.adj < 0.05). **C)** GO terms identified using Gene Set Enrichment Analysis (GSEA). GSEA was applied to a ranked gene list based on the fitness for proliferative cells and survival for quiescent cells estimated by linear regression modeling. The false discovery rate (FDR) was set at 0.05. Positive enrichment scores (red) indicate functions that have increased fitness or survival relative to WT control. Negative enrichment scores (blue) indicate functions that when impaired result in decreased fitness or survival. Set size indicates the gene number in each enriched term. **D)** The 8 genes defined in **Figure 2.2C** and their corresponding phenotypic readout in different conditions and cellular states.

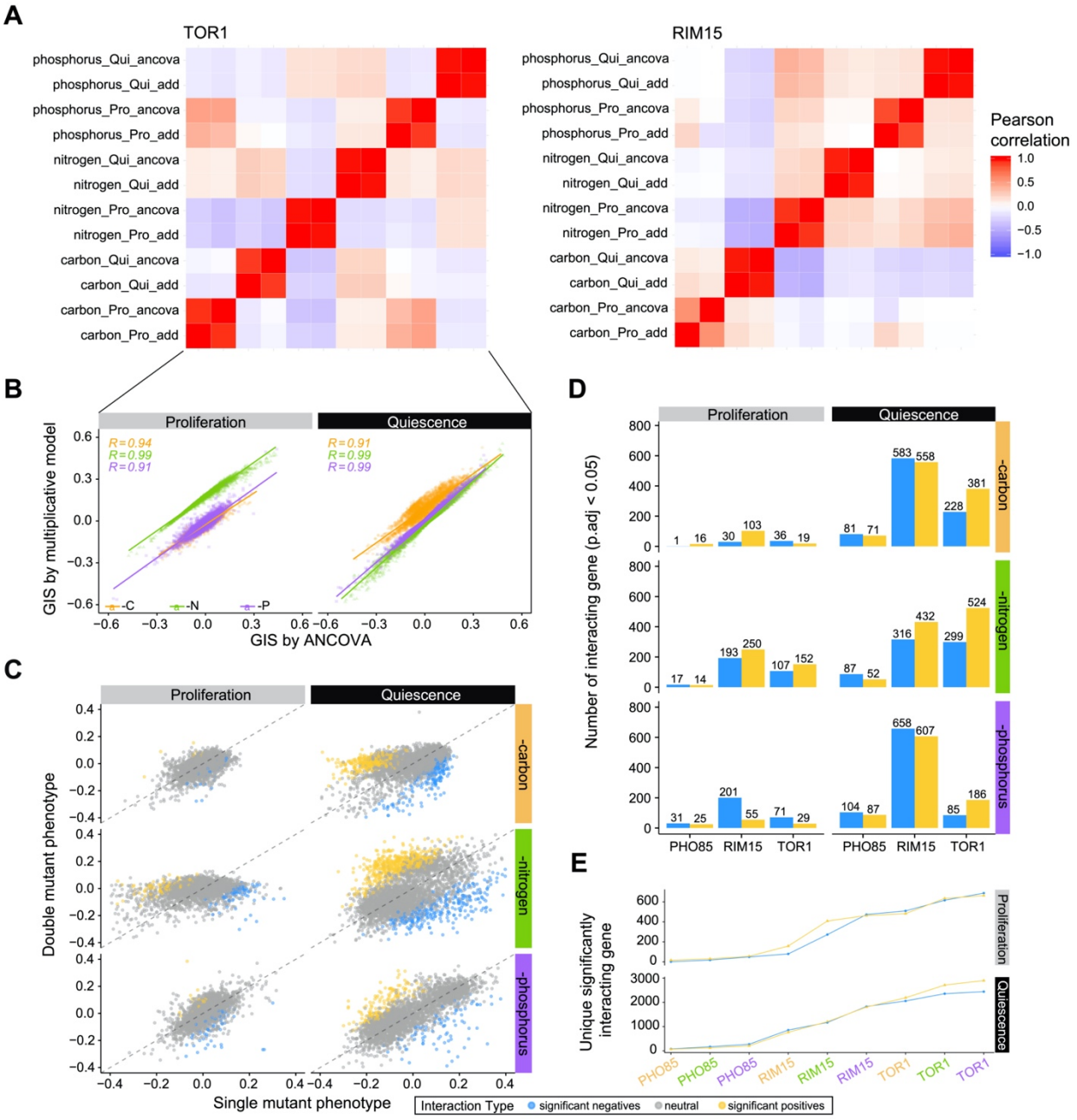

Figure 2.S3. Genetic interaction quantification comparison and summary.

A) Comparison of genetic interaction profiles for kinase gene *TOR1*(left panel) and *RIM15* (right panel) between different quantification models (add-multiplicative). **B)** Comparison of genetic interaction score estimated by ANCOVA and multiplicative model for different cellular states (TOR1). A linear regression line is plotted for each condition for each cellular state. **C)** Scatter plot of fitness and survival estimated in double mutation background (*tor1Δ0 xxx$_n$Δ0*: y-axis) and single mutation background (*xxx$_n$Δ0*: x-axis). The dashed diagonal line is colored grey. **D)**

Quantitative summary of significantly interacting genes with each kinase in proliferation and quiescence. **E)** Cumulative plot of unique genetic interactions detected with each kinase in three nutrient media.

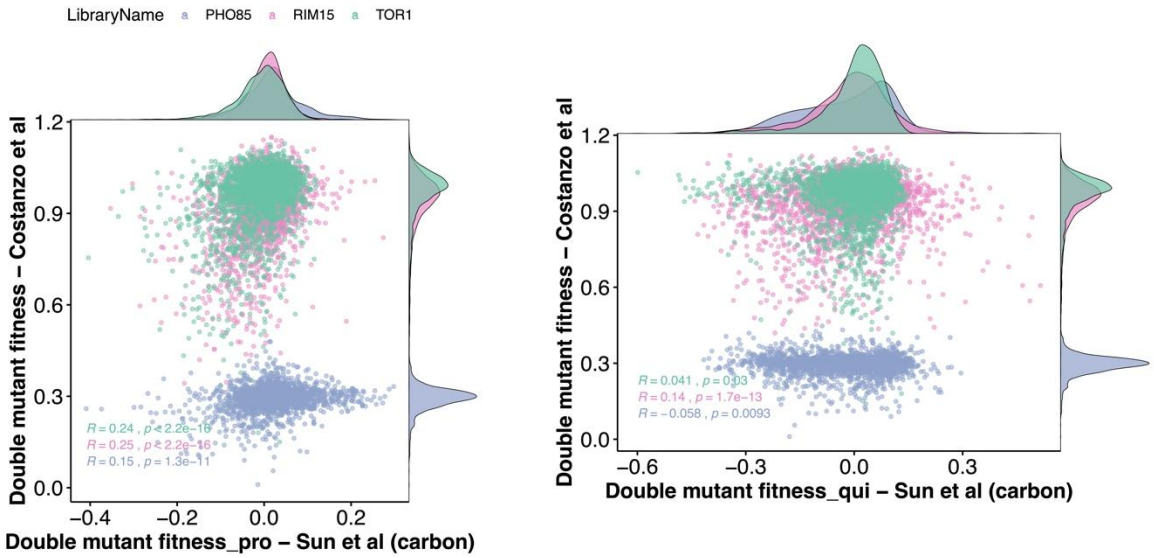

Figure 2.S4. Double mutant fitness and survival profiles comparison with the data from Costanzo et al's study.

Comparison of single mutant fitness/survival profiles between our study (carbon starvation) and Costanzo et al's study for all three kinases. Pearson correlation score is labeled in the plot with p-value.

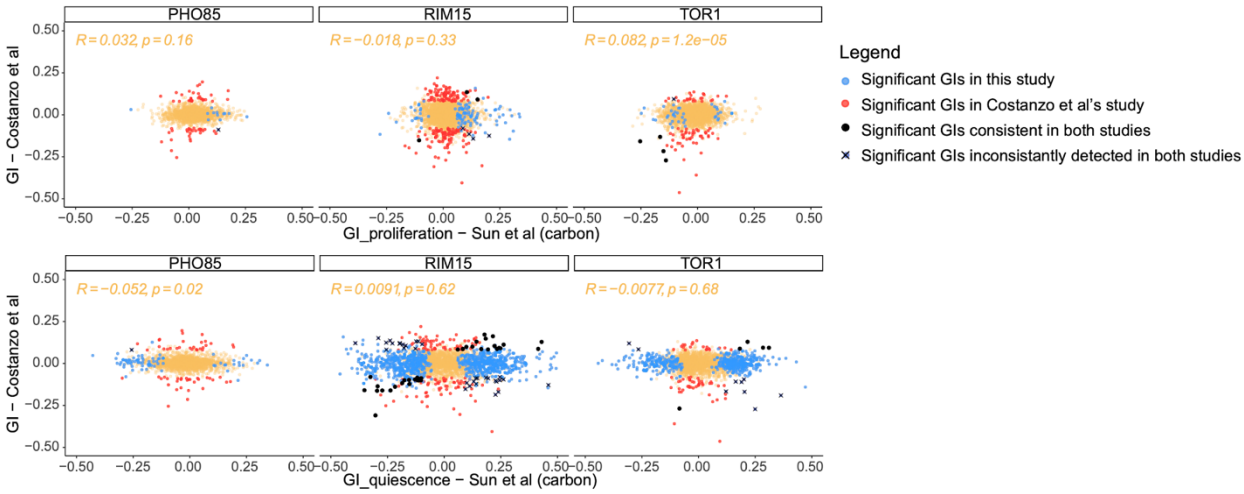

Figure 2.S5. Comparison of genetic interactions between data from our study and Costanzo et al's study.

Comparison of genetic interaction profiles between our study (carbon starvation) and Costanzo et al's study for all three kinases. Pearson correlation score is labeled in the plot with p-value (color code: yellow - carbon limitation, green - nitrogen limitation, purple - phosphorus limitation, blue - significant GIs in our study, red - significant GIs in Costanzo et al's study, black dot - Significant GIs consistent in both studies, black cross - significant GIs inconsistently detected in both studies).

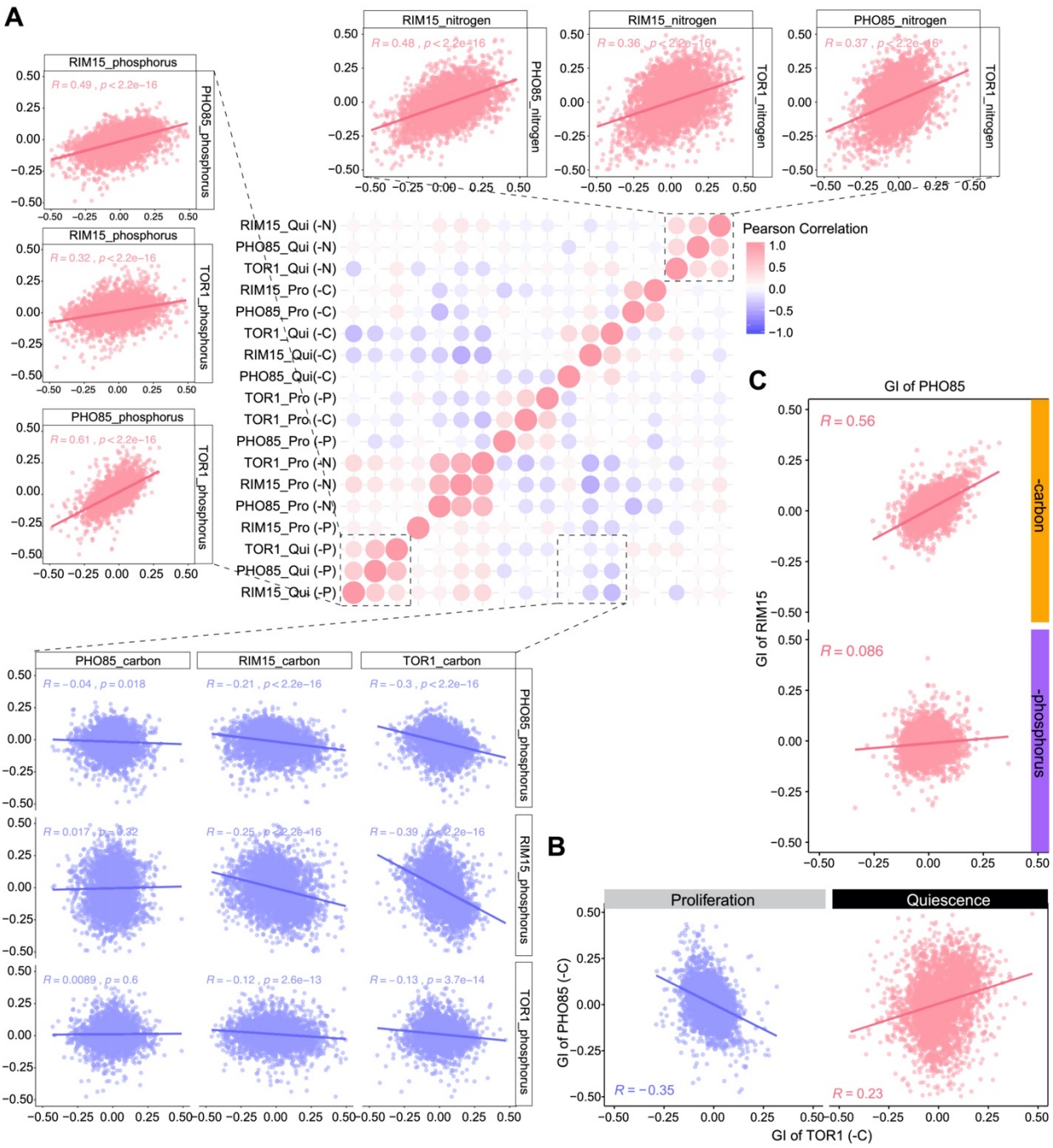

Figure 2.S6. Genetic interaction profiles with kinases across different conditions.

A) Correlation heatmap of genetic interaction profiles for each kinase under two cellular states in response to different nutritional restrictions. Samples are orders based on hierarchical clustering. Pearson correlation score is labeled in the plot with p-value < 0.05. **B)** comparison of

genetic interaction profiles of *TOR1* and *PHO85* between carbon restricted proliferative and carbon starved quiescent cells. Calculate pearson correlation is plotted on the bottom right of each panel with p-value < 0.05. **C)** Comparison of genetic interaction profiles between *PHO85* and *RIM15* in carbon- (top) or phosphorus- (bottom) restricted proliferating cells. Pearson correlation score is labeled in the plot with p-value < 0.05.

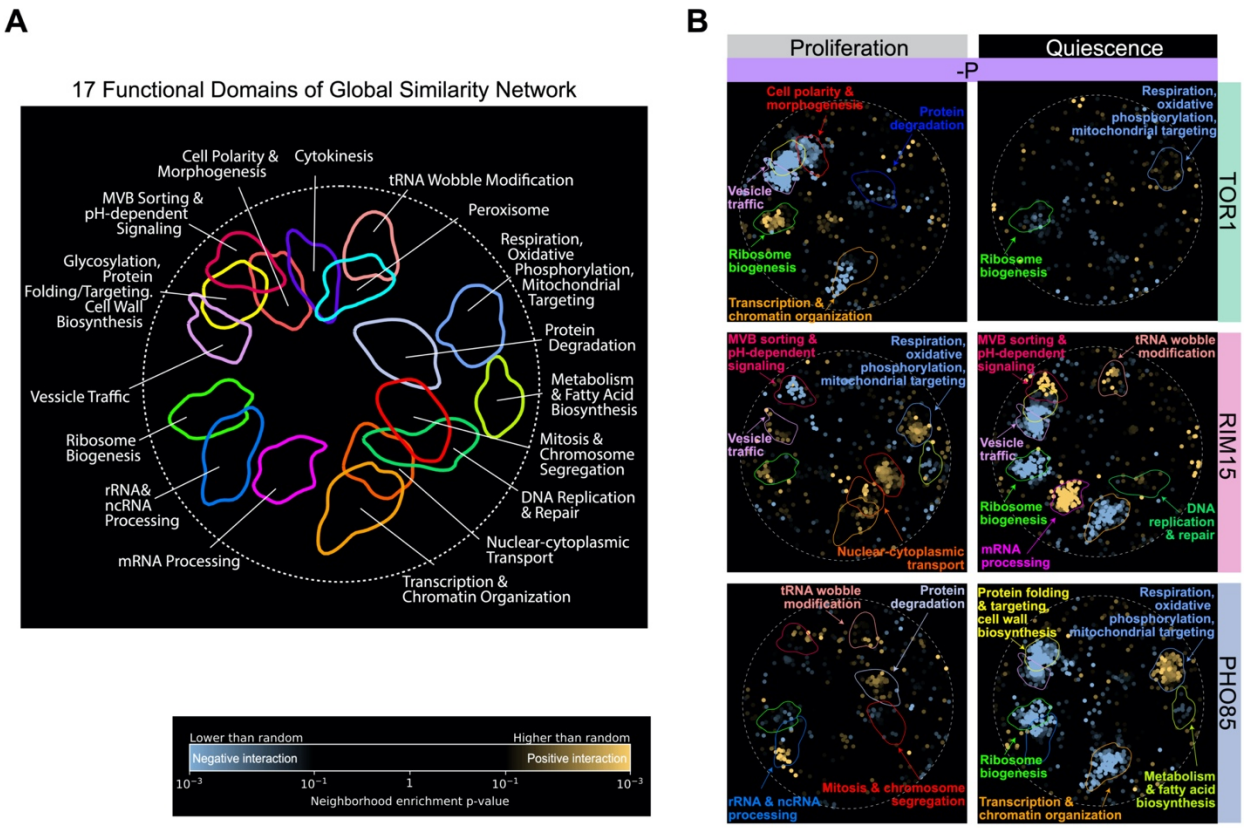

Figure 2.S7. A global network of genetic interaction profiles similarities.

A) A global genetic profile similarity network encompassing ~3,971 nonessential and essential genes from Costanzo et al., 2016. The global similarity network was annotated using the Spatial Analysis of Functional Enrichment (SAFE) (Baryshnikova 2016), identifying network regions enriched for similar GO biological process terms, which are color-coded (Costanzo et al., 2016). **B)** Genetic interaction enrichment landscape of *TOR1, RIM15, PHO85* in proliferating and quiescent cells under phosphorus (-P) restriction. Each dot represents one gene. Blue dots represent genes that have negative interactions with corresponding kinase (row-wise) in each condition (column-wise), and yellow dots represent genes with positive interactions.

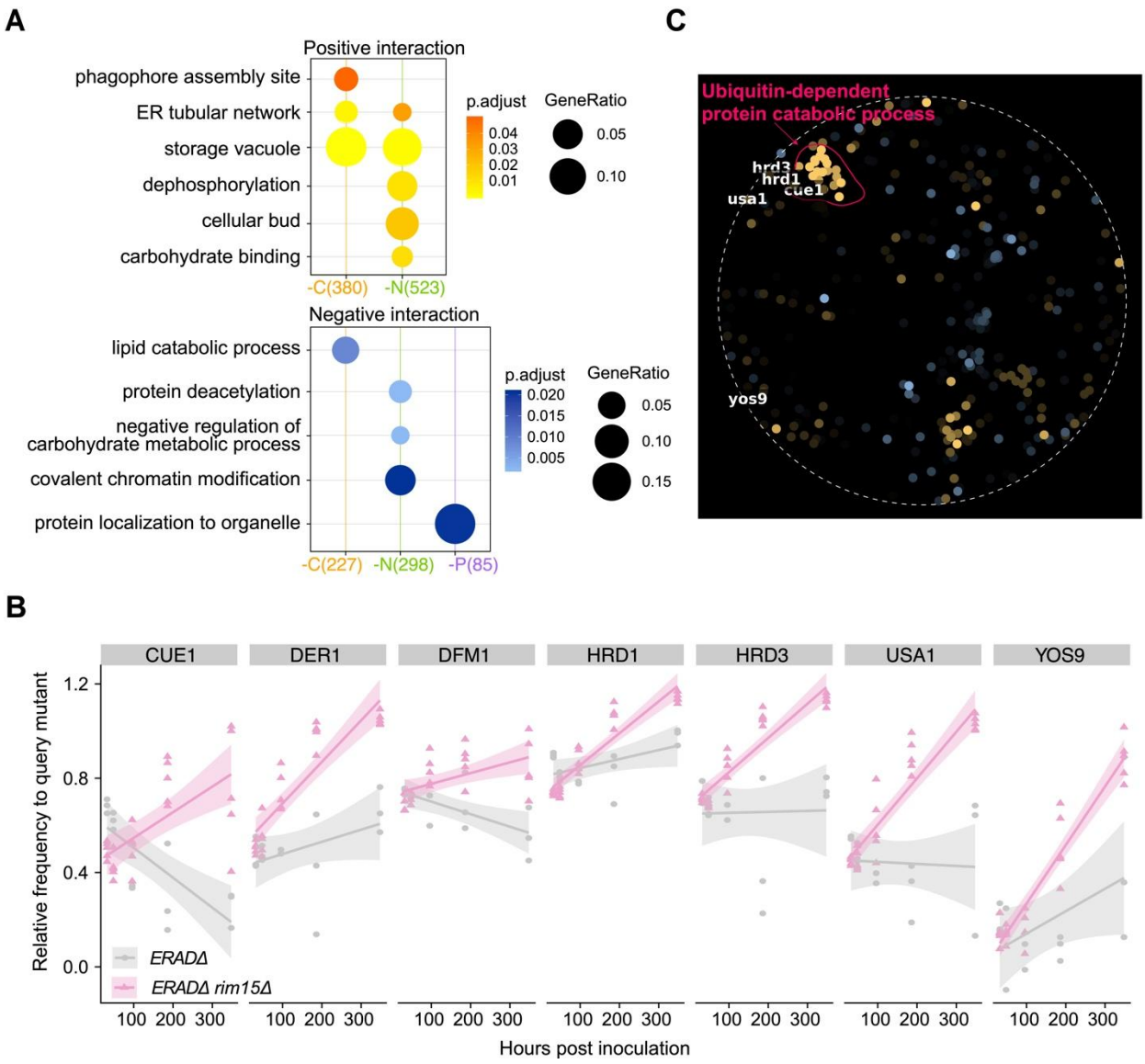

Figure 2.S8. Functional analysis of significantly interacting genes with different kinases.

A) GOterm enrichment analysis for genes that significantly interact with TOR1 in each different nutrient starvation condition. Only GOterms with significant representation are shown (p.adj < 0.05). The same color schemes are used to represent different interaction types (yellow - positive, blue - negative). The intensity of the dot color represents the significance, e.g. the lighter the color is, the smaller p-value. The size of the dot represents the gene group size within each term, given the significant interacting genes under each condition (colored parentheses on x-axis). B) Relative frequency of each double (*ERADΔ0 rim15Δ0*) and single mutant (*ERADΔ0*) as a function of time in response to nitrogen starvation. C) SAFE analysis for genes interacting with RIM15 in nitrogen starvation conditions.

Chapter 3 : Proteome and phosphoproteome remodeling and its regulation by *Rim15* during quiescence initiation

This chapter is based on the research paper “Integrative proteomics and phosphoproteomics profiling reveals dynamic signaling pathways underlying diverse quiescence entry” by Siyu Sun, Daniel Tranchina and David Gresham. I generated all of the data for all figures and tables, wrote the text, and generated all of the supplementary figures. This chapter will be submitted as a prepint to *bioRxiv* and for peer review to the journal *Molecular Biology of the Cell* in December 2020.

3.1 Abstract

The molecular circuits by which yeast cells enter quiescence in response to different nutritional starvations remain poorly understood. We combined temporal profiling of the whole proteome and phosphoproteome via stable isotope labeling with amino acids in cell culture (SILAC) and functional perturbation by deletion of the regulatory kinase *Rim15*, to systemically reconstruct regulatory networks underlying quiescence establishment. We find that different nutritional starvations activate quiescence by remodeling the proteome and phosphoproteome with different kinetics, characterized by greater dynamic range of protein phosphorylation and evidence of continued signal transduction after establishment of quiescence without concomitant changes in the proteome. Upregulation of mitochondrial proteins is essential for quiescence entry and undergoes distinct kinetics in a nutrient dependent manner. Genetic perturbation revealed a conserved pleiotropic role for the Serine/Threonine kinase *Rim15* in quiescence establishment by coordinating both transcription (RNA metabolism) and translation (amino acid metabolism) in response

to different starvations. Our multi-layer omics profiling and functional studies define the landscape of the quiescent proteome and phosphoproteome and reveal signaling, biogenesis and bioenergetics pathways that mediate initiation of cellular quiescence.

3.2 Introduction

Regulation of cell proliferation and growth in response to extracellular cues like growth factors, hormones and/or nutrients critically affects development and life span in virtually every biological system (J. V. Gray, Petsko, and Johnston 2004). In the absence of stimulatory signals, cells may enter into a reversible quiescent state that is typically characterized by low metabolic activity, including low rates of transcription and protein synthesis. In metazoans, quiescence is induced in response to growth factors and hormones, whereas in simpler, unicellular organisms' quiescence is primarily triggered by nutrient starvation to ensure long-term survival. The capacity of cells to maintain a viable non-proliferative state for prolonged periods is also referred to as chronological life span (CLS). Despite the universal importance of the quiescent state, the mechanisms regulating entry into and survival in quiescence remain poorly understood.

Quiescence and CLS have been studied in yeast primarily in cells starved in nutrient rich media. As with many microbes, however, quiescence in yeast can be initiated in response to a variety of nutrient deprivations (Lillie and Pringle 1980; Gresham et al. 2011; Klosinska et al. 2011; Yanagida 2009; S. Sun et al. 2020). Starvation for essential nutrients other than glucose, such as nitrogen, phosphorus and sulfur result in many of

the same characteristics including arrest as unbudded cells, thickened cell walls, increased stress resistance and an accumulation of storage carbohydrates compare to quiescent cells induced by glucose starvation (Lillie and Pringle 1980; Klosinska et al. 2011; Schulze et al. 1996). The ability to effectively initiate, maintain and exit quiescence confers a significant selective advantage across diverse environments resulting in a powerful evolutionary drive for effective cellular quiescence (O'Farrell 2011).

Initiation of the quiescence program in yeast requires downregulation of conserved nutrient-responsive signal transduction pathways. Specifically, inhibiting the kinase activities of the Target Of Rapamycin Complex 1 (TORC1), the protein kinase A (PKA) or PHO80-PHO85 (PHO) pathways drive cells into a quiescent state and significantly extend CLS (Kaeberlein, Burtner, and Kennedy 2007; Powers et al. 2006; Yang et al. 2010). Similarly, starvation for specific nutrient sensed by each pathway (carbon ➞ PKA/TORC1, nitrogen ➞ TORC1, phosphorus ➞ PHO) can also reduce pathway activity and drive cells into quiescence. However, how those different signaling pathways are integrated and mount a common transition into quiescence is not well understood.

Rim15, an evolutionary conserved serine/threonine kinase has been found to be regulated by those pathways across multiple studies. It has been proposed to be a nutrient signal integrator to coordinate quiescence entry by activating the PP2ACdc55 inhibitor Igo1 which in turn regulates the phosphorylation status and activity of both mRNA decay and transcription factors, such as Gis1 in response to glucose starvation (Bontron

et al. 2013). Typically, *Rim15* is inactivated by sequestration in the cytoplasm, where it is maintained in a phosphorylated state. When nutrients become scarce or the aforementioned pathways are downregulated, *Rim15* is derepressed via dephosphorylation and relocalizes to the nucleus (Ivo Pedruzzi et al. 2003; Wanke et al. 2008, 2005). The molecular pathways linking *Rim15* to distal readouts including the expression of specific nutrient-regulated genes, trehalose and glycogen accumulation, extension of CLS, and induction of autophagy have only been partially characterized in stationary phase cultures grown in nutrient rich conditions (I. Pedruzzi 2000; Wei et al. 2008; Yorimitsu et al. 2007). Whether *Rim15* regulates quiescence initiation via conserved mechanisms under different starvation conditions is unknown.

Increased protein turnover during the transition from proliferation to quiescence is essential for protein homeostasis and ensuring viability and long term survival (Marguerat et al. 2012; Zakrajšek, Raspor, and Jamnik 2011). Whether cells remodel their proteome differently according to different nutritional cues and utilize the same mechanisms for mediating protein homeostasis during this transition is not known. A recent systematic study has shown that *Rim15* genetically interacts with proteostasis genes that control protein translation and degradation (S. Sun et al. 2020), suggesting that *Rim15* has functions in quiescence beyond coordination of transcript levels. We hypothesized that *Rim15* is essential for sensing distinct nutrient signals to coordinate the protein expression state of quiescent cells. To test this, we developed a stable isotope labeling by amino acid in cell culture (SILAC) using prototrophic yeast strains that allowed us to profile the proteome and phosphoproteome during quiescence establishment. Using this

method, we quantified the proteome in response to three distinct starvation signals. We observed dramatic proteome remodeling in response to nitrogen, phosphorus, and carbon starvation and defined a common starvation response signature as well as signal specific expression changes. We found that the phosphoproteome exhibits larger scale changes compared to the entire proteome. By extending the study to *rim15Δ*, we found that *Rim15* differentially impacts the whole proteome and phosphoproteome dynamics during quiescence entry under different starvation conditions. Lastly, quantifying the differential expression phosphorylation events among conditions, we identified potential new targets of *Rim15* that are associated with protein synthesis and degradation. Overall, our finding broadens the functional spectrum of *Rim15* in regulating quiescence as a central mediator of transcription to translation.

3.3 Results

3.3.1 Prototrophic yeast strains efficiently incorporate exogenous lysine and arginine in SILAC medium

SILAC is a method for labeling auxotrophic cells by supplementing heavy isotopes containing amino acids in the culturing media. As auxotrophs cannot synthesize lysine or arginine, they efficiently import and assimilate exogenously provided amino acids. However, studying quiescence using auxotrophic cells may affect the establishment of quiescence. It has been recently demonstrated that proteins in prototrophic yeast strains can be efficiently labeled with isotope-labeled lysine (Lys-8), because amino acid incorporation from the culture medium is less energetically demanding than their internal

biosynthesis (Fröhlich, Christiano, and Walther 2013). To test whether SILAC can be applied to both prototrophic strains with different genotypes, we first tested labeling efficiency by inoculating cells from different strains in the same SILAC medium (**Figure 3.1A**). We found that both prototrophic and auxotrophic wildtype and *Rim15* null mutants have similar doubling time in standard SILAC media (i.e. synthetic complete media containing 2% glucose) containing either heavy or medium isotopes. We collected cells from all three strains and performed LC-MS/MS to check isotope incorporation efficiency. The incorporation level for each protein was calculated by dividing the intensity from the expected channel by the total intensity. By considering the density for each protein in each sample, we found that over 98% of the signal for each protein is labeled with the expected isotope (**Figure 3.1B**). There was no significantly reduced incorporation level found in either wild type or *rim15Δ* prototrophic cells in comparison to auxotrophic cells.

To differentiate biological alterations between proteomes identified using different wild type strains, we inspected the whole proteome between genotypes. Comparisons of wildtype cells in either a prototrophic or auxotrophic background are highly correlated: 0.93 for between samples in medium SILAC media (Lys-4 & Arg-6) and 0.95 between samples in heavy SILAC media (Lys-8 and Arg-10) (**Figure 3.S1A**). All data points are evenly distributed around the diagonal line with slope of one. The proteins with higher intensity tend to have higher correlation than those with lower intensities (**Figure 3.S1A**). By contrast, the correlation between wildtype and *rim15Δ* is reduced to 0.8 (**Figure 3.S1B & C**). Those results indicate that both labeling efficiency and peptide identification quality is not compromised when using prototrophic cells in SILAC as opposed to auxotrophs.

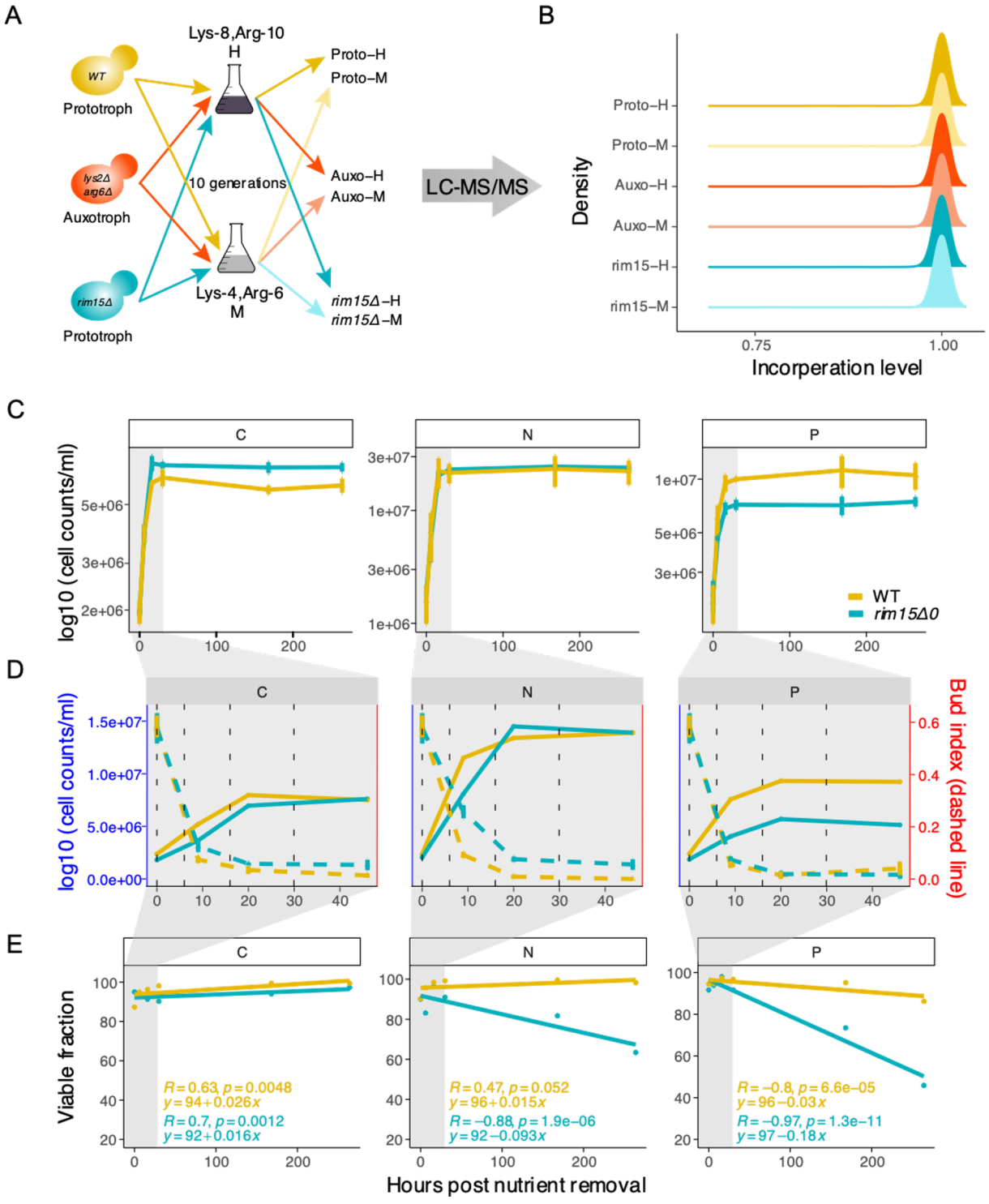
A
Lys-8,Arg-10
H
WT
Prototroph
Proto–H
Proto–M
lys2Δ
arg6Δ
Auxotroph
10 generations
Auxo–H
Auxo–M
LC-MS/MS
rim15Δ
Prototroph
Lys-4,Arg-6
M
rim15Δ–H
rim15Δ–M
B
Density
Proto–H
Proto–M
Auxo–H
Auxo–M
rim15–H
rim15–M
0.75
1.00
Incorperation level
C
log10 (cell counts/ml)
C
N
P
WT
rim15Δ0
D
log10 (cell counts/ml)
Bud index (dashed line)
E
Viable fraction
R = 0.63, p = 0.0048
y = 94 + 0.026x
R = 0.7, p = 0.0012
y = 92 + 0.016x
R = 0.47, p = 0.052
y = 96 + 0.015x
R = −0.88, p = 1.9e−06
y = 92 − 0.093x
R = −0.8, p = 6.6e−05
y = 96 − 0.03x
R = −0.97, p = 1.3e−11
y = 97 − 0.18x
Hours post nutrient removal

Figure 3.1. *rim15Δ* does not affect overall growth phenotype in all three nutrient restricted conditions.

Experimental design of amino acid incorporation test using prototrophic and auxotrophic strains. Briefly, prototrophic wild type (Proto-), auxotrophic (*lys2Δ arg6Δ*) wildtype (Auxo-), and prototrophic mutant (*rim15Δ*) cells were grown in either heavy ($^{13}C_6{}^{15}N_2$-lysine [Lys-8], $^{13}C_6{}^{15}N_4$-arginine [Arg-10]) or medium (D4-lysine [Lys-4], $^{13}C_6$-arginine [Arg-6]) isotope supplemented SILAC media (**Methods and materials**). Cells were collected for LC-MS/MS analysis after 10 generations. **B)** Incorporation levels of heavy (Lys-8, Arg-10) and medium (Lys-4, Arg-6) isotope-containing proteins for the auxotrophic *lysΔ, argΔ* and prototroph *S. cerevisiae* S288c strain. **C)** Growth curve of prototrophic wild type (yellow solid line) and *rim15Δ* (blue solid line) in response to three nutritional starvations: C - 0.06% glucose, N - 0mM nitrogen, P - 0mM phosphorus (n = 3) with addition of 100mM of lysine and arginine. T = 0 is the time at which cells were transferred into corresponding nutrient depleted conditions from the mid-log population growing in rich media. **D)** Tracking of growth curve (solid line) and bud-index (dashed line) for both wildtype (colored as yellow) and *rim15Δ* (colored as blue) in the first 46 hours post nutrient removal. *rim15Δ* cells ceased proliferation and were arrested at an unbudded stage around the same time as wild type cells. **E)** Viability of both wildtype and *rim15Δ* were tracked by PI/Syto9 staining followed by flow cytometry (**Methods and materials**).

3.3.2 Multiplexed quantitative analysis of whole proteome and phosphoproteome during quiescence initiation

To identify protein expression and phosphorylation events during quiescence establishment in response to different nutritional starvations, we used multiplexed SILAC and LC-MS/MS approaches to quantify the proteome and phosphoproteome of wild type cells in log-phase growth (0 hr) and 6 hr, 16 hr, and 30 hr after nutrient removal in biological triplicate. As depicted in **Figure 3.2A**, samples were cultured with different isotopically labeled Lys and Arg to enable multiplexing cells with different genotypes and to eliminate batch effects when quantifying proteomes from different genotypes across time. The samples were lysed, pooled, digested, and analyzed by LC-MS/MS (**Methods and materials**). 5% of the pool was used for whole proteome analysis, and the remaining

95% was subjected to further fractionation using titanium oxide columns for subsequent phosphoproteome profiling. In total, we quantified 1,277 proteins and 1,472 phosphorylation events (FDR < 1%), corresponding to a little under 25% of the expected proteome size.

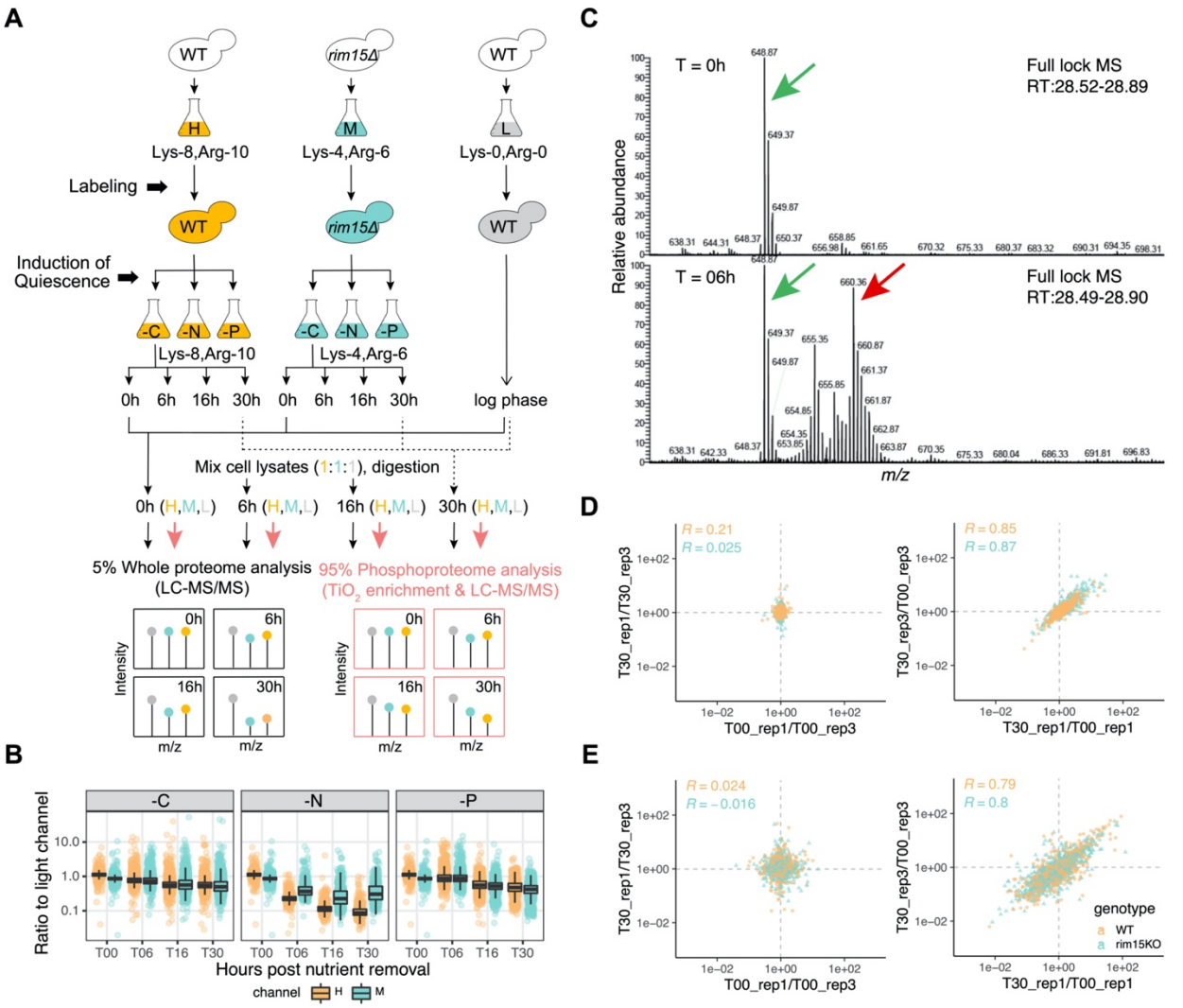

Figure 3.2. Multiplex SILAC identifies catabolism of lysine and arginine in nitrogen starvation condition.

A) Experimental setup for profiling proteome and phosphoproteome during quiescence initiation. **B)** Un-normalized ratios of heavy and medium channels show marked signal reduction in cells initiating quiescence in response to nitrogen starvation. See also **Figure 3.S2**. **C)** Cells

metabolize Lys-8/Arg-10 and incorporate heavy isotopes into other amino acids in random positions. MS/MS analysis on heavy isotope labeled cells collected T=0h and T=6h prior mixing. A representative spectrum indicates a second peak (red arrow) emerging in addition to the major peak (green arrow) detected in T=0h. **D)** Representative null comparisons of whole proteome (0h_rep1/0h_rep3 and 30h_rep1/30h_rep3) display markedly distinct patterns from true comparisons (30h_rep1/0h_rep1and 30h_rep3/0h_rep3 replicates). Correlation coefficient (r) for each comparison is indicated. **E)** Representative null comparisons of whole phosphoproteome (0h_rep1/0h_rep3 and 30h_rep1/30h_rep3) display markedly distinct patterns from true comparisons (30h_rep1/0h_rep1and 30h_rep3/0h_rep3 replicates) in carbon starvation. Correlation coefficient (r) for each comparison is indicated.

3.3.3 Amino acid catabolism results in widespread incorporation of isotopes during nitrogen starvation

Based on our experimental design we expected similar intensity distributions for each of the three channels from the same sample. We first checked technical variation by plotting the unnormalized ratio for each protein for heavy/light and medium/light. Surprisingly, we observed a significant discrepancy between distributions of heavy/light and medium/light specific to nitrogen starvation conditions across all biological replicates, owing to a marked reduction in detected heavy label (**Figure 3.2B & Figure 3.S2A**). To determine the source of this abnormal reduction in nitrogen starved cells, and exclude the possibility of technical confounders during mass spec analysis, we analyzed samples from nitrogen starvation conditions that were cultured in heavy labeling conditions (Lys-8 & Arg-10) and analyzed without subsequent mixing with samples containing light or medium label. We first checked the possibility of a reduced labeling efficiency and found that the incorporation level is not reduced as a function of time of starvation (**Figure 3.S2B**). Then we checked whether samples from the later time point had less MS scans that were further analyzed by the instrument. Interestingly, similar MS scans were found for both

MS1 and MS2(MS/MS) (**Figure 3.S2C**). However, less MS2 scans were identified as a function of time of starvation, which results in an increase in peptides that cannot be matched with the reference database and reduced intensity (**Figure 3.S2D**). We then inspected the raw spectra from the same samples at different time points. Interestingly, a second peak (red arrow) emerges in addition to the major peak (green arrow) at 6 hrs post nitrogen removal and is maintained in samples at later time points (**Figure 3.2C**). Together, these results suggest incorporation of isotopes into amino acids other than Lys/Arg in nitrogen starved quiescent cells. This is most likely caused by the fact that in the absence of nitrogen, cells start to catabolize heavy SILAC amino acids (Lys-8 & Arg-10) from the media or from protein degradation and use them as building blocks for synthesis of other amino acids. Unfortunately, the current experimental setup does not allow us to quantitatively assay proteome remodeling during quiescence establishment under nitrogen starvation, so we excluded these samples from subsequent analysis and focused on the response to carbon and phosphorus starvations using normalized ratios (**Methods and materials**).

To differentiate technical variation from biological variation, we compared replicate data at T=0 hour and T=30 hour for both whole proteome and phosphoproteome. Here, only carbon starvation samples were shown as representation. A comparison of technical variation shows a random distribution (**Figure 3.2D, left**), with the phosphoproteome data being more variable than the whole proteome data (**Figure 3.2D, right**), probably due to the transient nature of protein phosphorylation. In contrast, comparisons of biological variation show significant differences between proliferating and quiescent cells that are

consistent between replicates (**Figure 3.2E**). Principal-component analysis (PCA) of proteins and phosphopeptides (**Figure 3.S3**) further supports biological variation as the main source of variance in the data.

3.3.4 Mitochondrial proteins are continuously upregulated in response to carbon starvation

To test agreement of our data with similar studies we performed an initial comparative analysis. Expression of specific proteins from proteomic profiling (**Figure 3.S3C&D**) are in agreement with results from a study screening GFP fusion proteins (Davidson et al. 2011). We found that of the 125 proteins that were found to be upregulated in either stationary phase cultures or quiescent cells fractionated using a percoll gradient (Davidson et al. 2011; Allen et al. 2006) 44 are detected across all timepoints and conditions in our study. We fit a linear regression model to these proteins using their normalized ratios (across all replicates) against time. We found that 7 proteins have a negative slope but larger than -0.01, indicating that those proteins are not changing much overtime (**Figure 3.S3E**). The other 37 proteins have a positive coefficient, although with larger variation, that is consistent with upregulation during quiescence establishment in carbon starvation condition (**Figure 3.S3E**). Notably, 25 out of 37 quiescence specific upregulated proteins (note: ATP3 was counted twice in the original paper, who claimed 38 proteins instead of 37) are also found in carbon starved quiescent cell in ours study, i.e. CIT1, ATP3/4/5, COX4/6, KGD1/2, SDH2, CYT1, GDH2, FAA1, PIL1, LEU4, TPS1, PYC1, STI1, SAC6, AIP1, YRA1, UGA1, ABP1, PTC3 (**Figure 3.S3C & 3D**). At least 50% of these proteins (11/20) were reported to localize to mitochondria (Davidson et al. 2011).

Overall, our results in carbon starved quiescent cells agree with previous findings which used an orthogonal method, thereby validating the reliability of our profiling approach.

Interestingly, the majority of those proteins are overall down-regulated in response to phosphorus starvation **(Figure 3.S3E)**. Different from the continued increase under carbon starvation, the expression of those proteins all peaked at T = 6h and then attenuate afterwards (**Figure 3.S3C & D**). This transient upregulation of mitochondrial proteins in phosphorus starvation may suggest a different regulatory mechanism of quiescence, but still imply the importance of mitochondrial function in quiescence programming as previously showed in nutrient rich conditions (Allen et al. 2006; Aragon et al. 2008).

3.3.5 Proteome remodeling in quiescence entails multiple condition dependent functional modules

To model the dynamics of proteome changes during the initiation of quiescence in response to distinct starvation signals we adapted a two-step computational pipeline (**Figure 3.3A**) (Tan et al. 2017). We first identified proteins significantly changed between any two time points, genotype or starvation condition using three-way ANOVA, resulting in identification of 1,067 differentially expressed (DE) ones during quiescence establishment (FDR < 5%). We then applied Weighted Gene Correlation Network Analysis (WGCNA) to these DE proteins to identify modules of highly correlated protein dynamics, to relate modules to sample traits (e.g. starvation conditions, different genotypes, and time course), and to identify key hub proteins within modules that are

related to the traits. WGCNA applications in clinical studies are well suited at relating modules with phenotypic traits (e.g. height, weight). In our case, different genotypes (WT, *rim15Δ*) and nutritional starvations (C, P) are treated as binary traits, and time is treated as a continuous numerical trait (**Methods and materials**). Using WGCNA on the whole proteome dataset, we were able to group the majority of the DE proteins (1,067) into six co-expression clusters modules (named WPMs for whole proteome modules) with clear different expression patterns when related to the metadata (traits) (**Figure 3.3B**).

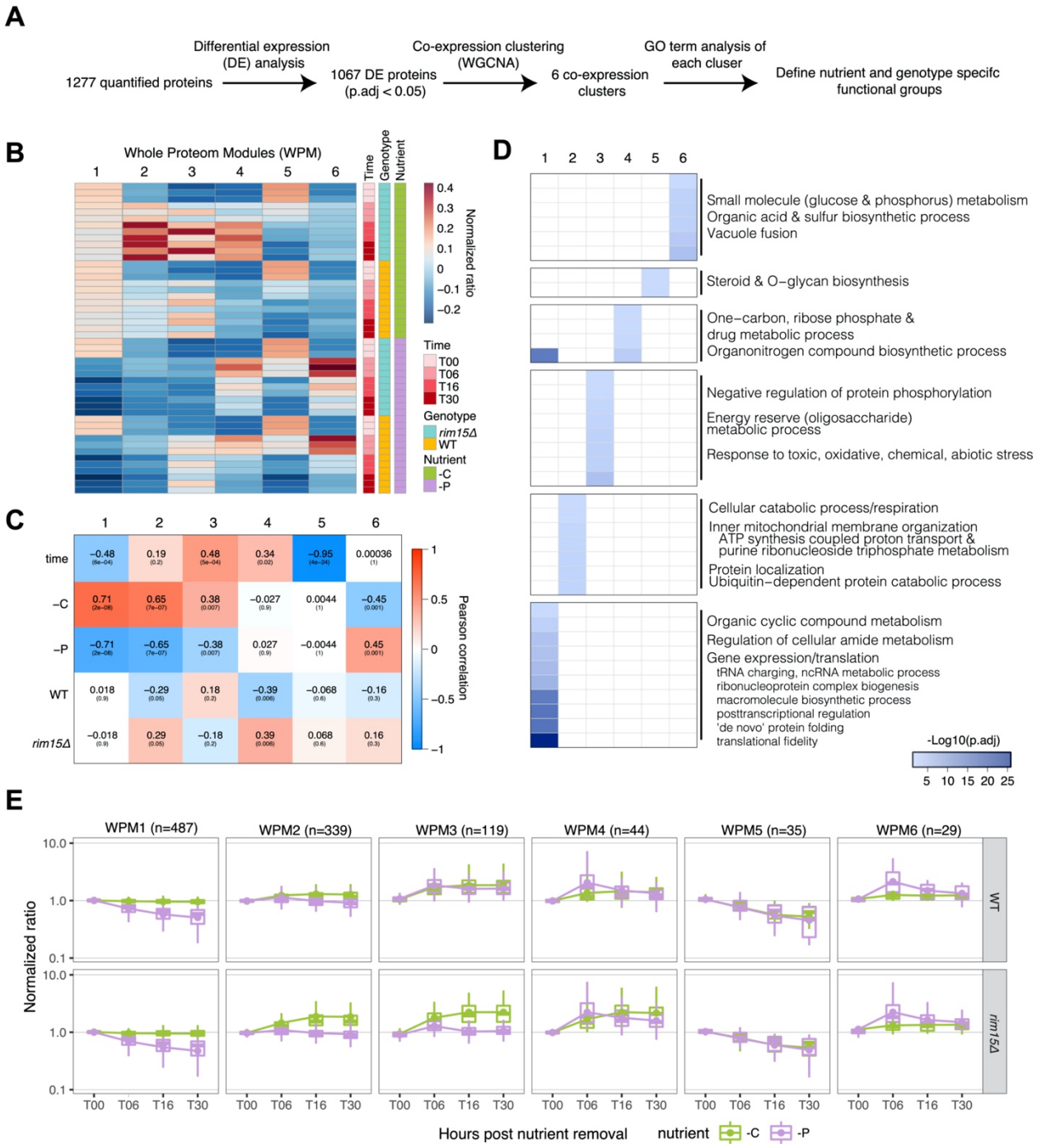

Figure 3.3. Temporal expression profiling of the whole proteome reveals key co-expression modules during initiation of quiescence.

A) Overview of computational workflow. **B)** Expression of consensus eignegenes for each whole proteome module (WPM). Each column indicates one module and each row indicates one sample. **C)** Module to trait relationships indicated by correlation scores and significance. **D)**

Functional annotations of WPMs by Gene Ontology enrichment and KEGG pathway annotation (FDR < 5%). **E)** Dynamics of proteins in six co-expression WPMs. The expression distribution for all proteins in each module is plotted (colored by starvation conditions) and the mean of each distribution per cluster is connected by lines with the same color code.

To confirm the feasibility of using binary traits in quantifying module-trait relationships, we compared the expression of consensus einegenes in each module (**Figure 3.3B**) with the correlation of module-trait relationships (**Figure 3.3C**). Six modules have quite different expression patterns when relating to their corresponding “traits” and the module-trait correlation analysis provides a quantitative measure of the strength of their relationships. Overall, 4/6 modules have significant correlations with nutrient starvation conditions: WPM1, 2, 4, 6 to different extents. WPM1, WPM2 and WPM6 primarily depend on the type of starvation, with a secondary dependence on time for WPM1, and on genotype for WPM2 (**Figure 3.3C & 3.3E**). Proteins in WPM3 and WPM5 primarily change expression as a function of time of starvation, but WPM3 also significantly correlates with the starvation nutrient condition. Although the correlation between WPM3 and genotype is not statistically significant, an expression difference between genotypes in response to phosphorus starvation can still be clearly seen (**Figure 3.3B)**. WPM4 is the only module in which genotype is the dominant factor, and this effect is marked in the carbon starvation condition. Functional annotations of each module show minimal overlap when integrating results from different functional annotations such as KEGG pathway and Gene Ontology (GO) analysis (**Figure 3.3D**), suggesting modular regulation of the proteome during quiescence establishment.

3.3.6 Wildtype cells deploy distinct reprogramming strategies for entering quiescence in response to different nutrient starvation signals

Proteins with the same function exhibit distinct expression dynamics in response to different nutrient starvations. For example, WPM1 is significantly and gradually down regulated in phosphorus starvation conditions compared to carbon starvation **(Figure 3.3E**). Functional annotation of proteins in WPM1 reveals protein homeostasis regulation roles at all levels from post-transcriptional modification, tRNA charging to translation fidelity and protein folding (**Figure 3.3D**). Similarly, proteins in WPM2 have a strong positive correlation with carbon starvation, with the signal peaking at T = 06 hours in both starvations. It subsequently remains stable throughout the time course in carbon starvation, but expression dynamics are attenuated at later time points in phosphorus starvation (**Figure 3.3E**). The previously discussed mitochondrial proteins (**Figure 3.S3B**) were clustered into this module. Indeed, functional annotation of proteins in WPM2 revealed the involvement of proteins localizations in mitochondrial & cellular respiration. The genes encode those proteins were found to be essential for survival in quiescent cells induced by carbon starvation (Klosinska et al. 2011), which again emphasize an essential function of mitochondria in adapting cells in response to starvations.

Proteins in WPM4 and WPM6 reach a similar steady state after 16 hours in both starvation conditions but via different paths in response to those two starvations. Proteins in WPM4 and WPM6 are remarkably upregulated at T = 6h and declined afterwards in phosphorus starvation. However, those proteins are gradually upregulated in carbon starvation and reached a similar expression as in phosphorus later on (**Figure 3.3E**).

Proteins in these modules are enriched in amino acid and metabolic and biosynthetic pathways likely reflecting the need for recycling basic building blocks for survival via different mechanisms (**Figure 3.3D**).

Overall, most proteome remodeling occurs during the first two time points with some additional dynamics during the third time point (T16). After that, there is only minimal downregulation in some of the modules specifically under phosphorus starvation (**Figure 3.3E**). This is consistent with the physiological behavior of the whole population (**Figure 3.1C**), in the first two time points the cells sense the starvation signals, start preparing for entering quiescence probably by largely remodeling expression and complete the last round of cell division, whereas in the second two timepoints the cells already arrest growth and are only fine tuning proteins expressions to maintain minimal cellular activities. WPM5 is a module with exceptional consistency between carbon and phosphorous starvation, which is composed of proteins involved in steroid and O-glycan biosynthesis pathways (**Figure 3.3D & 3.3E**). The consistent down regulation of proteins in WPM5 may suggest a common strategy for energy conservation in support of other activities in quiescence regardless of the starvation signals.

3.3.7 *Rim15* coordinates biosynthetic pathways and mitochondrial metabolism in quiescence entry

Rim15 impacts proteome reprogramming dynamics in a condition dependent manner. For example, we find no difference in WPM2 under phosphorus starvation conditions in the absence of *Rim15*, but observe that *Rim15* results in amplified upregulation of WPM2

proteins under carbon starvation (**Figure 3.S4A**). A similar effect of *Rim15* deletion was also found for proteins in WPM3 and WPM4 under carbon starvations. Those results suggest a repressive or rapid degradative function of *Rim15* on those proteins particularly in carbon starvation. Interestingly, in WPM3, proteins are down regulated in the absence of *Rim15* under phosphorus starvation exclusively (**Figure 3.S4A**). Those proteins are primarily involved in protein dephosphorylation, energy preservation and stress response (**Figure 3.3D**) suggesting that preserving energy during quiescence initiation is a key function of *Rim15* in preparing cells for long-term survival.

To further elucidate the function of *Rim15* in proteome remodeling we used analysis of covariance (ANCOVA) to compute *Rim15*'s impact on protein overall trend in the two starvation conditions (**Methods and materials**). In total, 298 proteins and 82 proteins are found to be differentially regulated (p.adj < 0.05) as a function of *Rim15* genotype in carbon starvation and phosphorus starvation, respectively. In accordance with the results from WGCNA analysis (**Figure 3.S4A**), ~ ¾ of the identified differentially expressed proteins are upregulated in the absence of *Rim15* under carbon starvation, which may suggest a repressive or degradative function of *Rim15* on those proteins (**Figure 3.S4B)**.

However, in contrast to carbon starvation, a similar number of proteins are found to be either up or down regulated in phosphorus starvation (43 ⇑ & 39 ⇓ in *rim15Δ*). Although far fewer proteins (i.e. 39) are found to be repressed by *Rim15* under phosphorus starvation, a significant number of them (18) are common to both conditions

(p.adj < 0.01, hypergeometric test) (**Figure 3.S4D & Table 3.1**). The majority of these proteins are enzymes involved in carboxylic acid catabolic, mitochondrial metabolism process and amino acid synthesis (8 proteins), chaperons, protein translation, folding, stability, and transport into various organelles (7), sub-cellular morphology regulation (2), and transcriptional regulation (2).

Table 3.1. Proteins upregulated in the absence of *Rim15* in both starvation conditions.

ORF	Gene name	Function
YLR153C	ACS2	Acetyl-coA synthetase isoform
YDL066W	IDP1	Mitochondrial NADP-specific isocitrate dehydrogenase
YMR083W	ADH3	Mitochondrial alcohol dehydrogenase isozyme III
YDL131W	LYS21	Homocitrate synthase isozyme; catalyzes the condensation of acetyl-CoA and alpha-ketoglutarate to form homocitrate
YDR304C	CPR5	Peptidyl-prolyl cis-trans isomerase (cyclophilin) of the ER
YBL050W	SEC17	Alpha-SNAP cochaperone, required for vesicular transport between ER and Golgi.
YIL038C	NOT3	Component of the CCR4-NOT core complex, involved in mRNA decapping; involved in transcription initiation and elongation
YJR076C	CDC11	Component of the septin ring that is required for cytokinesis
YIR006C	PAN1	Part of actin cytoskeleton-regulatory complex Pan1p-Sla1p-End3p
YLR259C	HSP60	prevents aggregation and mediates protein refolding after heat shock

YIL051C	MMF1	Mitochondrial protein required for transamination of isoleucine, interacts genetically with mitochondrial ribosomal protein genes
YCL043C	PDI1	Protein disulfide isomerase; multifunctional oxidoreductase of the ER lumen
YGL026C	TRP5	Tryptophan synthase
YDL185W	VMA1	Subunit A of the V1 peripheral membrane domain of V-ATPase; involved in methionine restriction extension of chronological lifespan in an autophagy-dependent manner
YDL078C	MDH3	Peroxisomal malate dehydrogenase, involved in the glyoxylate cycle
YBR222C	PCS60	Peroxisomal CoA-dependent Synthetase, that binds mRNA
YKL112W	ABF1	DNA binding protein with possible chromatin-reorganizing activity; involved in transcriptional activation, gene silencing, and DNA replication and repair
YMR226C	NA	NADP(+)-dependent serine dehydrogenase and carbonyl reductase

To further investigate the functional role of differentially expressed proteins in each condition, we ranked the proteins whose DE is statistically significant (p.adjust < 0.05) and applied Gene Set Enrichment Analysis (GSEA) on the ranked list (**Methods and materials**). Interestingly, upregulated proteins in carbon starved *rim15Δ* cells are mostly membrane transport proteins that are essential for energy production and synthesis in mitochondria (**Figure 3.S4C**). Many of these proteins (13) were previously found to be uniquely localized to mitochondria in quiescent cells under carbon starvation, which was known upregulated in carbon starved wildtype cells (**Figure 3.S3**) (Davidson et al. 2011).

Table 3.2. Proteins that are upregulated and genetically required for quiescence under carbon starvation

ORF	Gene names	Function
YBL087C	RPL23A	Ribosomal 60S subunit protein L23A
YBR025C	OLA1	P-loop ATPase, interacting with proteasome
YBR118W	TEF2	Translational elongation factor EF-1 alpha
YCL050C	APA1	Phosphorylase, catalyzes phosphorolysis of dinucleoside oligophosphates
YGR034W	RPL26B	Ribosomal 60S subunit protein L26B
YHL034C	SBP1	Protein that binds eIF4G and has a role in repression of translation
YHR021C	RPS27B	Protein component of the small (40S) ribosomal subunit
YHR108W	GGA2	Protein that regulates Arf1p, Arf2p to facilitate Golgi trafficking
YLR325C	RPL38	Ribosomal 60S subunit protein L38
YLR432W	IMD3	Inosine monophosphate dehydrogenase; catalyzes the rate-limiting step in the de novo synthesis of GTP
YML035C	AMD1	AMP deaminase - catalyzes the deamination of AMP to form IMP and ammonia

However, distinct sets of DE proteins were found in phosphorus starvation, which may explain the reduced viability of mitochondrial mutants in phosphorus starvation. These results support the essentiality of upregulating mitochondrial proteins under starvation induced quiescence, as phosphorus starved *rim15Δ* cells fail to activate those proteins (**Figure 3.S4C)** likely contributing to the poor viability of these cells (**Figure 3.1C**).

An alleviated upregulation of those proteins may be the key for survival to compensate for the other effect of missing *Rim15*. As mitochondria is known to undergo major morphological changes in response to carbon starvation to enable long term survival (Laporte, Gouleme, et al. 2018), it is possible that failed upregulation of those proteins will not be able to accomplish this morphological re-organization and therefore cannot support the cells for long-term survival.

To test whether *Rim15* dependent expression is functionally essential for surviving during quiescence, we compared the DE expression dynamic (as a function of time of starvation) with the survival rate when the corresponding gene is deleted. 11/51 proteins that are upregulated (p.adj < 0.05) and genetically required for survival (p.adj < 0.05) in carbon starvation (**Table 3.2**) and 13/39 are upregulated and genetically required for survival in phosphorus starvation (**Table 3.3**). Those results differ from previous findings based on studies on transcript levels, which found that the genes with increased transcript abundance do not overlap with those that are needed in order to survive starvation conditions (Klosinska et al. 2011). Those results may indicate a discrepancy between RNA and protein abundance in quiescence, which is consistent with the conclusion from an earlier quantitative study in fission yeast (Marguerat et al. 2012).

Table 3.3. Proteins that are upregulated and genetically required for quiescence under phosphorous starvation

ORF	Gene names	Function
YDL168W	SFA1	Bifunctional alcohol dehydrogenase and formaldehyde dehydrogenase

YDR214W	AHA1	Co-chaperone that binds Hsp82p and activates its ATPase activity
YDR368W	YPR1	NADPH-dependent aldo-keto reductase; reduces multiple substrates including 2-methylbutyraldehyde and D,L-glyceraldehyde, expression is induced by osmotic and oxidative stress
YGL037C	PNC1	part of the NAD(+) salvage pathway; required for life span extension by calorie restriction
YGR130C	NA	Component of the eisosome with unknown function; GFP-fusion protein localizes to the cytoplasm
YHR008C	SOD2	Mitochondrial manganese superoxide dismutase
YIR036C	IRC24	Putative benzil reductase;(GFP)-fusion protein localizes to the cytoplasm and is induced by the DNA-damaging agent MMS
YLR109W	AHP1	Thiol-specific peroxiredoxin; reduces hydroperoxides to protect against oxidative damage
YML004C	GLO1	Monomeric glyoxalase I
YML070W	DAK1	Dihydroxyacetone kinase; required for detoxification of dihydroxyacetone (DHA); involved in stress adaptation
YMR110C	HFD1	Dehydrogenase involved in ubiquinone and sphingolipid metabolism
YNL255C	GIS2	Translational activator for mRNAs with internal ribosome entry sites
YOR007C	SGT2	Glutamine-rich cytoplasmic cochaperone, protein trafficking

3.3.8 Phosphoproteome profiling identifies condition dependent signaling pathways

In our phosphoproteome profiling, we quantified 1,472 unique phosphorylations, out of which 1,340 phosphorylation events were differentially expressed as a function of

genotype, nutrient starvation or time (**Figure 3.4A**). WGCNA co-expression clustering of phosphorylation events identified eight modules (PEMs; **Figure 3.4B**), and functional enrichment was performed for each cluster (**Figure 3.4C**). In contrast to the limited number of proteins that are down-regulated in carbon starvation (WPM1-4 & 6 from **Figure 3.3E**), hundreds of protein phosphorylation events are reduced immediately post carbon removal (see PEM1, 4, 6, 7 from **Figure 3.4D**). However, distinct sets of modules were found to be downregulated at the onset of phosphorus starvation (see PEM 1,5,7). PEM1 is the only and largest cluster (n = 452) for which the dynamics show minimal conditional dependency. The proteins in PEM1 are enriched for functions in the cell cycle and MAPK signaling pathways, translation initiation factor binding, histone binding, and enzyme activities (**Figure 3.4C**). Proteins involved in those functions are dephosphorylated immediately after nutrient depletion no matter what type of the starvation is in. Whereas other down-regulated modules are prone to be condition dependent. For example, PEM4 is enriched for translation initiation and having a stronger and continuous downregulation in carbon starvation, and PEM5 & 7 are enriched for autophagy and enzyme functions, being constantly downregulated in phosphorus starvation (**Figure 3.4C & 3.4D**).

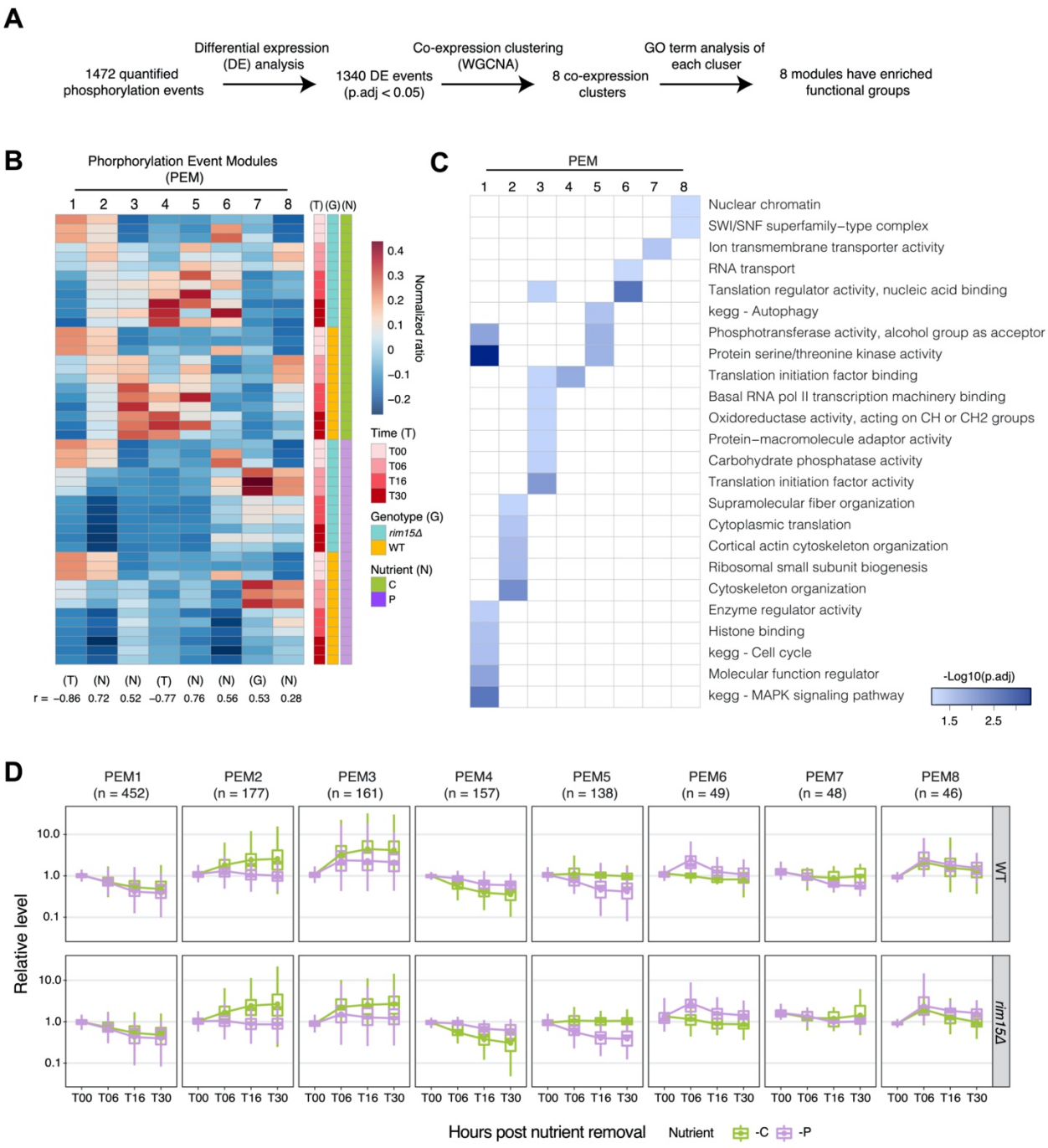

Figure 3.4. Phosphoproteome profiling reveals co-expression clusters that are condition dependent.

A) Overview of computational analysis for the phosphoproteome. **B)** Mean expression of consensus eignegenes in each module of phosphorylation events (PEMs). Each column indicates one module and each row is its expression in one sample. **C)** Functional annotations of PPCs by GO and KEGG (FDR < 0.05). **D)** Dynamics of phosphorylation events in eight co-

expression PEMs. Expression distribution for all proteins in each module is plotted (colored by starvation conditions) and the mean of each distribution per cluster is connected by lines (colored by starvation conditions).

As with proteome remodeling, protein phosphorylation events during quiescence establishment are also tightly coupled with starvation signals. For example, proteins in PEM2 and PEM3 share similar dynamic patterns under carbon starvation but have distinct patterns in phosphorus starvation, indicating that phosphorylation events of proteins involved in cytoskeleton organization are not drastically remodeled under phosphorus starvation. Surprisingly and in contrast to proteome dynamics, the phosphoproteome continues to change long after initiation of quiescence showing significant changes between 16h and at 30hr. This observation is consistent with quiescence not entailing a complete shutdown of all cellular activities, such that signaling pathway changes are actively regulating quiescent cells. Moreover, clusters of phosphorylation events sharing similar temporal patterns with proteomes do not functionally overlap; for example, PEM5 - WPM1, PEM1 - WPM1, PEM2 - WPM2, PEM6 - WPM6, PEM3 - WPM3 all share similar expression patterns between proteome and phosphoproteome. This suggests limited coordinated regulation between translation and phosphorylation, which is the opposite to what has been found in quiescent T-cell re-activation (Tan et al. 2017).

Proteins in PEM6 and PEM8 show similar temporal patterns in phosphorus starvation with peak levels occurring at T = 6 and subsequent attenuation. Again, the dynamics in response to carbon depletion are distinct. Functional annotation of proteins in PEM8 shows that proteins regulating nuclear chromatin including SWI/SNF complex are upregulated during the quiescence initiation in response to both starvations. This

result is in line with previous findings that chromatin condensation is one of the mechanisms to globally repress transcription during quiescence initiation. In support of these results, previous screens have also shown that SWI/SNF complexes are essential for quiescence entry (L. Li, Miles, and Breeden 2015; Spain, Braceros, and Tsukiyama 2018).

3.3.9 *Rim15* regulates functional similar phosphorylation events in response to different starvations

In general, the global phosphoproteome dynamic pattern in both widltype and *rim15Δ* are similar but there are two exceptional modules: PEM3 and PEM7 (**Figure 3.S5B**). In PEM3, *rim15Δ* shows consistent reduced upregulation during quiescent entry, which suggests that the phosphorylation levels of those proteins are positively affected by *Rim15*. The opposite case is found for PEM7, in which removing *Rim15* results in an overall increased phosphorylation of proteins that are involved in ion transporter activities (**Figure 3.4C**). Those results suggest an antagonistic relationship between *Rim15* and those phosphorylation events. Overall, *Rim15* was found to have a regulatory impact on protein and phosphorylation events associated with translational regulation (WPM 2, 3, 4 & PEM 3, 6, 7) (**Figure 3.3 & 3.4**).

To further investigate the potential phosphorylation substrates and proteins of *Rim15* during quiescence establishment under two nutritional starvation conditions, we used analysis of covariance (ANCOVA) to compute the significance of *Rim15*'s impact on the overall dynamic of every phosphorylation event in two starvation conditions (**Methods**

and materials). Comparable numbers of significant differentially phosphorylated sites were found in both starvation conditions. Specifically, 46 phosphorylation sites were upregulated in wildtype when starved for carbon, 49 were upregulated in wildtype when starved for phosphorus (**Figure 3.5A)**. We applied GSEA onto the ranked proteins list whose phosphorylation events are differentially expressed (p.adjust < 0.05) (**Methods and materials**). Interestingly, proteins of phosphorylation events involved in similar functions (process involved in translation) were upregulated in wild type cells in both starvations (**Figure 3.5B**). Those results are consistent with our hypothesis that the functional targets of *Rim15* in regulating quiescence are primarily related to translational activity.

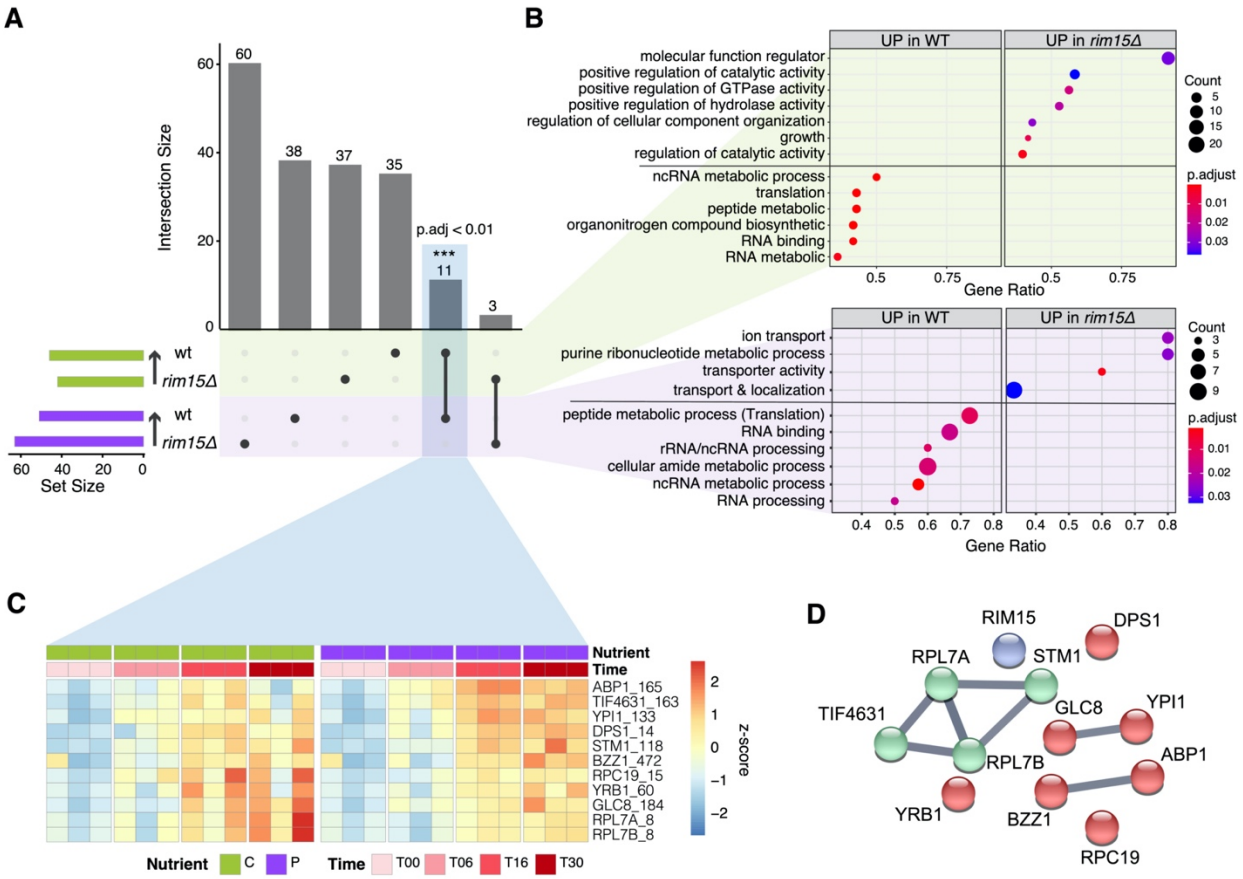

Figure 3.5. Functional annotation of *Rim15* on proteome and phosphoproteome profiling during quiescence establishment.

A) Summary of common and distinct differential protein phosphorylation events between wildtype (wt) and *rim15Δ* calculated as a function of time of starvation. **B)** GSEA for significant DE phosphorylation events between wt and *rim15Δ* in response to carbon (light green shade) and phosphorus starvation (light purple shade). **C)** Heatmap of 11 upregulated proteins in wildtype cells under both carbon and phosphorus starvations. DE dynamics Log2(wt/*rim15Δ*) for each timepoint and replica during quiescence entry. **D)** Known relationships among 11 proteins whose phosphorylation is dependent on *Rim15*.

3.3.10 Eleven novel potential targets of *Rim15*

Interestingly, 11 protein phosphorylation events were found to be commonly regulated by *Rim15* in both starvation conditions (p.adj < 0.01, hypergeometric test) (**Figure 3.5A & 3.5C**). To further check the differential expression of each phosphorylation site and the corresponding proteins over time, we calculated the fold change (expressed as a log2 value) of each phosphorylation event between WT and *rim15Δ* at each timepoint, and plotted the z-score scaled value for visualization purposes. An obvious gradual up-regulation was seen for all phosphorylation events over time with slightly different dynamics (**Figure 3.5C**), which is not a result of increased protein levels (**Figure 3.S5C**). The defined phosphorylation events are found to be involved in diverse biological processes. These proteins are composed of three functional groups: **1)** actin associated proteins (2 proteins): ABP1 (165) & BZZ1 (472) where ABP1 is an actin binding protein, which is mediated by PHO85 and BZZ1 in regulating actin polymerization. **2)** Subunits of protein phosphatase 1 (Glc7p) (2 proteins): YPI1 (133) - phosphatase inhibitor, overproduction will repress the production of glycogen, which is a key metabolite that quiescent cells accumulated for long term survival; GLC8 (184) - involved in glycogen metabolism and chromosome segregation. **3)** Proteostasis associated proteins (7): translation initiation factor - TIF4631(163), ribosome proteins - RPL7A (8) & RPL7B (8), STM1(118) - required for optimal translation under nutrient stress, RPC19(15) - RNA polymerases I and III, DPS1(14) - tRNA synthetase, YRB1(60) - ubiquitin-mediated protein degradation during the cell cycle. We searched for known protein-protein relationships between these proteins using the STRING database. Although some

proteins are known to interact with each other none of those proteins has previously been identified as being a direct target of *Rim15* (**Figure 3.5D**).

To further analyze the functional requirements of putative phosphorylation targets of *Rim15* in each condition, we examined the previously quantified survival of genes (S. Sun et al. 2020) encoding these proteins. Overall, there are 20 and 30 genes/proteins were found in both studies for carbon and phosphorus starvation, respectively. Not all proteins whose phosphorylation events are dependent on *Rim15* have a reduced survival in quiescence. 6/20 (-C) and 17/30 (-P) have a negative survival rate in our genetic screening, with the extreme case of SNF1 in carbon starvation and IGO1 in phosphorus starvation.

3.4 Discussion

In this study, we undertook a thorough analysis of proteome and phosphoproteome dynamics during quiescence initiation in response to distinct nutrient starvations: carbon and phosphorus. Our analysis of expression of 1,277 proteins and 1,472 phosphorylation events, ascribed to 785 phosphoproteins, reveals that proteome and phosphoproteome remodeling in quiescent cells is largely dependent on the pro-quiescent signals. In contrast to the global downregulation in the proteome with no substantial changes after T16 (cell established quiescence), the phosphoproteome continues to exhibit dynamic changes after entering quiescence.

Consistent with previous studies, mitochondrial proteins were found to be upregulated in quiescence under carbon starvation (Davidson et al. 2011). However, those proteins are only transiently upregulated in phosphorus starvation. These results suggest that mitochondrial activity is essential for preparing cells for quiescence independent of the starvation signals. This hypothesis is further supported by removing *Rim15*. *rim15Δ* cells do not affect survival in carbon starvation nor the expression of mitochondrial proteins. However, in the absence of *Rim15*, cells failed to survive long-term under phosphorus starvation or upregulate mitochondrial proteins. Our results are in line with a previous study of amino acid starvation, in which it was show that successful starvation response is correlated with expression of genes encoding oxidative stress response and mitochondrial functions regardless of the starvation nutrient (Petti et al. 2011). These observations may be functionally related to mitochondrial re-organization during quiescence entry (Laporte, Gouleme, et al. 2018), and the causative relationship between mitochondrial re-organization and the upregulation mitochondrial proteins would be an interesting topic for future investigation.

Genetic perturbation revealed new roles of the evolutionary conserved Serine/Threonine kinase *Rim15* in quiescence establishment by mediating the phosphorylation of proteins involved in both transcription and translation. We have also assessed the role of *Rim15* on proteome and phosphoproteome of quiescent cells and found that *Rim15* has different functional impacts on proteome remodeling when starved for different nutrients, but minimal impacts were found on the remodeling dynamics of phosphoproteome between conditions (**Figure 3.S4A & Figure 3.S5B**). By looking at the

overall trend of differentially expressed phosphorylation events between wildtype and *rim15Δ*, we found additional evidence for *Rim15* in regulating protein homeostasis via mediating the phosphorylation of proteins involved in translation and amino acid metabolism (**Figure 5B**). Interestingly, common functional enrichment was found for those proteins whose phosphorylation is regulated by *Rim15* between starvations including processes involved in RNA processing (including rRNA, ncRNA and mRNA) and translation (peptide metabolism). Our finding broadens the functional spectrum of *Rim15* in regulating quiescence as a central mediator of transcription to translation.

We have demonstrated the possibility of using SILAC with prototrophic strains in both rich and minimal starvation conditions. However, a reduced identification of heavy isotope ($^{13}C_6{}^{15}N_2$-lysine/$^{13}C_6{}^{15}N_4$-arginine) labeled samples was exclusively found in nitrogen starvation regardless of the genotype. Similarly, medium isotope (D4-lysine/$^{13}C_6$-arginine) labeled samples also show reduced identification but to a milder extent. This probably is caused by different amino acid catabolism mechanisms in response to nitrogen starvation. A literature research have shown that in response to nitrogen starvation, cells start to accumulate basic amino acids (e.g. lysine and arginine) in vacuoles, and this accumulation will change the concentration gradient in the cytoplasm which in turn will inhibit the intake of exogenous amino acids (Woodward and Cirillo 1977). In combination with the highly activated autophagy pathway under nitrogen starvations (Tyler and Johnson 2018), cells catabolize internal amino acids and incorporate derivatives with heavy atoms on amino acids other than lysine and arginine.

Overall, our multi-layer proteomics profiling and functional studies define the landscape of the quiescent proteome and phosphoproteome and reveal dynamics of signaling, biogenesis, bioenergetics pathways and the functional basis of *Rim15* in quiescence entry of yeast cells. Our study provides a comprehensive resource of proteome regulation and protein phosphorylation events during quiescence entry in budding yeast across different starvations conditions, uncovers that *Rim15* signaling impinges on multiple pathways in the balancing proteome synthesis and degradation, and lays the groundwork for future mechanistic studies of the regulation of protein turnover at the systems level.

3.5 Methods and materials

3.5.1 Strains, Cell Culture Conditions and SILAC Labeling

All experiments were done with s288c isogenic strains. In the incorporation test, three s288c isogenic strains were used: prototrophic FY4 (*MATa*), auxotrophic strain derived from FY4 (*MATa* lys2Δ0 arg6Δ0) and prototrophic *rim15Δ* (*MATa* rim15::kanMX) created from FY4 - deletion confirmed by PCR and whole genome sequencing. In the proteomic and phosphoproteomic experimental setup, prototrophic FY4 (*MATa*) and *rim15Δ0* (*MATa* rim15::kanMX) were used. SILAC experiments for incorporation tests were performed in cells with three different genotypes grown in SD medium containing the amino acid dropout mixture depleted in arginine and lysine. SILAC media were then supplemented with light, medium or heavy isotopes of arginine and lysine (L-lysine/L-

arginine, D4-lysine/$^{13}C_6$-arginine, $^{13}C_6{}^{15}N_2$-lysine/$^{13}C_6{}^{15}N_4$-arginine – sigma). For quantitative SILAC experiments in starvation conditions, cells were first cultured in SILAC medium supplemented with either of the three combinations of isotopes labeled medium for 10 generations for isotope incorporation and then cells with the same genotype were pelleted and washed twice with water before transferring into the corresponding isotope supplemented nutrient limited medium. Cells after labeled in SILAC medium were split into three equal portions and inoculated into 300ml of nutrient depleted/limited medium: for glucose- (C, 0.06% glucose), ammonia- (N, 0 mM nitrogen), and phosphorus- (P, 0 mM phosphorus) with an initial concentration around 2 x 10^6 cells/ml. A small amount of glucose was added in glucose depleted medium for allowing cells to double for 2-3 times after nutrient removal to match with the growth phenotype observed in nitrogen and phosphorus depleted conditions. For viability quantification at each time point, 1 × 10^7 cells were collected and subsequently washed once with sterilized DI water and one more time with PBS. The washed cell pellet was resuspended with 1mL 1 x PBS and stained with 3.34μM of SYTO® 9 and 20μM of propidium iodide for 20 minutes. The stained samples were then analyzed by flow cytometry (BD Accuri™ C6). To track the proteome and phosphoproteome remodeling during quiescence establishment in response to three nutritional starvations, we performed three independent experiments for each genotype (wt and *rim15Δ*) per nutrient limiting conditions. In total, we had 2 genotypes collections × 3 biological replicates × 3 nutrient limiting conditions. To model the dynamics of protein and phosphoproteome remodeling, we collected three time points after transferring the

sample into a nutrient depleted medium at T=6h, T=16h, and T=30h. T00 samples were collected from the SILAC medium right before cell transfer.

3.5.2 Protein extraction, pooling and digestion

3 x 10^8 cells were pelleted and washed twice with ice cold PBS before flash freezing, a technical replica was also collected. Sample were randomized for protein extraction and digestion for minimizing technical variations. After thaw on ice, cells were disrupted by glass-bead agitation at 4 °C in standard buffer: 50 mM Tris-HCl pH 7.5, 150 mM NaCl, 20 mM iodoacetamide (IAM), 1x cOmplete protease inhibitor (Roche) and 1x phosphatase inhibitor cocktail (PhosphoSTOP, Roche). The extract was cleared by centrifugation and protein concentration was determined by Bradford assay (BioRad). Cell lysate extracted from different genotypes under the same starvation treatment at the same time point were then mixed at equal amount with the external spike-in (wild type cells in log stage from rich medium) at 1:1:1. Approximately 600 µg of the mixed light/medium/heavy/ protein sample was processed for in-solution digestion as previously described (Monteoliva et al. 2011). Proteins were reduced with 5 mM DL-Dithiothreitol (DTT) for 30 min at 37°C and alkylated with 10 mM iodoacetamide for 30 min at 30°C. Samples were diluted six times with 25 mM ammonium bicarbonate, trypsin/lysC (Promega, Spain) was added to the protein mixture at a 25:1 protein:protease ratio (w/w), and samples were incubated overnight at 37°C. Digestion was stopped by addition of formic acid.

3.5.3 Phosphopeptide enrichment

Enrichment for phosphopeptide was done using Pierce™ TiO2 Phosphopeptide Enrichment and Clean-up Kit. All digested peptides were desalted with C18 according to previous study (Villén and Gygi 2008). Then, an aliquot of 10 µg peptides was separated to be further processed and analyzed without phosphopeptide enrichment. All rest samples were then processed with the TiO2 according to the user manual. Samples representing the whole proteome were solubilized in 15 ul of 2% ACN 0.5% AcOH and 2 ul were analyzed by LC-MS/MS. Enriched phosphopeptides were solubilized in 10 ul of 2% ACN 0.5% AcOH and 5 ul were analyzed by LC-MS/MS.

3.5.4 Mass Spectrometry

LC separation was performed online on EASY-nLC 1000 (Thermo Scientific) utilizing Acclaim PepMap 100 (75 um x 2 cm) precolumn and PepMap RSLC C18 (2 um, 100A x 50 cm) analytical column. Peptides were gradient eluted from the column directly to Orbitrap HFX mass spectrometer using 160 min ACN gradient from 5 to 26 % B in 118 min followed by ramp to 40% B in 20 min and final equilibration in 100% B for 15 min (A=2% ACN 0.5% AcOH / B=80% ACN 0.5% AcOH). Flowrate was set at 200 nl/min.

For whole cell digests high resolution full MS spectra were acquired with a resolution of 120,000, an AGC target of 3e6, with a maximum ion injection time of 32 ms, and scan range of 400 to 1600 m/z. Following each full MS scan 20 data-dependent HCD MS/MS scans were acquired at the resolution of 7,500, AGC target of 2e5, maximum ion time of

32 ms, one microscan, 1.4 m/z isolation window, nce of 27 and dynamic exclusion for 45 seconds.

For phosphopeptides analysis high resolution full MS spectra were acquired with a resolution of 120,000, an AGC target of 3e6, with a maximum ion injection time of 100 ms, and scan range of 400 to 1600 m/z. Following each full MS scan 20 data-dependent HCD MS/MS scans were acquired at the resolution of 30,000, AGC target of 5e5, maximum ion time of 100 ms, one microscan, 1.4 m/z isolation window, nce of 27 and dynamic exclusion for 45 seconds.

3.5.5 Protein identification

MS data were analyzed using MaxQuant software version 1.6.3.4 and searched against the *S. Cerevisiae* reference database (http://www.uniprot.org/) containing 6,721 entries. Multiplicity was set to three, matching the number of SILAC labels used (“light,” “medium,” and “heavy”) in each experiment; Lys-4/Arg-6 and Lys-8/Arg-10 were specified as medium and heavy labels, respectively. Database search was performed in Andromeda integrated in the MaxQuant environment. A list of 248 common laboratory contaminants included in MaxQuant was also added to the database as well as reversed versions of all sequences. For searching, the enzyme specificity was set to trypsin with the maximum number of missed cleavages set to 2. The precursor mass tolerance was set to 20 ppm for the first search used for non-linear mass re-calibration and then to 6 ppm for the main search. Oxidation of methionine was searched as variable modification; carbamidomethylation of cysteines was searched as a fixed modification. For

phosphopeptides samples phosphorylation of serine, threonine and tyrosine residues was also included as a variable modification. The false discovery rate (FDR) for peptide, protein, and site identification was set to 1%, the minimum peptide length was set to 6. To transfer identifications across different runs, the 'match between runs' option in MaxQuant was enabled with a retention time tolerance of one minute (after data-dependent nonlinear retention time recalibration).

3.5.6 Data analysis

Subsequent data analysis was performed using the R environment for statistical computing and graphics. The triple SILAC experiments were combined to get a ratio profile for each protein and phosphorylation event across the four time points relative to the "light labeled" internal control. The median normalized ratios were used for downstream analysis, with the maximum variation between genotypes and minimum variation across biological replicates. Only proteins and phosphorylation events (P-events) that have valid value over 75% out of the passed filter samples (including 3 biological replicate, 2 genotypes, 2 nutritional conditions and 4 timepoints) were considered for further quantitative analysis to get a full dataset by imputing the rest 15% data in R.

3.5.6.1 Differential expression analysis of proteome and phosphoproteome

DE events during quiescence entry were defined by identifying proteins/peptides with between-timepoint, genotype, nutrient variance significantly larger than within-replicate variance using ANOVA (analysis of variance). Specifically, we applied a two-step

procedure to define DE events as follows: (i) Calculate F statistic and P values (defined as the ratio of between-group variance relative to within-group variance) for each protein. The P value distributions are skewed towards 0 (data not shown), indicating a large number of DE proteins and peptides during quiescence entry (ii) Correct P values for multiple testing. We applied the Benjamini-Hochberg (BH) method, and then selected the DE proteins and phosphorylation events by applying a threshold of corrected P value (0.05).

3.5.6.2 Weighted gene co-expression network analysis (WGCNA) clustering analysis

The analysis (B. Zhang and Horvath 2005) was carried out with the WGCNA R package (Langfelder and Horvath 2008). To define whole proteome co-expression module (i.e. WPMs), only the 1,067 DE proteins were considered. Pearson correlation matrix (with direction, i.e. for building signed co-expression network) was calculated using the 42 passed filtered samples of these DE proteins, and an adjacency matrix was calculated by raising the correlation matrix to a power of 6 using the scale-free topology criterion (B. Zhang and Horvath 2005) with modifications. Co-expression modules were defined by hybrid dynamic tree-cutting method (Langfelder, Zhang, and Horvath 2008) with the minimum height for merging modules at 0.25. For each co-expression module, a consensus trend was calculated based on the first principal component (also known as eigengene) and cluster membership was defined as Pearson correlation between individual protein and the consensus of the WPM. Proteins were assigned to the most

correlated co-expression cluster (i.e. WPM) with a cutoff of r of at least 0.7. Individual WPM was annotated using two pathway databases (Gene Ontology and KEGG) by Fisher's exact test (with BH FDR < 0.05). Phosphoproteome co-expression modules (PEMs) were also defined by the same procedure but with an adjacency matrix calculated by raising the correlation matrix to a power of 8 using the scale-free topology criterion.

3.5.6.3 Differential expression dynamic quantification using ANCOVA

In each model per protein or per phosphorylation event, the two different genotypes (wt and *rim15Δ*) are treated as independent categorical variables, sampling time is the covariate, and the normalized ratio at different time points is the dependent variable. We quantified the dynamic difference for each protein and phosphorylation events using ANCOVA in R by the following function:

$$lm\,(Normalized\,ratio\ \sim\ Time\ *\ Genotype)$$

Where $Time$ is the hours post nutrient removal being: 0hr, 6hr, 16hr, 30hr. $Genotype$ is the proteome and phosphoproteome profiling for cells with two different genotype backgrounds: wt and *rim15Δ.* The different genotypes in this function is the interaction term, which was used to test for statistical significance. The P value distributions are skewed towards 0 (data not shown), indicating a large number of DE proteins and peptides during quiescence entry. We then correct P values for multiple testing by applying the Benjamini-Hochberg (BH) method, and then select the DE proteins and

phosphorylation events by applying a threshold of corrected P value (0.1). The resulting lists for both proteomic and phosphoproteomic data were then subject to Gene Set Enrichment Analysis using $clusterProfiler$function in R(Guangchuang Yu et al. 2012).

3.6 Supplementary figures

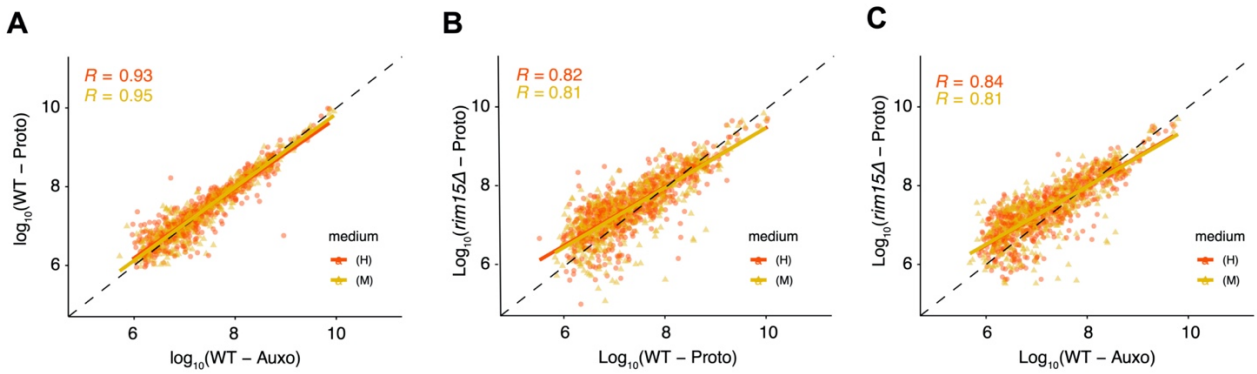

Figure 3.S1. Whole proteome comparison between SILAC studies using different genotypes.

A) Scatter plot for proteomes identified by SILAC using auxotrophic (*lys2Δ arg6Δ*) wildtype (x-axis) and prototrophic wildtype (y-axis). Pearson correlation is indicated with the same color code. **B)** Scatter plot for proteomes identified by SILAC using prototrophic wildtype cells (x-axis) and prototrophic *rim15Δ* cells (y-axis). **C)** Scatter plot for proteomes identified by SILAC using auxotrophic wildtype cells (x-axis) and prototrophic *rim15Δ* (y-axis).

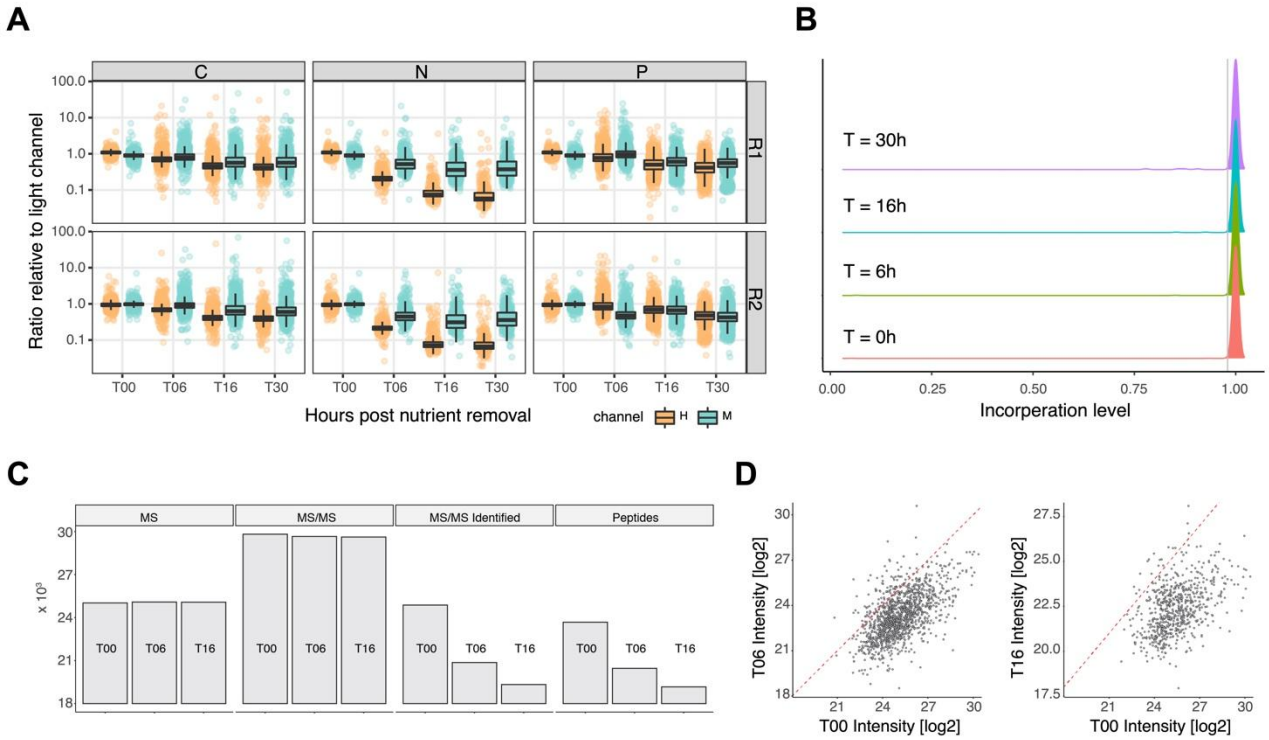

Figure 3.S2. Reduced identification of nitrogen starved protein is caused by incorporation of heavy isotopes into amino acids other than lysine or arginine.

A) Un-normalized ratios of heavy and medium channels from two biological replicates show striking signal reduction as cells initiate quiescence in response to nitrogen starvation. **B)** Incorporation efficiency is not reduced over time. Density function of heavy label (Lys-8, Arg-10) incorporation of all isotope-containing peptides for prototroph *S. cerevisiae* S288c strain. A 98% incorporation level is indicated on the plot as a vertical grey line. **C)** MS/MS analysis of heavy isotope labeled cells collected at T=0h, T=6h, and T=16h prior to mixing with heavy isotope labeled cells. **D)** Scatter plot showing the intensity for all identified proteins over time.

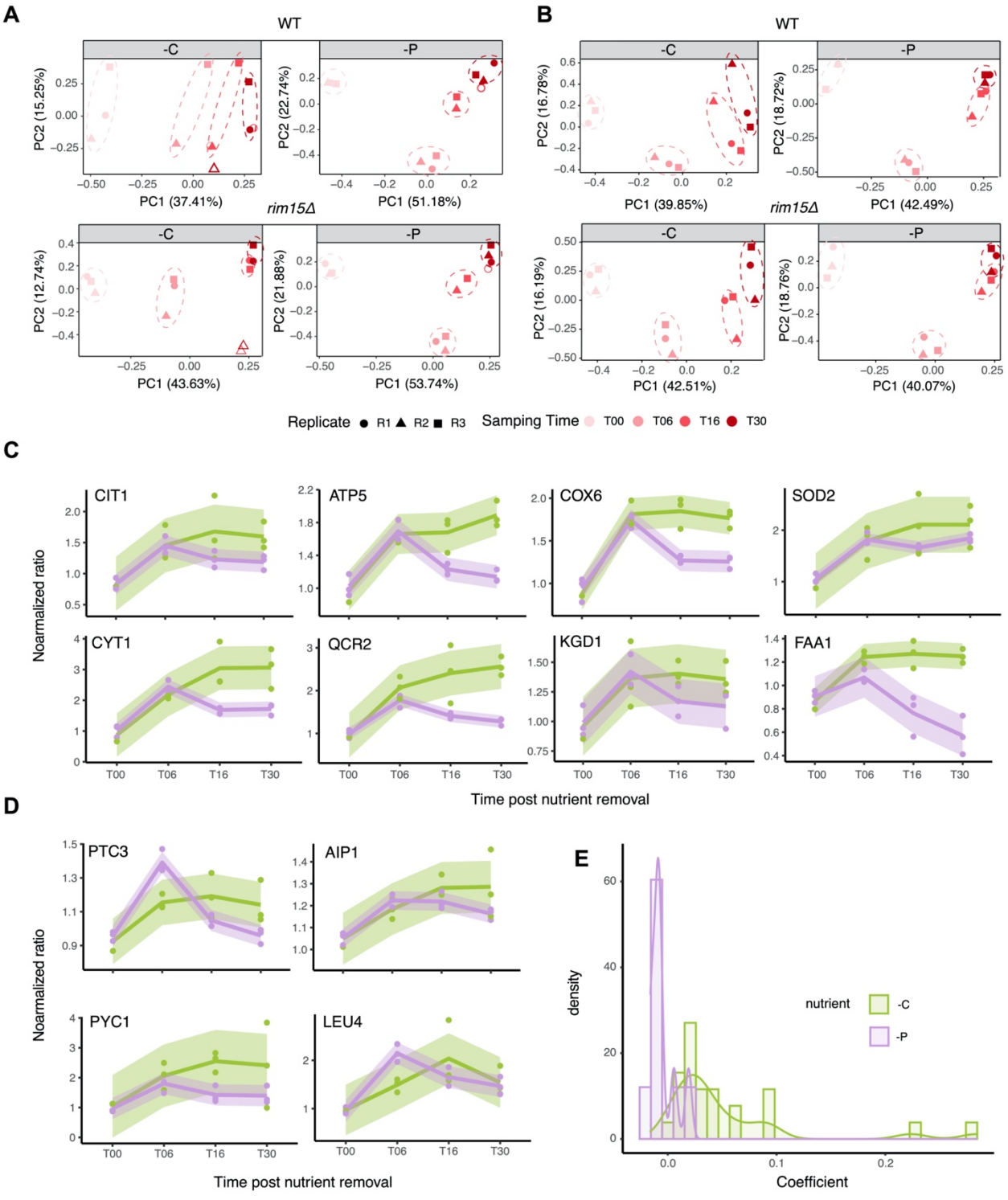

Figure 3.S3. Quality check of our data with published results.

A) Principal-component analysis of whole proteome data. Replicates from different time points

(red gradient color) post nutrient restriction cluster together and are dispersed largely along the 1st principal component. **B)** Principal-component analysis of phosphoproteome data. Replicates from different time points (red gradient color) post nutrient restriction cluster together and are dispersed largely along the 1st principal component. **C)** Representative examples of known quiescence-specific upregulated proteins that are uniquely localized to mitochondria (Davidson et al. 2011) in carbon (green line) and phosphorus (purple line) starvation induced quiescent wild type cells. Solid line is connecting the mean at each timepoint with the shadow indicating standard error. **C)** Representative examples of additional quiescence-specific upregulated proteins (Davidson et al. 2011) in carbon (green line) and phosphorus (purple line) starvation induced quiescent wild type cells. **E)** Density plot for all coefficients of the linear regression model fitted for 44 proteins in wild type cells under carbon or phosphorus starvation.

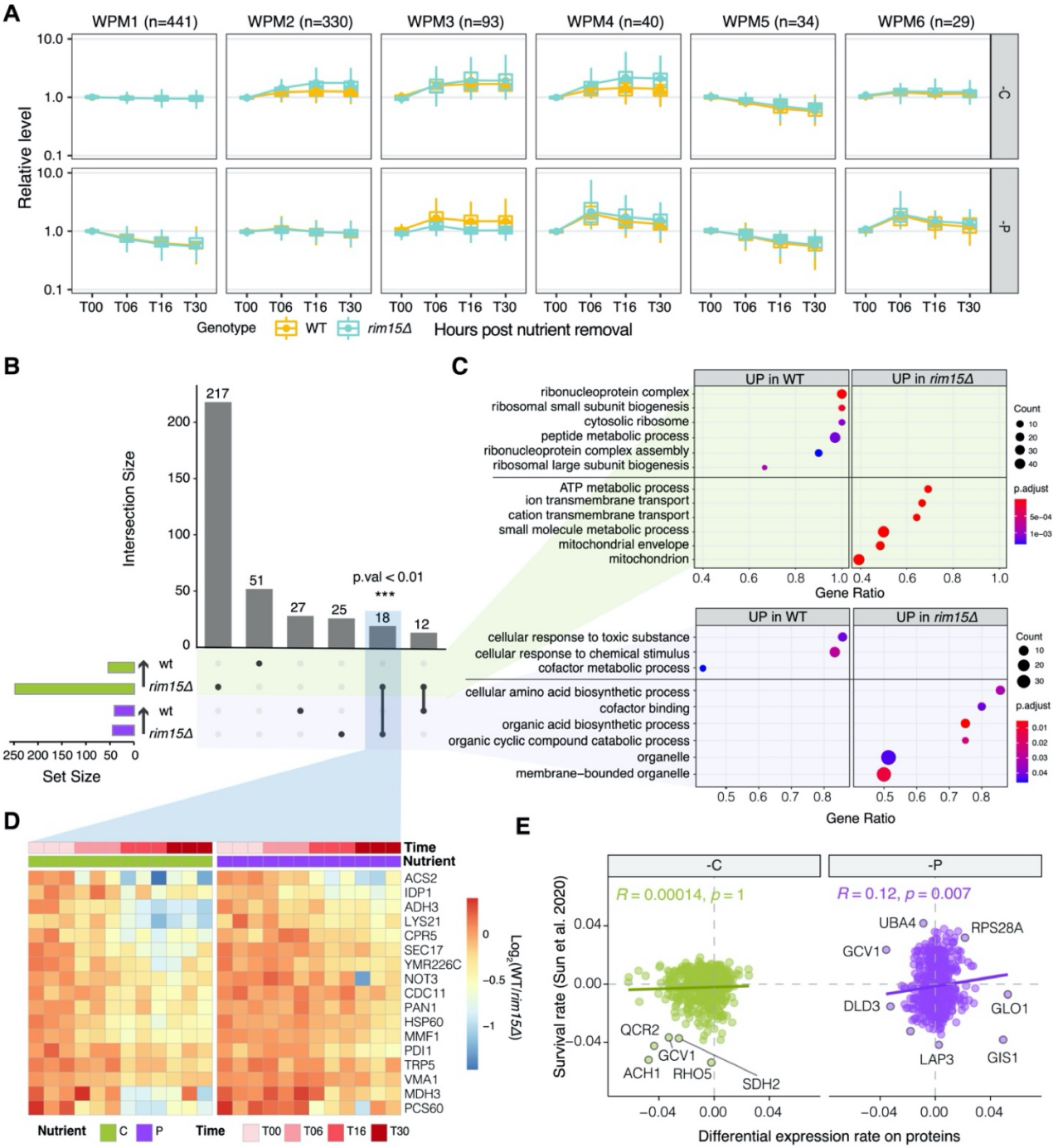

Figure 3.S4. Functional impact of Rim15 on whole proteome profiling.

A) Proteome dynamics of six co-expression whole proteome modules (WPMs) in two different starvation conditions. The expression distribution for all proteins in each module is plotted (colored by genotypes, yellow - wiltype; sky blue - *rim15Δ*) and the mean of each distribution per cluster is connected by lines. **B)** Summary of common and distinct differentially expressed

proteins between wt and *rim15Δ* calculated as a function of time of starvation. One single protein was found to be upregulated in wild type cells in both conditions: SBP1 (did not shown on the plot), which binds to eIF2 and represses translation and forms P bodies by binding to mRNAs under carbon starvation (Segal, Dunckley, and Parker 2007). **C)** GSEA for significant DE proteins between wt and *rim15Δ* in response to carbon (light green shade) and phosphorus starvation (light purple shade). **D)** Differential expression [Log_2(wt/*rim15Δ*)] patterns of 18 commonly up regulated proteins in *rim15Δ* under both starvations over time. **E)** Comparison between survival rate (y-axis) estimated by gene deletion analysis (S. Sun et al. 2020) and the dynamics of differential expressed proteins (x-axis). Pearson correlation is indicated with the same color code on the plot.

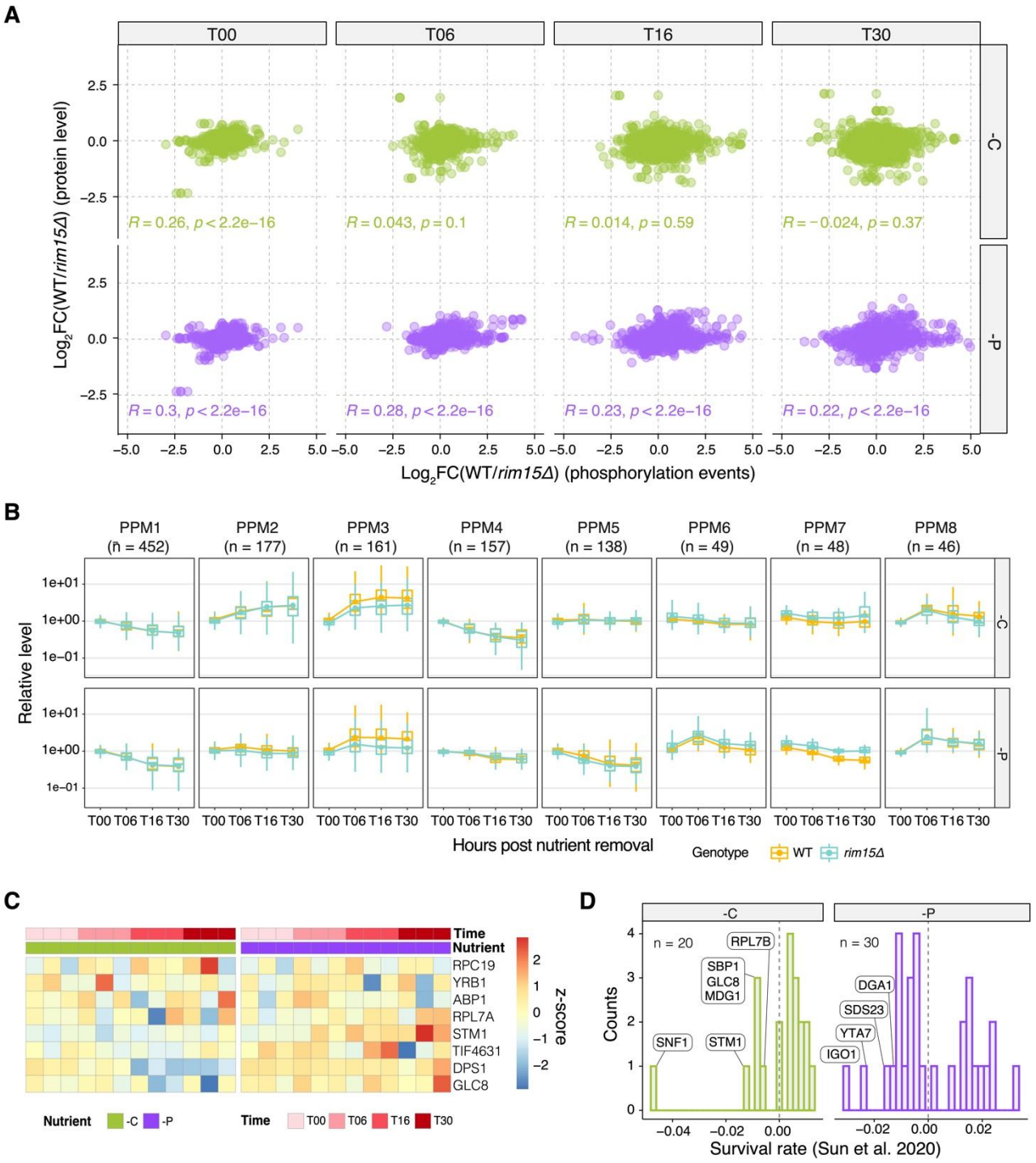

Figure 3.S5. Functional impact of Rim15 on phosphoproteome.

A) Distribution of phosphoproteome dynamics in eight co-expression modules of phosphorylation sites (PPM) in both cell types. Expression distribution for all proteins in

each module is plotted (colored by starvation conditions, purple - phosphorus starvation; green - carbon starvation) and the mean of each distribution per cluster is connected by lines. **B)** Expression of 11 proteins whose phosphorylation events are found to be commonly regulated by Rim15 in both starvation conditions (**Figure 5A**). For visualization purposes, data were scaled by rows. **C)** Viability of significant differential protein phosphorylation sites per condition (S. Sun et al. 2020).

Chapter 4 : Characterization of molecular and biophysical properties of quiescent cells

4.1 Abstract

A couple of technical obstacles in studying quiescence are impeding our understanding of quiescence, including: 1) lacking a consensus definition of quiescence; 2) difficult to collect a large quantity of non-dividing cells; 3) most experimental tools are only optimized for proliferative cells. Although multiple physical and cellular alterations occur in quiescent cells, none of them is individually well-suited as a marker of quiescence as discussed in Chapter 1. Lack of a universal marker that can be used for identifying and isolating quiescent cells induced under different pro-quiescence cues has precluded progress in understanding quiescence. Identification of an evolutionarily conserved marker of quiescent cells would represent a significant technical advance. Toward this goal, we tested the feasibility of using physical markers and molecular markers for identifying and isolating quiescent cells induced by different nutritional starvations. We find that isolation of quiescent cells using percoll gradient separation based on increased density is the most efficient way to isolate a large quantity of quiescent cells across all starvation conditions. No molecular marker was founded to be suitable as their expression level in quiescent cells largely overlaps with that observed in proliferative cells. Lastly, we compared the biophysical properties of the cytoplasm in quiescent cells induced under different starvations and found that molecular crowding is increased in quiescent cells starved for different essential nutrients. This suggests a universal strategy used by cells

to survive different starvations as quiescent cells.

4.2 Introduction

Although quiescent yeast cells have distinct physiological features that distinguish them from proliferating cells, (**Figure 1.1B**) (Lillie and Pringle 1980), we still lack a universal marker that can be used for identifying and isolating quiescent cells induced under different starvations or pro-quiescence cues. Previous quiescent studies in budding yeast have mostly been limited to considering all cells in the stationary phase, which is a highly heterogeneous and dynamic population composed of quiescent and senescent cells. These cellular states are hardly distinguishable without triggering proliferation resumption, hampering thus the study of quiescent cells properties. Multiple strategies have been proposed for isolating quiescent sub-populations out of stationary phase mixture based on different physical characteristics (Allen et al. 2006; L. Li, Miles, and Breeden 2015). One of these methods is percoll gradient fractionation that isolates denser and faster migrating quiescent cells which usually have increased storage of carbohydrate and reduced cell volume. Alternatively, the Breeden lab has developed a staining method using SytoxGreen (a DNA intercalating dye) that makes use of the fact that quiescent cells have fortified cell walls that makes dye penetration inefficient. Both methods provide tools for enriching quiescent cells, but further assessment is needed for applying these methods in different contexts, such as in response to different pro-quiescent signals.

Quiescence entry is usually accompanied with global repression of multiple cellular

activities including transcription, translation, and metabolism. Nonetheless, there are certain genes whose expression is upregulated in quiescent cells compared to cells in proliferative growth (H. a. Coller 2011; Klosinska et al. 2011; H. A. Coller, Sang, and Roberts 2006). One study found that the whole transcriptome is dramatically remodeled at the onset of starvation and distinct expression signatures were found in response to distinct starvation signals (Klosinska et al. 2011). However, as time progresses, a common transcriptional program was found across all conditions. Overall, 82 genes were identified as being transcriptionally upregulated in all starvation (carbon, nitrogen and phosphorus) induced quiescent cells with more than two-fold change compared to cells in log phase(Klosinska et al. 2011). It is worth noting that those genes do not exhibit a growth rate-specific pattern of expression, which suggests their increased expression is specific to quiescent cells. However, whether those quiescence specific transcripts are also upregulated at the protein level is not known.

The transition from proliferation to quiescence is also coupled with various physicochemical changes at the cellular level, such as lowered cytosolic pH and decreased macromolecule mobility in the cytoplasm (Joyner et al. 2016; Ashe, De Long, and Sachs 2000; Munder et al. 2016). Cytoplasmic crowding in a cell is highly dynamic and changes in response to stress conditions such as heat shock, osmotic stress, energy depletion, and nutrient starvation (Marini et al. 2020; Mourão, Hakim, and Schnell 2014; Delarue et al. 2018; Riback et al. 2017; Munder et al. 2016). Dysregulated homeostasis of cytoplasmic crowding can contribute to cell death (Neurohr et al. 2019). In yeast, the cytoplasm appears to undergo a transition from a fluid like material to a glass like material

under glucose starvation, which may be important for long-term survival under stress conditions (Munder et al. 2016). As the majority of metabolic reactions, protein translation, and signaling processes take place in the cytoplasm, induced changes in its physicochemical properties of the cytoplasm may be required for the cell to transition into a quiescent state. However, the extent to which the biophysical properties of the cytoplasm change in response to different pro-quiescence signals and the dynamics, functional consequences, and regulators of these changes are largely unknown.

In this chapter, I first tested the utility of established methods for defining quiescent cells in different nutrient starvation conditions using the yeast strain, S288c. Then I screened known transcriptionally up-regulated genes in defined starvation conditions and tested their utility as universal molecular markers of quiescent cells. Lastly, I compared the biophysical properties of quiescent cells induced by different types of starvation.

4.3 Results

4.3.1 Testing established isolation methods in defined nutritional starvations

To test the feasibility of extending previously described methods for isolating quiescent cells induced by different nutrient starvations, wild type cells were cultured in three different nutrient limited conditions: carbon (-C, 0.08%), nitrogen (-N, 800μM), and phosphorus (-P, 5mg/L) (**Table 2.2**). Samples were collected 2 days post inoculation, at which point all cells had arrested growth. We tested two protocols: percoll gradient separation (Allen et al. 2006) and SytoxGreen staining (L. Li, Miles, and Breeden 2015)

(**Methods and materials**). We successfully used both methods to isolate and identify quiescent cells from YPD cultures (**Figure 4.1B & C**). In percoll gradient separation, two separate bands were also observed for all defined nutrient starvations, but cells reached equilibrium at different densities (**Figure 4.1B**). Using viability quantification by PI/Syto9 staining, the viable proportion in lower percoll gradient fraction is significantly higher than the overall population (data not shown). Overall, both methods have been successfully tested in the three defined nutritional starvations, but with slightly different outcomes.

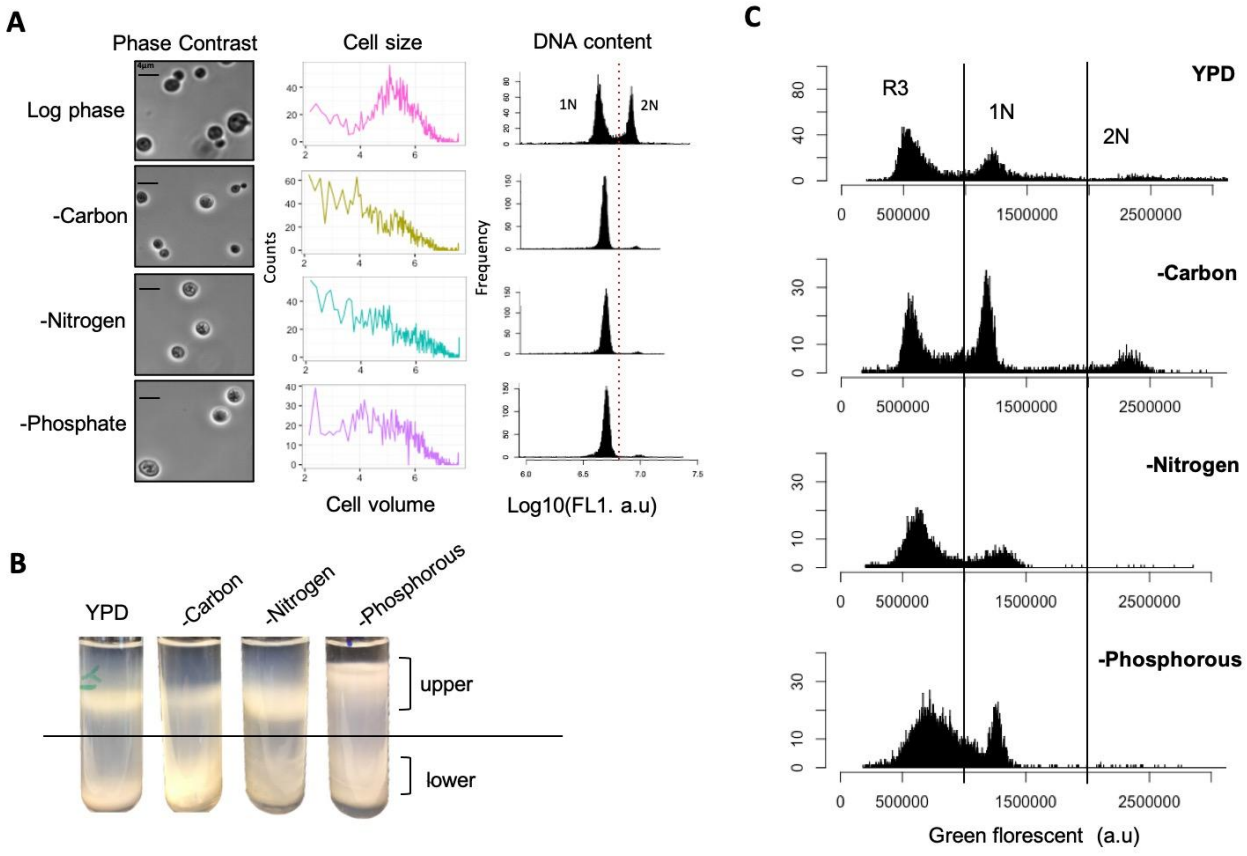

Figure 4.1. Phenotypic characterization in different nutritional starvation induced quiescent cells.

A) Phenotype, cell size and DNA content of cells in log phase and carbon, nitrogen,

phosphorous starved quiescent cells. **B)** Fractionated population in percoll gradient. Upper band is reported as composed of mostly non-quiescent cells, and the lower fraction is enriched for quiescent cells. **C)** Dynamic of R3 population (quiescent cells, with fortified cell wall) during quiescence initiation of carbon, nitrogen and phosphorous starvations.

4.3.2 Screening for universal molecular markers in quiescence

Unlike cells in the mitotic cycle, there are no known genes that specifically and commonly turn on in quiescent cells under multiple stimuli. Previous whole transcriptome analysis found 87 genes are commonly upregulated more than two fold in quiescent cells in the three defined starvations (Klosinska et al. 2011). Those are the genes with the highest potential for being used as molecular markers in quiescence. To verify this, we analyzed 43 genes of those genes at the protein level based on their availability in the existing GFP-fusion library. The 43 protein fusion strains were cultured on a 96 well plate with 1mL medium culture that is limited for one of each nutrient in biological triplicate. The GFP intensity of each strain was determined using flow cytometer (Becton Dickinson Accuri). Samples were analyzed at two timepoints: T=0h (log-phase) and T=48h (quiescence). To eliminate the effects of cell size difference, the GFP signal was normalized by cell size (i.e. forward scatter) before comparison.

Overall, 4 proteins (FLR1, SLX8, JJJ1, and ERG24) out of 43 have consistent upregulation with more than two-fold increase in median signal across three biological replicates in all tested conditions (**Figure 4.2**). These proteins play diverse functions in cellular activities required for maintenance of homeostasis within the cell. For example, FLR1 is known as a multidrug transporter whose expression is essential for survival under drug stress (Alarco, Balan, Talibi, Mainville, & Raymond, 1997). SLX8 is the subunit of

Slx5-Slx8 SUMO-targeted ubiquitin ligase (STUbL) complex that is necessary for the proteolysis of couple proteins involved in DNA replication stress (Schweiggert, Stevermann, Panigada, Kammerer, & Liakopoulos, 2016). JJJ1 is a co-chaperone that stimulates the ATPase activity and is required for ribosome biogenesis (Lee et al. 2016) and ERG24 functions in ergosterol biosynthesis. However, we find that expression of these proteins is not exclusive to quiescent cells, and the expression difference is insufficient for accurate separation of growing and quiescent cells. Consistent with this finding, none of these proteins were recovered in the whole proteomic analysis (Chapter 3).

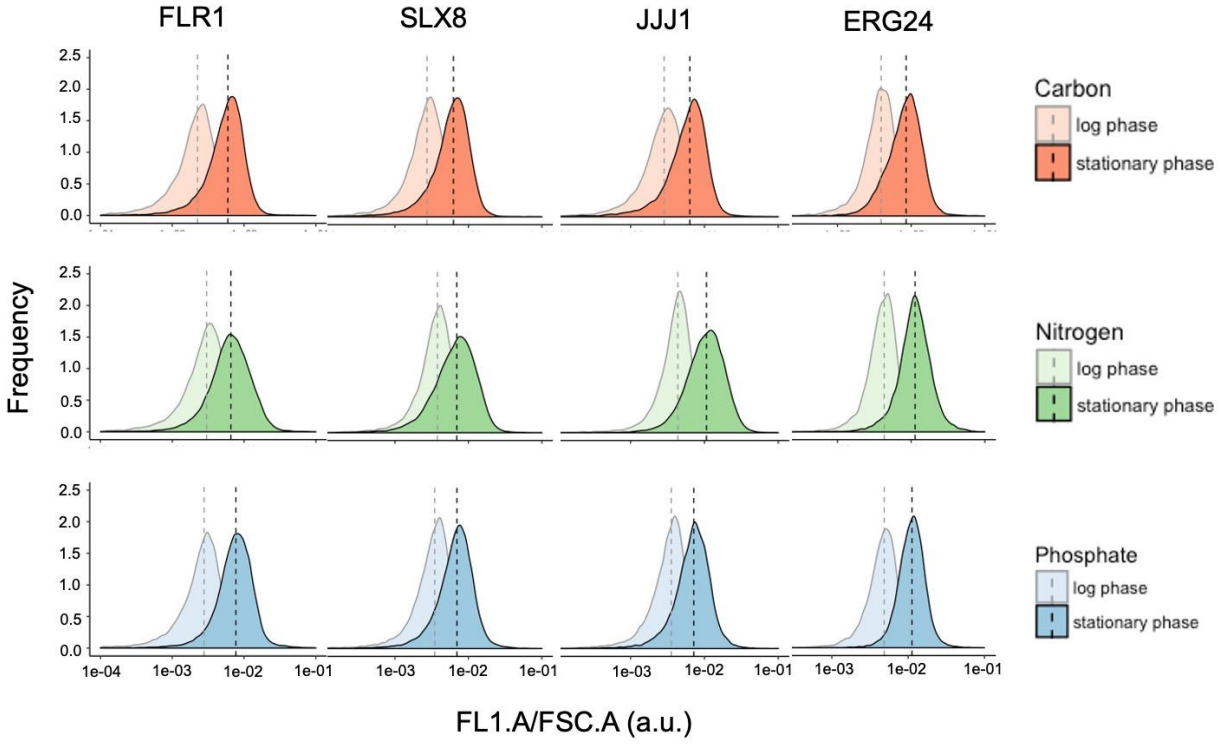

Figure 4.2. GFP signals of four candidate proteins between log phase and stationary phase (quiescence).

The dashed line indicates the median of each distribution. FLR1: Plasma membrane multidrug

transporter. SLX8: subunit of Slx5-Slx8 SUMO-targeted ubiquitin ligase (STUbL) complex. JJJ1: TypeIII J-protein, Co-chaperone that stimulates the ATPase activity of Ssa1p. ERG24: C-14 sterol reductase that acts in ergosterol biosynthesis.

4.3.3 Measuring cytoplasmic crowding in quiescent cells using Genetically Encoded Multimeric nanoparticles (GEMs)

To define the biophysical properties of quiescent cells, we used genetically encoded multimeric nanoparticles (GEMs) as an indicator of cytoplasm crowding. Briefly, a GEM is composed of a single gene that encodes a scaffold protein fused to a fluorescent protein under the same promoter. When the whole cassette is translated, it is assembled into a multimeric protein complex with GFP proteins on the surface, which forms bright fluorescent foci that can be tracked by microscopy (Delarue et al. 2018). The size of GEMs we used is 40nM, which is in the size range of multi-subunit assemblies such as ribosomes. Thus, the movement of GEMs within the cells is informative of the concentration of macromolecular complexes within the cell.

In collaboration with the Holt Lab at NYUSoM, we transformed a plasmid carrying the GEM into a prototrophic S288c withtype strain. To study changes in cytoplasmic crowding in quiescent cells, we starved the GEM strain for the three starvations aforementioned and monitored molecular crowding by tracking GEMs using fluorescent microscopy (**Methods and materials**). As quiescence results in reduced ribosome abundance, which is typically observed in nutrient-deprived cells, we expected molecular crowding to decrease in quiescent cells. However, cells that are starved for carbon exhibit a marked increase in molecular crowding as the GEMs diffusion coefficient is reduced significantly compared to cells in log phase (**Figure 4.3A**), and the fluorescenting particles

tend to aggregat and stuck in the cytoplasm in quiescent cells in contrast to the discrete foci in proliferating cells (**Figure 4.3B**). Interestingly, this increase in crowding is reversible as refeeding cells with carbon results in an increase in the diffusion coefficient of GEMs. These observations are consistent with studies that have relied on the movement of fluorescently tagged proteins in carbon starved cells to assess cytoplasmic properties (Munder et al. 2016; Joyner et al. 2016). Similarly, in response to nitrogen and phosphorus starvation, a reversible increase cytoplasmic crowding was also observed but to different extents, indicating that increased cytoplasmic crowding is a property of all quiescent states.

Increases in molecular crowding in quiescent cells may be a common causative factor underlying changes in macromolecular and organelle structures. Previous studies suggest that decreases in cellular volume may contribute to increased molecular crowding (Joyner et al. 2016). We quantified the cell volume of quiescent cells using a Coulter Counter and found that cell volume decreases in all starvation conditions (**Figure 4.1A**). Using brightfield microscopy we observed that the vacuole is enlarged in quiescent cells compared to proliferative cells in rich medium (**Figure 4.3B**). Those results are consistent with the previous finding that nutrient limitation induces vacuolar fusion, resulting in one enlarged vacuole (Baba et al. 1994). Overall, the expansion of the vacuole may be an important factor contributing to changes in the cytoplasmic properties of quiescent cells to ensure long term survival.

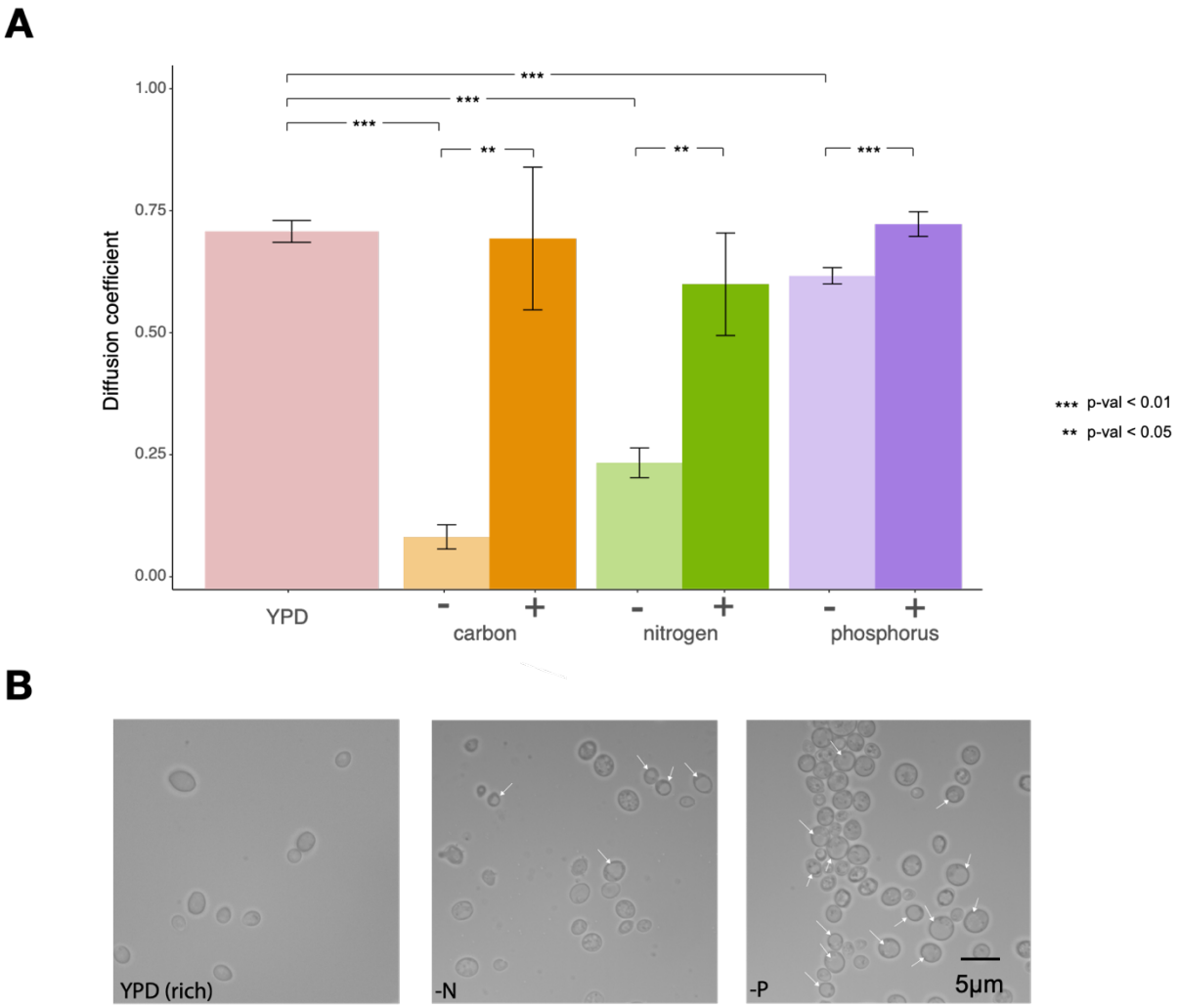

Figure 4.3. Inferring cytoplasmic crowding by estimating diffusion coefficient of GEMs in defined nutritional starvations.

A) Diffusion coefficient of GEM particles in the indicated conditions. Proliferating cells in YPD, 24 hours after carbon, nitrogen and phosphorus starvation (-), 2hours after refeeding cells with the corresponding missing nutrient (+). **B)** Morphology check of vacuoles in cells at proliferative (YPD), nitrogen or phosphorus starved quiescent cells with increased vacuoles indicated by white arrows.

4.4 Discussion

4.4.1 Separation methods based on physical properties are optimized for quiescence isolation in rich medium

In this chapter, I characterized the phenotypic and biophysical feature of quiescent cells under different starvations and found that all three starvation conditions result in quiescent cells with decreased volume, enlarged vacuole, increased cytoplasm crowding and arrested at G0/G1 state with a single copy of the genome (**Figure 4.1A**). In defined starvations, percoll gradient centrifugation allowed us to obtain two distinct layers of cells, with the lower fraction having higher viability compared to the upper layer. However, the migration distance is different based on the nutrient starvation. Similarly, phosphorus starved cells have a less distinguishable R3 population compared to the other two starvations (data not shown). These results suggest that 1) slightly different physical properties are achieved in quiescent cells starved for different nutrients 2) these methods are optimized in YPD medium. Using physical properties to differentiate quiescent cells induced by different means requires further assessment and adjustment in different conditions.

4.4.2 Four proteins show potential as molecular markers

To screen for a universal gene expression marker for defining and isolating quiescent cells, we screened 43 known transcriptionally upregulated genes by quantifying their protein expression using GFP fusion strains. In total, only four genes: FLR1, SLX8, JJJ1, and ERG24 whose median fluorescent signal was found to be upregulated more than

two-fold in all conditions are potentially suitable candidates (**Figure 4.2**). However, their expression is not exclusive to quiescent cells, and the expression difference is not significant enough to separate quiescent cells from the signal found in proliferating cells. The number of genes we screened may limit the conclusions of this study as we have only tested half of the known transcriptionally upregulated candidates. However, our results are still in line with a study in fission yeast that showed a discrepancy between RNA and protein expression (Marguerat et al. 2012). Moreover, use of a single gene marker might be challenging due to the nature of the heterogeneity in quiescent cells, for example different genes might be activated at different degrees within quiescence (**Figure 1.2**). A promising future direction would be finding combinations of genes using multi-colors or combining other labeling metrics such as DNA and RNA labeling.

4.4.3 Cytoplasmic crowding is increased in quiescent cells

Surprisingly, cytoplasmic crowding is increased in quiescent cells in all defined starvations despite the reduced production of ribosomes. This suggests that increased molecular crowding in quiescent cells may be a common causative factor underlying changes in macromolecular and organelle structures. Observation of morphology of quiescent cells indicates that the increased cytoplasmic crowding may be a result of decreased cell volume coupled with enlarged vacuole. However, how different factors coordinately reorganize cytoplasm and prepare cells for quiescence is not known. To further test this hypothesis, a strain that carries free cytoplasmic mCherry and GFP-tagged VPH1 have been constructed in wildtype background. VPH1 is a subunit of the

vacuolar-ATPase V0 domain that effectively stains the membrane of the vacuole (Toulmay and Prinz 2013). This strain will allow us to quantify the ratio of cytoplasmic and vacuoles by imaging fluorescent signals using confocal during quiescence entry, and quantitatively tracking the changing ratio of cells and cytoplasm/vacuole. In addition, this system can be introduced with other strains that carry mutations of interest, such as Rim15, for future testing of the functional impact of vacuole expansion in cytoplasmic crowding and quiescence.

4.5 Methods and materials

4.5.1 Strains and growth conditions

FY4 (s288c *MATa*) haploid cells were used in this experiment. Strains were cultured at 30°C with aeration in YPD + 2% glucose, to mid-log and then washed with water for two times, pellet cells, and transferred into corresponding nutrient limited conditions. I inoculated 1×10^7 cells into 100ml of nutrient limited medium: for glucose- (C, 4.4mM carbon), ammonia- (N, 0.8mM nitrogen), and phosphorus- (P, 0.04mM phosphorus) and collect desired amount of cells at 48 hours post nutrient limitation for downstream analysis. The GEM strain was constructed by transforming the plasmic that was constructed as previously described (Delarue et al. 2018) into the FY3 (s288c *MATa ura3-52*).

4.5.2 Percoll gradient fractionation

Percoll density gradients (GE Healthcare) were prepared using the manufacturer's preformed gradient protocol with modifications. Percoll was diluted 9:1 (vol/vol) with 1.5

M NaCl, for a final NaCl concentration of 167 mM. To form the gradients, 10 ml of the Percoll solution was put into 15-ml Corex tubes and centrifuged at 13,800 RPM (19,240 gav) for 15 min at 20°C. Approximately 2 × 10^9 cells (200 OD600) were pelleted, resuspended in 1 ml Tris buffer, overlaid onto the preformed gradient, and centrifuged at 400 gav for 60 min in a tabletop centrifuge equipped with a swinging bucket rotor (Beckman Instruments) at 20°C. Fractions were collected, washed once in a 40 ml Tris buffer, pelleted, and resuspended in ddH_20 or conditioned medium for subsequent assays. Cell counts for each fraction were determined using a particle count and size analyzer (Z2; Beckman Instruments).

4.5.3 Flow cytometry

4.5.3.1 Sytox Green staining

The growth of the cells was stop and cells were fixed overnight at 4 degree by adding 200 mL of ethanol. These cells were then pelleted and washed once with H_2O. Cells were resuspended in 80 mL of 0.2 mg/mL RNaseA in 50 mM Tris-HCl, pH 7.5, and incubated at 37 for 4 hr. Then, 80 mL of Proteinase K in 50 mM Tris-HCl pH 7.5 was added to the cultures at a final concentration of 2 mg/mL, and cultures were incubated at 50 for 1 hr, then 40 mL of 50 mM Tris-HCl with SYTOX Green nucleic acid stain (Invitrogen, Carlsbad, CA) was added to the cultures at final concentration of 1.0 mM. DNA content analysis was performed in the 96-well format using a BD FACS Canto II-2 flow cytometer and Flowjo software (BD Biosciences).

4.5.3.2 Viability quantification using propidium iodide & SYTO® 9

For viability quantification at each time point, 1 × 10^7 cells were collected and subsequently washed once with sterilized DI water and one more time with PBS. The washed cell pellet was resuspended with 1mL 1 x PBS and stained with 3.34μM of SYTO® 9 and 20μM of propidium iodide for 20 minutes. The stained samples were then analyzed by flow cytometry (BD Accuri™ C6).

4.5.4 Imaging, direct particle tracking, and extraction of the rheological parameters

All analyses were done as previously described (Delarue et al. 2018). Briefly, the GEM particles were imaged using TIRF Nikon TI Eclipse microscope in partial TIRF mode at 488 nm excitation, and fluorescence was recorded with a scMOS camera (Zyla, Andor) with a 100x objective (pixel size: 0.093 mm) at a rate of one image every 10 ms. The tracking of particles was performed with the Mosaic suite of FIJI, using the following typical parameters: radius =3; cutoff = 0; 10% of fluorescence intensity, a link range of 1, and a maximum displacement of 8 px, assuming Brownian dynamics. Various parameters were extracted from the particle trajectories. For every trajectory, we calculated the time-averaged mean-square displacement (MSD), as defined in (Munder et al. 2016) as well as the ensemble-average of the time-averaged MSD. The diffusion of the tracer particle is subdiffusive, and generally obeys the following law:

$$MSD\ (\tau)\ =\ 4K\tau^{\alpha}$$

where α is the power exponent of the anomalous diffusion, and α < 1 in the case of a

subdiffusive behavior. In this case, the apparent diffusion coefficient, K, is in units of $\mu m^2/s^\alpha$. To characterize individual particle trajectories, we calculated apparent diffusion coefficients by fitting MSD with a linear (diffusive) time dependence (less than 100 ms for GEMs). To do this, we calculated theMSD and truncated it to the first 10 points, and fit it with the following linear relationship:

$$MSD_{truncated}(\tau) = 4D_{eff}\tau$$

where D_{eff} is the effective coefficient of diffusion of the tracer particle.

Chapter 5 : Conclusions

5.1 Summary and discussion

A central challenge in biology is understanding how cells adjust their physiological characteristics to constantly changing environment to ensure long term survival. This dissertation aims to gain insights on the functional role of signaling kinases in regulating quiescence, a way to survive long term under different environmental stresses in *S. cerevisiae*. *S. cerevisiae* can enter quiescence under different nutritional starvations, but knowledge about quiescence induced by nutrients other than glucose is limited. Although significant progress has been made in understanding quiescence in yeast, there are several key questions and issues that await resolution. Given the increasing appreciation of the importance of cellular quiescence, addressing these questions as a coordinated community-wide effort is required to make progress in our understanding cellular quiescence. A comprehensive review that highlight key features and remaining questions was presented in Chapter 1. In this thesis, I adapt several methods that have been applied in proliferating cells (e.g. Bar-seq, native SILAC, GEMs) to the study of quiescence. My results reveal the importance of the environmental role in regulating cellular quiescence and shed light on the coordination of cellular components and gene expression in quiescence initiation, maintenance and exit.

5.1.1 Genetic interaction profiles of signaling kinases are condition and cellular state dependent

In Chapter 2, I addressed two questions: 1) Does quiescence induced by different starvation cues require the same set of genes? 2) What are the functional relationships between signaling pathways in quiescent cells and how do those relationships differ from proliferating cells? Toward this goal, I performed genome-wide mutant screening for about 4,800 single mutants and genetic interaction quantification for TOR1, RIM15 and PHO85 using Bar-seq in three different nutrient-restricted conditions in both proliferative and quiescent cells. I find that both individual gene effects and genetic interaction profiles vary depending on the specific pro-quiescence signal with limited overlaps. Only eight non-essential genes are commonly required for quiescence, which does not differ from what would be expected by chance (Fisher's exact test, $p > 0.05$) (**Figure 2.2D & Figure 2.S2D**). There genes have not previously been reported as required for quiescence. Three genes have unknown functions, three genes function in metabolism, and two gene are involved in protein folding and degradation (**Figure 5.1**). Functional annotations of interaction phenotypes provided additional evidence of RIM15 being a master regulator for quiescence by integrating signals from multiple pathways and mediating vacuole related protein recycling (**Figure 5.1**).

Chapter 2 provides an extendable method for studying the interaction of signaling kisses systematically of cells at different stages and provides insights of functional relationships among kinases that are condition dependent. However, my fundings are just the tip of the iceberg given the complexity and heterogeneity of quiescence. A

comprehensive understanding of quiescence regulation and the interaction between cells and environment begs a systems-level study of the regulatory pathways. Ultimately, studies of quiescence in yeast and other organisms will yield a deeper understanding of the life cycle of cells and has the potential to lead to important advances in our understanding of the function of cells with potential therapeutic insights.

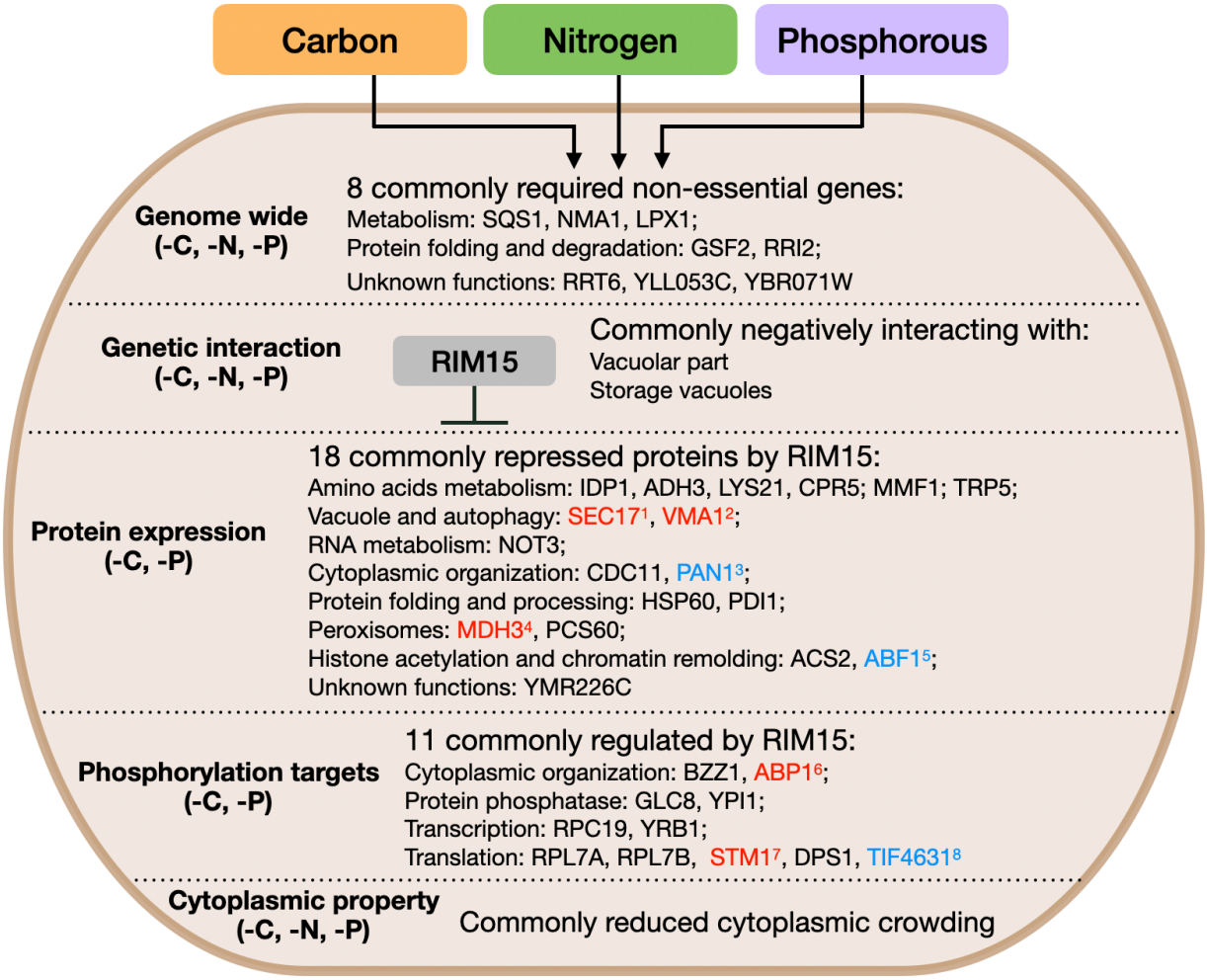

Figure 5.1 . Summarized commonalties of quiescent cells induced by different starvation signals.

The common set of genes, proteins, phosphorylation events were grouped based on molecular function. The bolded text on the left are experiments in which the common features are

detected. The text in the parenthesis are the starvation conditions in which those commonalities were found (-C, carbon starvation; -N, nitrogen starvation; -P phosphorous starvation). Most of the genes and proteins listed in the figure are novel (black). Some proteins have either directly (red) or indirectly (blue) reported to have a functional impact on quiescence establishment or maintenance. [1.](Sajiki et al., 2009); [2.](Wood et al., 2020); [3.](Benbadis et al., 2009); [4.] (Allen et al., 2006); [5.](Poramba-Liyanage et al., 2020); [6.](Van Dyke et al., 2013); [7.](Berset et al., 1998).

5.1.2 Profiling of proteome and phosphoproteome dynamics during quiescence entry in response to diverse starvation signals

To further dissect the molecular circuits by which yeast cells enter quiescence in response to different nutritional starvations, I combined temporal profiling of the whole proteome and phosphoproteome via Stable Isotope Labeling with Amino acids in Cell culture (SILAC) approach. The main questions I addressed in Chapter 3 are: 1) Do cells exhibit the same proteome remodeling dynamics in response to different starvations? 2) How does RIM15 impact proteome remodeling? 3) As rim15 is a serine/threonine kinase, does it phosphorylate the same set of proteins within the signaling cascade in response to different starvations?

I first successfully demonstrated the feasibility of using SILAC in prototrophic strains (**Figure 3.1 & Figure 3.S1**). My temporal profiling analysis revealed that different nutritional starvations activate quiescence by remodeling the proteome and phosphoproteome with different dynamics. In response to carbon starvation, protein dephosphorylation and energy preservation (mitochondrial associated function) are marked by early dynamics; however, pathways involved in metabolism, biosynthesis and vacuole fusion peak at early time points under phosphorus starvation. Moreover, proteins involved in translation were downregulated early in carbon starvation suggesting a global translational shutdown, which is not observed in phosphorus starvation.

Genetic perturbation revealed new roles of evolutionary conserved Serine/Therinion kinase RIM15 in quiescence establishment by mediating the phosphorylation of proteins involved in translation and protein degradation. 18 proteins were repressed by RIM15 in both carbon and phosphorous starvations, whereas only 5 proteins have been previously reported either directly or in-directly related with quiescence (**Figure 5.1**). Functional annotation of those genes reveals the importance of some biological pathways that are commonly regulated in quiescence in response to different starvation signals. Those pathways include macromolecular metabolism (e.g. RNA, amino acids, fatty acids, reactive oxygen species), protein homeostasis (e.g. protein folding, degradation and processing), cytoplasmic organization and chromatin remodeling. Moreover, 11 phosphorylation targets were found to be commonly phosphorylated by RIM15 either directly or in-directly in response to carbon and phosphorous starvations (**Figure 5.1**). Altogether, my multi-condition proteomics profiling and functional studies defined landscapes of the quiescent proteome and phosphoproteome and reveal dynamics of signaling, biogenesis, bioenergetics pathways and the functional basis of RIM15 in quiescence entry in budding yeast.

Nonetheless, we have only recovered a limited number of proteins and phosphorylation events. To increase the recovery, an additional fractionation step is needed. Our current experimental setup cannot differentiate the turnover of molecules (e.g. RNAs and proteins) during quiescence establishment, maintenance and development. It would be more informative to distinguish newly synthesized RNA and proteins and from extant molecules. In addition, our analysis was all done in a bulk sample,

but because of the heterogeneity of the quiescent population, single cell based high-throughput sequencing approaches may be well-suited to defining the dynamics of gene expression during quiescence entry. Approaches to metabolic labeling of mRNAs (Neymotin, Athanasiadou, and Gresham 2014) and proteins (de Godoy et al. 2008; Snider et al. 2019) would allow us to differentiate the turnover of mRNA and proteins.

5.1.3 Vacuole fusion and cell volume decreasing result in increased cytoplasmic crowding

The aim of Chapter 4 was to characterize the physical, molecular and biophysical properties of quiescent cells that are induced via different nutrient starvations with the goal of finding a universal marker of quiescence. Unfortunately, no such gene was found. I then tested established methods that take advantage of the physical properties of quiescent cells: Percoll gradient fractionation (quiescent cells are denser than dead cells) and adapted SytoxGreen staining (thickened cell wall in quiescent cell reduces staining efficiency). Although the expected separation was seen in all starvation conditions, the quality and efficiency of the separation needs to be further optimized in a given condition.

Lastly, I laid the foundation for studying the interaction between organelle reorganization (particularly vacuoles) and cytoplasmic crowding. In preliminary studies, I found that cytoplasmic crowding is increased in all starvation induced quiescent cells, but to different extents. For example, a higher crowding was found in carbon starvation, whereas phosphorus starvation has a milder effect. Interestingly, this increased crowding can be reversed within 2 hours after refeeding. I hypothesize that the increased

cytoplasmic crowding might be a combinatorial result of decreased cell size and enlargement of vacuole.

My studies have shown that the quiescent state is differently regulated in response to different starvation signals. Nonetheless, we find limited but novel overlap signatures that shed light on understanding of commonality of quiescence regulation in different contexts (**Figure 5.1**). Overall, my results have important implications for studying quiescence on systematic level: 1) the definition of an “essential gene” is dependent on the condition in which essentiality is assessed; 2) genome-wide genetic interaction mapping is extensible to additional phenotypes and conditions. Analyzing condition-specific phenotypes may increase the sensitivity for identifying novel regulatory relationships; 3) RIM15 has “pleiotropic” effects in regulating gene expression in quiescent cells that mediates cellular homeostasis on transcription and translation levels.

5.2 Perspective and future directions

Although significant progress has been made in understanding quiescence in yeast and other organisms, there are several key questions and issues that await resolution. Given the increasing appreciation of the importance of cellular quiescence, addressing these questions as a coordinated community-wide effort is clearly the most expedient approach to making progress in our understanding cellular quiescence. Central to this aim is consensus among researchers on the definitions (cells have reversibly exited the cell cycle), contexts (different starvation signals), stages (initiation, maintenance and exit),

characteristics (large-scale remodeling of gene expression, organelles and metabolism), and analytical methods for studying quiescence in yeast (**Figure 5.2**), which I hope will be stimulated by this dissertation.

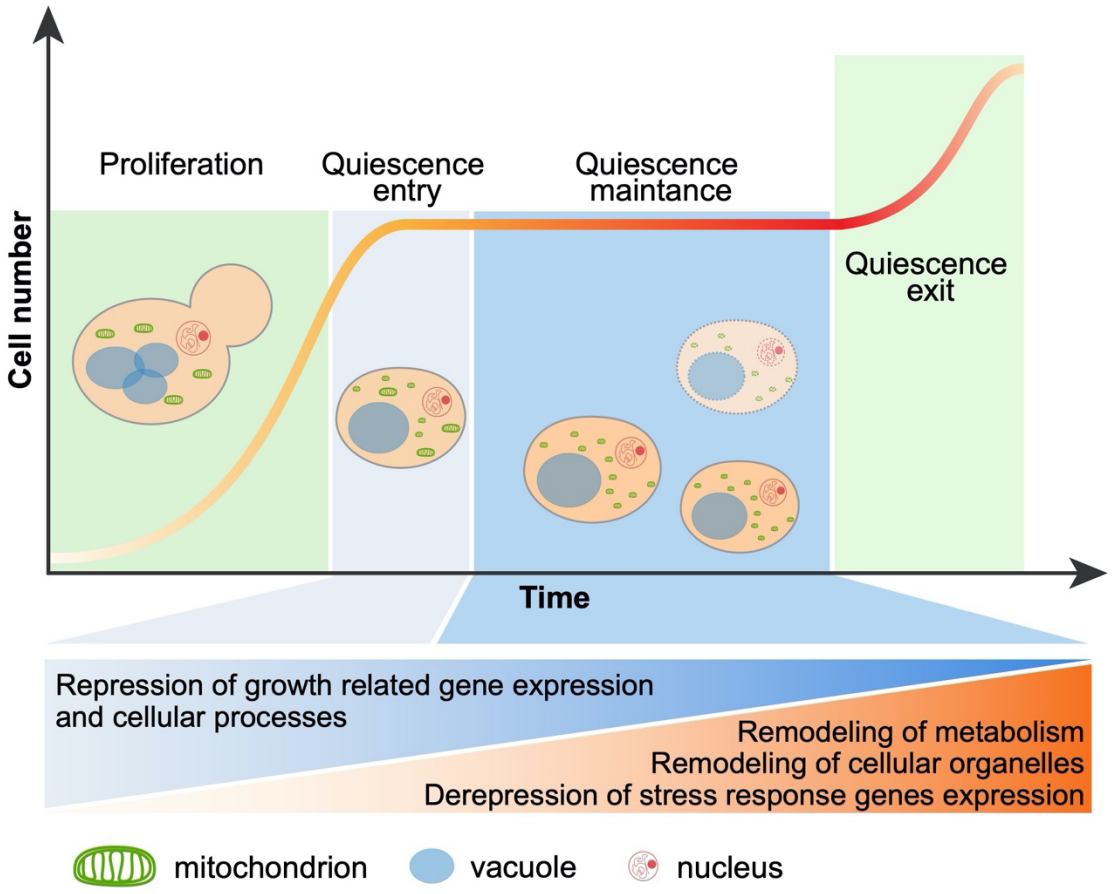

Figure 5.2. Three phases of quiescence in budding yeast and the known changing features associated with quiescence progression.

The processes that underlie the initiation, maintenance and exit from quiescence are likely distinct, but interrelated.

First, the identification of an evolutionarily conserved marker of quiescent cells would represent a significant technical advance. Although myriad cellular alterations

occur in quiescent cells (**Figure 1.1B**), none of them is individually well-suited as a marker of quiescence because 1) they are not specific to quiescence, 2) their relevance in different quiescence inducing conditions has not been demonstrated (Sagot et al., 2006), and 3) they are not amenable to high-throughput studies (e.g. FACS-based isolation). We believe that expanding and refining the molecular characterization of quiescent cells will be useful for identifying specific quiescent cell markers.

The turnover of molecules (e.g. RNAs and proteins) during quiescence establishment, maintenance and development is unknown. For example, it would be informative to distinguish newly synthesized RNA or proteins from extant molecules. Because of the heterogeneity of quiescent population, single cell based high-throughput sequencing approaches may be well-suited to defining the dynamics of gene expression during quiescence. Approaches to metabolic labeling of mRNAs (Neymotin et al., 2014) and proteins (de Godoy et al., 2008) would allow distinction of mRNA synthesis and degradation rates during the different stages of quiescence.

The significance of remodeling of cellular organelles in quiescence is a particularly exciting area of research. Cell biological studies of organelle function have typically been performed in proliferating cells and many organelles - including mitochondria and vacuoles - exhibit striking differences in quiescent cells. Studies have shown that the cytoplasm of quiescent cells undergoes dramatic changes in its physical properties. Ribosome concentration appears to have important impacts on this property in a TORC1-dependent manner (Delarue et al., 2018). Understanding the regulatory and functional

connections between quiescence regulating pathways and organelle and cytoplasmic properties during quiescence presents a major challenge for future studies.

Expansion of current approaches to assess the role of natural variation warrants increased attention. The vast majority of quiescence studies in yeast have been performed in laboratory adapted strains. As quiescence is of primary importance in many natural environments, natural variation is likely to be informative. Both QTL mapping and methods such as insertional mutagenesis (Michel et al., 2017; Segal et al., 2018) would be informative approaches. Efforts should also be made to expand the study of quiescence in fungal species beyond model organisms. Human pathogens, such as *C. albicans*, are readily amenable to many of the approaches that have been used in *S. cerevisiae* and *S. pombe*, and studies of such organisms yield findings of clinical utility. Expansion of studies to other fungal species will also facilitate identification of evolutionarily conserved mechanisms.

Quiescence also provides a unique opportunity to understand how signaling pathways sense different signals and converge on related processes. As yeast cells respond to diverse nutritional signals to initiate quiescence, it seems likely that these pathways converge on related cellular processes required for quiescence. This begs a systems-level approach, using the power of genome-wide methods and the resolution of single-cell approaches, to understand how this signal integration occurs. Ultimately, studies of quiescence in yeast and other organisms will yield a deeper understanding of the life cycle of cells with potential therapeutic insights.

References

Agudo, Judith, Eun Sook Park, Samuel A. Rose, Eziwoma Alibo, Robert Sweeney, Maxime Dhainaut, Koichi S. Kobayashi, et al. 2018. “Quiescent Tissue Stem Cells Evade Immune Surveillance.” *Immunity* 48 (2): 271–85.e5.

Alberts, Bruce, Dennis Bray, Alexander Johnson, Julian Lewis, Martin Raff, Keith Roberts, and Peter Walter. 2013. “How Cells Obtain Energy from Food.” *Essential Cell Biolog*. https://doi.org/10.1201/9781315815015-13.

Alexander, Barbara D., and John R. Perfect. 1997. “Antifungal Resistance Trends towards the Year 2000.” *Drugs* 54 (5): 657–78.

Allen, Chris, Sabrina Büttner, Anthony D. Aragon, Jason A. Thomas, Osorio Meirelles, Jason E. Jaetao, Don Benn, et al. 2006. “Isolation of Quiescent and Nonquiescent Cells from Yeast Stationary-Phase Cultures.” *The Journal of Cell Biology* 174 (1): 89–100.

Anderl, Jeff N., Frank Roe, and Philip S. Stewart. 2003. “Role of Nutrient Limitation and Stationary-Phase Existence in.” *Society* 47 (4): 1251–56.

Aragon, Anthony D., Angelina L. Rodriguez, Osorio Meirelles, Sushmita Roy, George S. Davidson, Phillip H. Tapia, Chris Allen, Ray Joe, Don Benn, and Margaret Werner-Washburne. 2008. “Characterization of Differentiated Quiescent and Nonquiescent Cells in Yeast Stationary-Phase Cultures.” *Molecular Biology of the Cell* 19 (3): 1271–80.

Ashe, M. P., S. K. De Long, and A. B. Sachs. 2000. “Glucose Depletion Rapidly Inhibits Translation Initiation in Yeast.” *Molecular Biology of the Cell* 11 (3): 833–48.

Aufschnaiter, Andreas, and Sabrina Büttner. 2019. “The Vacuolar Shapes of Ageing: From Function to Morphology.” *Biochimica et Biophysica Acta, Molecular Cell Research* 1866 (5): 957–70.

Augenlicht, L. H., and R. Baserga. 1974. “Changes in the G0 State of WI-38 Fibroblasts at Different Times after Confluence.” *Experimental Cell Research* 89 (2): 255–62.

Baba, M., K. Takeshige, N. Baba, and Y. Ohsumi. 1994. “Ultrastructural Analysis of the Autophagic Process in Yeast: Detection of Autophagosomes and Their Characterization.” *The Journal of Cell Biology* 124 (6): 903–13.

Balaban, Nathalie Q., Jack Merrin, Remy Chait, Lukasz Kowalik, and Stanislas Leibler. 2004. “Bacterial Persistence as a Phenotypic Switch.” *Science* 305 (5690): 1622–25.

Bandyopadhyay, Sourav, Monika Mehta, Dwight Kuo, Min-Kyung Sung, Ryan Chuang, Eric J. Jaehnig, Bernd Bodenmiller, et al. 2010. “Rewiring of Genetic Networks in Response to DNA Damage.” *Science* 330 (6009): 1385–89.

Baryshnikova, Anastasia. 2016. “Systematic Functional Annotation and Visualization of Biological Networks.” *Cell Systems* 2 (6): 412–21.

Baserga, Renato. 1968. “Biochemistry of the Cell Cycle: A Review.” *Cell Proliferation* 1 (2): 167–91.

Beltrao, Pedro, Gerard Cagney, and Nevan J. Krogan. 2010. “Quantitative Genetic Interactions Reveal Biological Modularity.” *Cell* 141 (5): 739–45.

Beristain, A. G., S. D. Molyneux, P. A. Joshi, N. C. Pomroy, M. A. Di Grappa, M. C. Chang, L. S. Kirschner, G. G. Privé, M. A. Pujana, and R. Khokha. 2015. “PKA Signaling Drives Mammary Tumorigenesis through Src.” *Oncogene* 34 (9): 1160–73.

Billmann, Maximilian, Varun Chaudhary, Mostafa F. ElMaghraby, Bernd Fischer, and Michael Boutros. 2018. “Widespread Rewiring of Genetic Networks upon Cancer Signaling Pathway Activation.” *Cell Systems* 6 (1): 52–64.e4.

Billmann, Maximilian, Thomas Horn, Bernd Fischer, Thomas Sandmann, Wolfgang Huber, and

Michael Boutros. 2016. “A Genetic Interaction Map of Cell Cycle Regulators.” *Molecular Biology of the Cell* 27 (8): 1397–1407.

Boer, Viktor M., Sasan Amini, and David Botstein. 2008. “Influence of Genotype and Nutrition on Survival and Metabolism of Starving Yeast.” *Proceedings of the National Academy of Sciences of the United States of America* 105 (19): 6930–35.

Boer, Viktor M., Christopher A. Crutchfield, Patrick H. Bradley, David Botstein, and Joshua D. Rabinowitz. 2010. “Growth-Limiting Intracellular Metabolites in Yeast Growing under Diverse Nutrient Limitations.” *Molecular Biology of the Cell* 21 (1): 198–211.

Bontron, Séverine, Malika Jaquenoud, Stefania Vaga, Nicolas Talarek, Bernd Bodenmiller, Ruedi Aebersold, and Claudio De Virgilio. 2013. “Yeast Endosulfines Control Entry into Quiescence and Chronological Life Span by Inhibiting Protein Phosphatase 2A.” *Cell Reports* 3 (1): 16–22.

Boone, Charles, Howard Bussey, and Brenda J. Andrews. 2007. “Exploring Genetic Interactions and Networks with Yeast. TL - 8.” *Nature Reviews. Genetics* 8 VN - re (6): 437–49.

Borst, P. 2012. “Cancer Drug Pan-Resistance: Pumps, Cancer Stem Cells, Quiescence, Epithelial to Mesenchymal Transition, Blocked Cell Death Pathways, Persisters or What?” *Open Biology* 2 (5): 120066.

Broach, James R. 2012. “Nutritional Control of Growth and Development in Yeast.” *Genetics* 192 (1): 73–105.

Brooks, R. F. 1976. “Regulation of Fibroblast Cell Cycle by Serum.” *Nature* 260 (5548): 248–50.

Bruschini, Sara, Gennaro Ciliberto, and Rita Mancini. 2020. “The Emerging Role of Cancer Cell Plasticity and Cell-Cycle Quiescence in Immune Escape.” *Cell Death & Disease*. https://doi.org/10.1038/s41419-020-2669-8.

Cameroni, Elisabetta, Nicolas Hulo, Johnny Roosen, Joris Winderickx, and Claudio De Virgilio. 2004. "The Novel Yeast PAS Kinase Rim 15 Orchestrates G0-Associated Antioxidant Defense Mechanisms." *Cell Cycle* 3 (4): 462–68.

Castro, Anna, and Thierry Lorca. 2018. "Greatwall Kinase at a Glance." *Journal of Cell Science*. https://doi.org/10.1242/jcs.222364.

Chen, Cuilan, Guisheng Zeng, and Yue Wang. 2018. "G1 and S Phase Arrest in Candida Albicans Induces Filamentous Growth via Distinct Mechanisms." *Molecular Microbiology* 110 (2): 191–203.

Cheung, Tom H., and Thomas A. Rando. 2013. "Molecular Regulation of Stem Cell Quiescence." *Nature Reviews. Molecular Cell Biology* 14 (6): 329–40.

Coller, H. a. 2011. "The Essence of Quiescence." *Science* 334 (6059): 1074–75.

Coller, Hilary A., Liyun Sang, and James M. Roberts. 2006. "A New Description of Cellular Quiescence." *PLoS Biology* 4 (3): 0329–49.

Costanzo, Michael, Anastasia Baryshnikova, Jeremy Bellay, Yungil Kim, Eric D. Spear, Carolyn S. Sevier, Huiming Ding, et al. 2010. "The Genetic Landscape of a Cell." *Science* 327 (5964): 425–31.

Costanzo, M., B. VanderSluis, E. N. Koch, A. Baryshnikova, C. Pons, G. Tan, W. Wang, et al. 2016. "A Global Genetic Interaction Network Maps a Wiring Diagram of Cellular Function." *Science* 353 (6306): aaf1420–aaf1420.

Daignan-Fornier, Bertrand, and Isabelle Sagot. 2011. "Proliferation/quiescence: The Controversial 'Aller-Retour.'" *Cell Division* 6 (1): 10.

Davidson, George S., Ray M. Joe, Sushmita Roy, Osorio Meirelles, Chris P. Allen, Melissa R. Wilson, Phillip H. Tapia, et al. 2011. "The Proteomics of Quiescent and Nonquiescent Cell Differentiation

in Yeast Stationary-Phase Cultures." *Molecular Biology of the Cell* 22 (7): 988–98.

Delarue, M., G. P. Brittingham, S. Pfeffer, I. V. Surovtsev, S. Pinglay, K. J. Kennedy, M. Schaffer, et al. 2018. "mTORC1 Controls Phase Separation and the Biophysical Properties of the Cytoplasm by Tuning Crowding." *Cell* 174 (2): 338–49.e20.

De Virgilio, C., and R. Loewith. 2006. "Cell Growth Control: Little Eukaryotes Make Big Contributions." *Oncogene* 25 (48): 6392–6415.

Dhawan, Jyotsna, and Sunil Laxman. 2015. "Decoding the Stem Cell Quiescence Cycle--Lessons from Yeast for Regenerative Biology." *Journal of Cell Science* 128 (24): 4467–74.

Díaz-Mejía, J. Javier, Albi Celaj, Joseph C. Mellor, Atina Coté, Attila Balint, Brandon Ho, Pritpal Bansal, et al. 2018. "Mapping DNA Damage-Dependent Genetic Interactions in Yeast via Party Mating and Barcode Fusion Genetics." *Molecular Systems Biology* 14 (5): e7985.

Du, Dan, Assen Roguev, David E. Gordon, Meng Chen, Si-Han Chen, Michael Shales, John Paul Shen, et al. 2017. "Genetic Interaction Mapping in Mammalian Cells Using CRISPR Interference." *Nature Methods* 14 (6): 577–80.

Elser, James J., Matthew E. S. Bracken, Elsa E. Cleland, Daniel S. Gruner, W. Stanley Harpole, Helmut Hillebrand, Jacqueline T. Ngai, Eric W. Seabloom, Jonathan B. Shurin, and Jennifer E. Smith. 2007. "Global Analysis of Nitrogen and Phosphorus Limitation of Primary Producers in Freshwater, Marine and Terrestrial Ecosystems." *Ecology Letters* 10 (12): 1135–42.

Epifanova, Olga I., and V. V. Terskikh. 1969. "ON THE RESTING PERIODS IN THE CELL LIFE CYCLE." *Cell Proliferation* 2 (1): 75–93.

Esposito, R. E., and S. Klapholz. 1981. "The Molecular Biology of the Yeast Saccharomyces: Life Cycle and Inheritance." *By JN Strathern, EW Jones and JR Broach, Cold Spring Harbor Laboratory*, 211.

Fabrizio, Paola, and Valter D. Longo. 2003. “The Chronological Life Span of Saccharomyces Cerevisiae.” *Methods in Molecular Biology* 371: 89–95.

Faubert, Brandon, Emma E. Vincent, Maya C. Poffenberger, and Russell G. Jones. 2015. “The AMP-Activated Protein Kinase (AMPK) and Cancer: Many Faces of a Metabolic Regulator.” *Cancer Letters* 356 (2 Pt A): 165–70.

Fischer, Bernd, Thomas Sandmann, Thomas Horn, Maximilian Billmann, Varun Chaudhary, Wolfgang Huber, and Michael Boutros. 2015. “A Map of Directional Genetic Interactions in a Metazoan Cell.” *eLife*. https://doi.org/10.7554/elife.05464.

Flanagan, Peter R., Ning-Ning Liu, Darren J. Fitzpatrick, Karsten Hokamp, Julia R. Köhler, and Gary P. Moran. 2017. “The Candida Albicans TOR-Activating GTPases Gtr1 and Rhb1 Coregulate Starvation Responses and Biofilm Formation.” *mSphere* 2 (6). https://doi.org/10.1128/mSphere.00477-17.

Freese, E. B., M. I. Chu, and E. Freese. 1982. “Initiation of Yeast Sporulation of Partial Carbon, Nitrogen, or Phosphate Deprivation.” *Journal of Bacteriology* 149 (3): 840–51.

Fröhlich, Florian, Romain Christiano, and Tobias C. Walther. 2013. “Native SILAC: Metabolic Labeling of Proteins in Prototroph Microorganisms Based on Lysine Synthesis Regulation.” *Molecular & Cellular Proteomics: MCP* 12 (7): 1995–2005.

Fuge, E. K., E. L. Braun, and M. Werner-Washburne. 1994. “Protein Synthesis in Long-Term Stationary-Phase Cultures of Saccharomyces Cerevisiae.” *Journal of Bacteriology* 176 (18): 5802–13.

Fujimaki, Kotaro, Ruoyan Li, Hengyu Chen, Kimiko Della Croce, Hao Helen Zhang, Jianhua Xing, Fan Bai, and Guang Yao. 2019. “Graded Regulation of Cellular Quiescence Depth between Proliferation and Senescence by a Lysosomal Dimmer Switch.” *Proceedings of the National*

Academy of Sciences of the United States of America 116 (45): 22624–34.

Garay, Erika, Sergio E. Campos, Jorge González de la Cruz, Ana P. Gaspar, Adrian Jinich, and Alexander DeLuna. 2014. “High-Resolution Profiling of Stationary-Phase Survival Reveals Yeast Longevity Factors and Their Genetic Interactions.” *PLoS Genetics* 10 (2): e1004168.

Godoy, Lyris M. F. de, Jesper V. Olsen, Jürgen Cox, Michael L. Nielsen, Nina C. Hubner, Florian Fröhlich, Tobias C. Walther, and Matthias Mann. 2008. “Comprehensive Mass-Spectrometry-Based Proteome Quantification of Haploid versus Diploid Yeast.” *Nature* 455 (7217): 1251–54.

Gookin, Sara, Mingwei Min, Harsha Phadke, Mingyu Chung, Justin Moser, Iain Miller, Dylan Carter, and Sabrina L. Spencer. 2017. “A Map of Protein Dynamics during Cell-Cycle Progression and Cell-Cycle Exit.” *PLoS Biology* 15 (9): e2003268.

Gray, Joseph V., Gregory a. Petsko, Gerald C. Johnston, Dagmar Ringe, Richard a. Singer, and Margaret Werner-washburne. 2004. “ Sleeping Beauty : Quiescence in Saccharomyces Cerevisiae ‘ Sleeping Beauty ’: Quiescence in Saccharomyces Cerevisiae †.” *Microbiology and Molecular Biology Reviews: MMBR* 68 (2): 187–206.

Gray, J. V., G. A. Petsko, and G. C. Johnston. 2004. “‘Sleeping Beauty’: Quiescence in Saccharomyces Cerevisiae.” *Microbiology*. https://mmbr.asm.org/content/68/2/187.short.

Gresham, David, Viktor M. Boer, Amy Caudy, Naomi Ziv, Nathan J. Brandt, John D. Storey, and David Botstein. 2011. “System-Level Analysis of Genes and Functions Affecting Survival during Nutrient Starvation in Saccharomyces Cerevisiae.” *Genetics* 187 (1): 299–317.

Guo, Yongfeng, Kerry Flegel, Jayashree Kumar, Daniel J. McKay, and Laura A. Buttitta. 2016. “Ecdysone Signaling Induces Two Phases of Cell Cycle Exit in Drosophila Cells.” *Biology Open* 5 (11): 1648–61.

Gutin, Jenia, Amit Sadeh, Ayelet Rahat, Amir Aharoni, and Nir Friedman. 2015. “Condition-Specific

Genetic Interaction Maps Reveal Crosstalk between the cAMP/PKA and the HOG MAPK Pathways in the Activation of the General Stress Response." *Molecular Systems Biology* 11 (10): 829.

Hall, Rebecca A. 2015. "Dressed to Impress: Impact of Environmental Adaptation on the Candida Albicans Cell Wall." *Molecular Microbiology* 97 (1): 7–17.

Hanahan, Douglas, and Robert A. Weinberg. 2011. "Hallmarks of Cancer: The next Generation." *Cell* 144 (5): 646–74.

Honigberg, Saul M. 2016. "Similar Environments but Diverse Fates: Responses of Budding Yeast to Nutrient Deprivation." *Microbial Cell Factories* 3 (8): 302–28.

Huang, Jin, Carl J. Mousley, Louis Dacquay, Nairita Maitra, Guillaume Drin, Chong He, Neale D. Ridgway, et al. 2018. "A Lipid Transfer Protein Signaling Axis Exerts Dual Control of Cell-Cycle and Membrane Trafficking Systems." *Developmental Cell* 44 (3): 378–91.e5.

Iwaki, Soichiro, Akio Kihara, Takamitsu Sano, and Yasuyuki Igarashi. 2005. "Phosphorylation by Pho85 Cyclin-Dependent Kinase Acts as a Signal for the down-Regulation of the Yeast Sphingoid Long-Chain Base Kinase Lcb4 during the Stationary Phase." *The Journal of Biological Chemistry* 280 (8): 6520–27.

Iwama, Ryo, and Yoshinori Ohsumi. 2019. "Analysis of Autophagy Activated during Changes in Carbon Source Availability in Yeast Cells." *The Journal of Biological Chemistry*, February. https://doi.org/10.1074/jbc.RA118.005698.

Jackson, Christopher A., Dayanne M. Castro, Giuseppe-Antonio Saldi, Richard Bonneau, and David Gresham. 2020. "Gene Regulatory Network Reconstruction Using Single-Cell RNA Sequencing of Barcoded Genotypes in Diverse Environments." *eLife* 9 (January). https://doi.org/10.7554/eLife.51254.

Jaffe, Mia, Adam Dziulko, Justin D. Smith, Robert P. St Onge, Sasha F. Levy, and Gavin Sherlock. 2019. “Improved Discovery of Genetic Interactions Using CRISPRiSeq across Multiple Environments.” *Genome Research* 29 (4): 668–81.

Johnston, G. C., R. A. Singer, and S. McFarlane. 1977. “Growth and Cell Division during Nitrogen Starvation of the Yeast Saccharomyces Cerevisiae.” *Journal of Bacteriology* 132 (2): 723–30.

Joyner, Ryan P., Jeffrey H. Tang, Jonne Helenius, Elisa Dultz, Christiane Brune, Liam J. Holt, Sebastien Huet, Daniel J. M??ller, and Karsten Weis. 2016. “A Glucose-Starvation Response Regulates the Diffusion of Macromolecules.” *eLife* 5 (MARCH2016): 1–26.

Kadosh, David, and Vasanthakrishna Mundodi. 2020. “A Re-Evaluation of the Relationship between Morphology and Pathogenicity in Candida Species.” *Journal of Fungi (Basel, Switzerland)* 6 (1). https://doi.org/10.3390/jof6010013.

Kaeberlein, Matt. 2010. “Lessons on Longevity from Budding Yeast.” *Nature* 464 (7288): 513–19.

Kaeberlein, Matt, Christopher R. Burtner, and Brian K. Kennedy. 2007. “Recent Developments in Yeast Aging.” *PLoS Genetics* 3 (5): e84.

Kaplon, Joanna, Loes van Dam, and Daniel Peeper. 2015. “Two-Way Communication between the Metabolic and Cell Cycle Machineries: The Molecular Basis.” *Cell Cycle* 14 (13): 2022–32.

Kim, Carla F. Bender, Erica L. Jackson, Amber E. Woolfenden, Sharon Lawrence, Imran Babar, Sinae Vogel, Denise Crowley, Roderick T. Bronson, and Tyler Jacks. 2005. “Identification of Bronchioalveolar Stem Cells in Normal Lung and Lung Cancer.” *Cell* 121 (6): 823–35.

Kim, L. C., R. S. Cook, and J. Chen. 2017. “mTORC1 and mTORC2 in Cancer and the Tumor Microenvironment.” *Oncogene* 36 (16): 2191–2201.

Klosinska, Maja M., Christopher a. Crutchfield, Patrick H. Bradley, Joshua D. Rabinowitz, and James

R. Broach. 2011. “Yeast Cells Can Access Distinct Quiescent States.” *Genes & Development* 25 (4): 336–49.

Kumar, Ravinder, and Sanjeeva Srivastava. 2016. “Quantitative Proteomic Comparison of stationary/G0 Phase Cells and Tetrads in Budding Yeast.” *Scientific Reports* 6 (August): 32031.

Kwon, Jungeun Sarah, Nicholas J. Everetts, Xia Wang, Weikang Wang, Kimiko Della Croce, Jianhua Xing, and Guang Yao. 2017. “Controlling Depth of Cellular Quiescence by an Rb-E2F Network Switch.” *Cell Reports* 20 (13): 3223–35.

Langfelder, Peter, and Steve Horvath. 2008. “WGCNA: An R Package for Weighted Correlation Network Analysis.” *BMC Bioinformatics* 9 (December): 559.

Langfelder, Peter, Bin Zhang, and Steve Horvath. 2008. “Defining Clusters from a Hierarchical Cluster Tree: The Dynamic Tree Cut Package for R.” *Bioinformatics* 24 (5): 719–20.

Laplante, Mathieu, and David M. Sabatini. 2012. “mTOR Signaling in Growth Control and Disease.” *Cell* 149 (2): 274–93.

Laporte, Damien, Laëtitia Gouleme, Laure Jimenez, Ines Khemiri, and Isabelle Sagot. 2018. “Mitochondria Reorganization upon Proliferation Arrest Predicts Individual Yeast Cell Fate.” *eLife* 7 (October). https://doi.org/10.7554/eLife.35685.

Laporte, Damien, Laure Jimenez, Laetitia Gouleme, and Isabelle Sagot. 2018. “Yeast Quiescence Exit Swiftness Is Influenced by Cell Volume and Chronological Age.” *Microbial Cell Factories* 5 (2): 104–11.

Laporte, Damien, Anne Lebaudy, Annelise Sahin, Benoît Pinson, Johanna Ceschin, Bertrand Daignan-Fornier, and Isabelle Sagot. 2011. “Metabolic Status rather than Cell Cycle Signals Control Quiescence Entry and Exit.” *The Journal of Cell Biology* 192 (6): 949–57.

Latgé, Jean-Paul, and Georgios Chamilos. 2019. “Aspergillus Fumigatus and Aspergillosis in 2019.” *Clinical Microbiology Reviews* 33 (1). https://doi.org/10.1128/CMR.00140-18.

Laughney, Ashley M., Jing Hu, Nathaniel R. Campbell, Samuel F. Bakhoum, Manu Setty, Vincent-Philippe Lavallée, Yubin Xie, et al. 2020. “Regenerative Lineages and Immune-Mediated Pruning in Lung Cancer Metastasis.” *Nature Medicine* 26 (2): 259–69.

Lee, Kanghyun, Ruchika Sharma, Om Kumar Shrestha, Craig A. Bingman, and Elizabeth A. Craig. 2016. “Dual Interaction of the Hsp70 J-Protein Cochaperone Zuotin with the 40S and 60S Ribosomal Subunits.” *Nature Structural & Molecular Biology* 23 (11): 1003–10.

Leeuwen, Jolanda van, Charles Boone, and Brenda J. Andrews. 2017. “Mapping a Diversity of Genetic Interactions in Yeast.” *Current Opinion in Systems Biology* 6 (December): 14–21.

Lemons, Johanna M. S., Hilary A. Coller, Xiao Jiang Feng, Bryson D. Bennett, Aster Legesse-Miller, Elizabeth L. Johnson, Irene Raitman, Elizabeth A. Pollina, Herschel A. Rabitz, and Joshua D. Rabinowitz. 2010. “Quiescent Fibroblasts Exhibit High Metabolic Activity.” *PLoS Biology* 8 (10). https://doi.org/10.1371/journal.pbio.1000514.

Lillie, S. H., and J. R. Pringle. 1980. “Reserve Carbohydrate Metabolism in Saccharomyces Cerevisiae: Responses to Nutrient Limitation.” *Journal of Bacteriology* 143 (3): 1384–94.

Li, L., S. Miles, and L. L. Breeden. 2015. “A Genetic Screen for Saccharomyces Cerevisiae Mutants That Fail to Enter Quiescence.” *G3: Genes|Genomes|Genetics* 5 (8): 1783–95.

Lin, Tara L., Cecilia Fu, and Kathleen M. Sakamoto. 2007. “Cancer Stem Cells: The Root of the Problem.” *Pediatric Research* 62 (3): 239.

Li, Sheena Claire, and Patricia M. Kane. 2009. “The Yeast Lysosome-like Vacuole: Endpoint and Crossroads.” *Biochimica et Biophysica Acta* 1793 (4): 650–63.

Litsios, Athanasios, Álvaro D. Ortega, Ernst C. Wit, and Matthias Heinemann. 2018. “Metabolic-Flux Dependent Regulation of Microbial Physiology.” *Current Opinion in Microbiology* 42 (April): 71–78.

Ljungdahl, Per O., and Bertrand Daignan-Fornier. 2012. “Regulation of Amino Acid, Nucleotide, and Phosphate Metabolism in Saccharomyces Cerevisiae.” *Genetics* 190 (3): 885–929.

Lynch, A. S., and G. T. Robertson. 2008. “Bacterial and Fungal Biofilm Infections.” *Annu.Rev.Med.* 59 (0066-4219 (Print)): 415–28.

Mani, Ramamurthy, Robert P. St Onge, John L. Hartman, Guri Giaever, and Frederick P. Roth. 2008. “Defining Genetic Interaction.” *Proceedings of the National Academy of Sciences of the United States of America* 105 (9): 3461–66.

Marguerat, Samuel, Alexander Schmidt, Sandra Codlin, Wei Chen, Ruedi Aebersold, and Jürg Bähler. 2012. “Quantitative Analysis of Fission Yeast Transcriptomes and Proteomes in Proliferating and Quiescent Cells.” *Cell* 151 (3): 671–83.

Marini, Guendalina, Elisabeth Nüske, Weihua Leng, Simon Alberti, and Gaia Pigino. 2020. “Reorganization of Budding Yeast Cytoplasm upon Energy Depletion.” *Molecular Biology of the Cell* 31 (12): 1232–45.

Martin, Humberto, Michael Shales, Pablo Fernandez-Piñar, Ping Wei, Maria Molina, Dorothea Fiedler, Kevan M. Shokat, Pedro Beltrao, Wendell Lim, and Nevan J. Krogan. 2015. “Differential Genetic Interactions of Yeast Stress Response MAPK Pathways.” *Molecular Systems Biology* 11 (4): 800.

McKnight, Jeffrey N., Joseph W. Boerma, Linda L. Breeden, and Toshio Tsukiyama. 2015. “Global Promoter Targeting of a Conserved Lysine Deacetylase for Transcriptional Shutoff during Quiescence Entry.” *Molecular Cell* 59 (5): 732–43.

Menoyo, S., N. Ricco, S. Bru, S. Hernández-Ortega, X. Escoté, M. Aldea, and J. Clotet. 2013.

"Phosphate-Activated Cyclin-Dependent Kinase Stabilizes G1 Cyclin to Trigger Cell Cycle Entry." *Molecular and Cellular Biology* 33 (7): 1273–84.

Miermont, Agnès, François Waharte, Shiqiong Hu, Megan Nicole McClean, Samuel Bottani, Sébastien Léon, and Pascal Hersen. 2013. "Severe Osmotic Compression Triggers a Slowdown of Intracellular Signaling, Which Can Be Explained by Molecular Crowding." *Proceedings of the National Academy of Sciences of the United States of America* 110 (14): 5725–30.

Miles, Shawna, and Linda Breeden. 2017. "A Common Strategy for Initiating the Transition from Proliferation to Quiescence." *Current Genetics* 63 (2): 179–86.

Miles, Shawna, Li Hong Li, Zephan Melville, and Linda L. Breeden. 2019. "Ssd1 and the Cell Wall Integrity Pathway Promote Entry, Maintenance, and Recovery from Quiescence in Budding Yeast." *Molecular Biology of the Cell* 30 (17): 2205–17.

Mitra, Mithun, Linda D. Ho, and Hilary A. Coller. 2018. "An In Vitro Model of Cellular Quiescence in Primary Human Dermal Fibroblasts." *Methods in Molecular Biology* 1686: 27–47.

Monteoliva, Lucia, Raquel Martinez-Lopez, Aida Pitarch, Maria Luisa Hernaez, Antonio Serna, Cesar Nombela, Juan Pablo Albar, and Concha Gil. 2011. "Quantitative Proteome and Acidic Subproteome Profiling of Candida Albicans Yeast-to-Hypha Transition." *Journal of Proteome Research* 10 (2): 502–17.

Mourão, Márcio A., Joe B. Hakim, and Santiago Schnell. 2014. "Connecting the Dots: The Effects of Macromolecular Crowding on Cell Physiology." *Biophysical Journal* 107 (12): 2761–66.

Munder, Matthias Christoph, Daniel Midtvedt, Titus Franzmann, Elisabeth Nüske, Oliver Otto, Maik Herbig, Elke Ulbricht, et al. 2016. "A pH-Driven Transition of the Cytoplasm from a Fluid- to a Solid-like State Promotes Entry into Dormancy." *eLife* 5: e09347.

Murray, P. J. 1999. "Defining the Requirements for Immunological Control of Mycobacterial Infections."

Trends in Microbiology 7 (9): 366–72.

Neurohr, Gabriel E., Rachel L. Terry, Jette Lengefeld, Megan Bonney, Gregory P. Brittingham, Fabien Moretto, Teemu P. Miettinen, et al. 2019. “Excessive Cell Growth Causes Cytoplasm Dilution And Contributes to Senescence.” *Cell* 176 (5): 1083–97.e18.

Neymotin, Benjamin, Rodoniki Athanasiadou, and David Gresham. 2014. “Determination of in Vivo RNA Kinetics Using RATE-Seq.” *RNA* 20 (10): 1645–52.

Nguyen, Dao, Amruta Joshi-Datar, Francois Lepine, Elizabeth Bauerle, Oyebode Olakanmi, Karlyn Beer, Geoffrey McKay, et al. 2011. “Active Starvation Responses Mediate Antibiotic Tolerance in Biofilms and Nutrient-Limited Bacteria.” *Science* 334 (6058): 982–86.

O’Farrell, P. H. 2011. “Quiescence: Early Evolutionary Origins and Universality Do Not Imply Uniformity.” *Philosophical Transactions of the Royal Society of London. Series B, Biological Sciences* 366 (1584): 3498–3507.

Olivares-Marin, Ivanna Karina, Luis Alberto Madrigal-Perez, Melina Canizal-Garcia, Blanca E. García-Almendárez, Juan Carlos González-Hernández, and Carlos Regalado-Gonzalez. 2018. “Interactions between Carbon and Nitrogen Sources Depend on RIM15 and Determine Fermentative or Respiratory Growth in Saccharomyces Cerevisiae.” *Applied Microbiology and Biotechnology*, 1–14.

Onodera, Jun, and Yoshinori Ohsumi. 2005. “Autophagy Is Required for Maintenance of Amino Acid Levels and Protein Synthesis under Nitrogen Starvation.” *The Journal of Biological Chemistry* 280 (36): 31582–86.

Owen, Thomas A., Dianne Robert Soprano, and Kenneth J. Soprano. 1989. “Analysis of the Growth Factor Requirements for Stimulation of WI-38 Cells after Extended Periods of Density-Dependent Growth Arrest.” *Journal of Cellular Physiology*. https://doi.org/10.1002/jcp.1041390227.

Parrish, N. M., J. D. Dick, and W. R. Bishai. 1998. “Mechanisms of Latency in Mycobacterium Tuberculosis.” *Trends in Microbiology* 6 (3): 107–12.

Patt, H. M., and H. Quastler. 1963. “Radiation Effects on Cell Renewal and Related Systems.” *Physiological Reviews* 43 (July): 357–96.

Pedruzzi, I. 2000. “Saccharomyces Cerevisiae Ras/cAMP Pathway Controls Post-Diauxic Shift Element-Dependent Transcription through the Zinc Finger Protein Gis1.” *The EMBO Journal*. https://doi.org/10.1093/emboj/19.11.2569.

Pedruzzi, Ivo, Frédérique Dubouloz, Elisabetta Cameroni, Valeria Wanke, Johnny Roosen, Joris Winderickx, and Claudio De Virgilio. 2003. “TOR and PKA Signaling Pathways Converge on the Protein Kinase Rim15 to Control Entry into G0.” *Molecular Cell* 12 (6): 1607–13.

Petti, Allegra A., Christopher A. Crutchfield, Joshua D. Rabinowitz, and David Botstein. 2011. “Survival of Starving Yeast Is Correlated with Oxidative Stress Response and Nonrespiratory Mitochondrial Function.” *Proceedings of the National Academy of Sciences of the United States of America* 108 (45): E1089–98.

Pluskal, Tomáš, Takeshi Hayashi, Shigeaki Saitoh, Asuka Fujisawa, and Mitsuhiro Yanagida. 2011. “Specific Biomarkers for Stochastic Division Patterns and Starvation-Induced Quiescence under Limited Glucose Levels in Fission Yeast.” *The FEBS Journal* 278 (8): 1299–1315.

Powers, R. Wilson, Matt Kaeberlein, Seth D. Caldwell, Brian K. Kennedy, and Stanley Fields. 2006. “Extension of Chronological Life Span in Yeast by Decreased TOR Pathway Signaling.” *Genes and Development* 20 (2): 174–84.

Quasem, Ishtiaque, Christopher J. Luby, Charles R. Mace, and Stephen M. Fuchs. 2017. “Density Separation of Quiescent Yeast Using Iodixanol.” *BioTechniques* 63 (4): 169–73.

Ramage, Gordon, Ranjith Rajendran, Leighann Sherry, and Craig Williams. 2012. “Fungal Biofilm

Resistance." *International Journal of Microbiology* 2012 (February): 528521.

Riback, Joshua A., Christopher D. Katanski, Jamie L. Kear-Scott, Evgeny V. Pilipenko, Alexandra E. Rojek, Tobin R. Sosnick, and D. Allan Drummond. 2017. "Stress-Triggered Phase Separation Is an Adaptive, Evolutionarily Tuned Response." *Cell* 168 (6): 1028–40.e19.

Rittershaus, Emily S. C., Seung Hun Baek, and Christopher M. Sassetti. 2013. "The Normalcy of Dormancy: Common Themes in Microbial Quiescence." *Cell Host & Microbe* 13 (6): 643–51.

Roguev, Assen, Sourav Bandyopadhyay, Martin Zofall, Ke Zhang, Tamas Fischer, Sean R. Collins, Hongjing Qu, et al. 2008. "Conservation and Rewiring of Functional Modules Revealed by an Epistasis Map in Fission Yeast." *Science* 322 (5900): 405–10.

Sagot, Isabelle, and Damien Laporte. 2019. "The Cell Biology of Quiescent Yeast – a Diversity of Individual Scenarios." *Journal of Cell Science*. https://doi.org/10.1242/jcs.213025.

Sagot, Isabelle, Benoît Pinson, Bénédicte Salin, and Bertrand Daignan-Fornier. 2006. "Actin Bodies in Yeast Quiescent Cells: An Immediately Available Actin Reserve?" *Molecular Biology of the Cell* 17 (11): 4645–55.

Sajiki, Kenichi, Mitsuko Hatanaka, Takahiro Nakamura, Kojiro Takeda, Mizuki Shimanuki, Tomoko Yoshida, Yuichiro Hanyu, Takeshi Hayashi, Yukinobu Nakaseko, and Mitsuhiro Yanagida. 2009. "Genetic Control of Cellular Quiescence in S. Pombe." *Journal of Cell Science* 122 (Pt 9): 1418–29.

Saldanha, Alok J., Matthew J. Brauer, and David Botstein. 2004. "Nutritional Homeostasis in Batch and Steady-State Culture of Yeast." *Molecular Biology of the Cell* 15 (9): 4089–4104.

Salmenperä, Pertteli, Piia-Riitta Karhemo, Kati Räsänen, Pirjo Laakkonen, and Antti Vaheri. 2016. "Fibroblast Spheroids as a Model to Study Sustained Fibroblast Quiescence and Their Crosstalk with Tumor Cells." *Experimental Cell Research* 345 (1): 17–24.

Sang, Liyun, Hilary A. Coller, and James M. Roberts. 2008. “Control of the Reversibility of Cellular Quiescence by the Transcriptional Repressor HES1.” *Science* 321 (5892): 1095–1100.

Schulze, U., G. Liden, J. Nielsen, and J. Villadsen. 1996. “Physiological Effects of Nitrogen Starvation in an Anaerobic Batch Culture of Saccharomyces Cerevisiae.” *Microbiology*. https://doi.org/10.1099/13500872-142-8-2299.

Segal, Scott P., Travis Dunckley, and Roy Parker. 2007. “Sbp1p Affects Translational Repression and Decapping in Saccharomyces Cerevisiae.” *Molecular and Cellular Biology*. https://doi.org/10.1128/mcb.02173-06.

Shi, Lei, Benjamin M. Sutter, Xinyue Ye, and Benjamin P. Tu. 2010a. “Trehalose Is a Key Determinant of the Quiescent Metabolic State That Fuels Cell Cycle Progression upon Return to Growth.” *Molecular Biology of the Cell* 21 (12): 1982–90.

———. 2010b. “Trehalose Is a Key Determinant of the Quiescent Metabolic State That Fuels Cell Cycle Progression upon Return to Growth.” *Molecular Biology of the Cell* 21 (12): 1982–90.

Shimanuki, Mizuki, Soo Yoel Chung, Yuji Chikashige, Yosuke Kawasaki, Lisa Uehara, Chihiro Tsutsumi, Mitsuko Hatanaka, Yasushi Hiraoka, Koji Nagao, and Mitsuhiro Yanagida. 2007. “Two-Step, Extensive Alterations in the Transcriptome from G0 Arrest to Cell Division in Schizosaccharomyces Pombe.” *Genes to Cells: Devoted to Molecular & Cellular Mechanisms* 12 (5): 677–92.

Smith, Andrew M., Lawrence E. Heisler, Joseph Mellor, Fiona Kaper, Michael J. Thompson, Mark Chee, Frederick P. Roth, Guri Giaever, and Corey Nislow. 2009. “Quantitative Phenotyping via Deep Barcode Sequencing.” *Genome Research* 19 (10): 1836–42.

Snider, Justin, Daifeng Wang, Daniel F. Bogenhagen, and John D. Haley. 2019. “Pulse SILAC Approaches to the Measurement of Cellular Dynamics.” *Advances in Experimental Medicine and*

Biology 1140: 575–83.

Spain, M. M., K. C. A. Braceros, and T. Tsukiyama. 2018. “SWI/SNF Coordinates Transcriptional Activation through Rpd3-Mediated Histone Hypoacetylation during Quiescence Entry.” *bioRxiv*. https://www.biorxiv.org/content/10.1101/426288v1.abstract.

St Onge, Robert P., Ramamurthy Mani, Julia Oh, Michael Proctor, Eula Fung, Ronald W. Davis, Corey Nislow, Frederick P. Roth, and Guri Giaever. 2007. “Systematic Pathway Analysis Using High-Resolution Fitness Profiling of Combinatorial Gene Deletions.” *Nature Genetics* 39 (2): 199–206.

Subramanian, Aravind, Pablo Tamayo, Vamsi K. Mootha, Sayan Mukherjee, Benjamin L. Ebert, Michael A. Gillette, Amanda Paulovich, et al. 2005. “Gene Set Enrichment Analysis: A Knowledge-Based Approach for Interpreting Genome-Wide Expression Profiles.” *Proceedings of the National Academy of Sciences of the United States of America* 102 (43): 15545–50.

Su, Chang, Yang Lu, and Haoping Liu. 2013. “Reduced TOR Signaling Sustains Hyphal Development in Candida Albicans by Lowering Hog1 Basal Activity.” *Molecular Biology of the Cell* 24 (3): 385–97.

Suda, Toshio, Fumio Arai, and Atsushi Hirao. 2005. “Hematopoietic Stem Cells and Their Niche.” *Trends in Immunology* 26 (8): 426–33.

Sudbery, Peter E. 2011. “Growth of Candida Albicans Hyphae.” *Nature Reviews. Microbiology* 9 (10): 737–48.

Sun, Dan, and Laura Buttitta. 2015. “Protein Phosphatase 2A Promotes the Transition to G0 during Terminal Differentiation in Drosophila.” *Development* 142 (17): 3033–45.

Sun, Siyu, Anastasia Baryshnikova, Nathan Brandt, and David Gresham. 2020. “Genetic Interaction Profiles of Regulatory Kinases Differ between Environmental Conditions and Cellular States.” *Molecular Systems Biology*. https://doi.org/10.15252/msb.20199167.

Swinnen, Erwin, Valeria Wanke, Johnny Roosen, Bart Smets, Frédérique Dubouloz, Ivo Pedruzzi, Elisabetta Cameroni, Claudio De Virgilio, and Joris Winderickx. 2006. “Rim15 and the Crossroads of Nutrient Signalling Pathways in Saccharomyces Cerevisiae.” *Cell Division* 1 (April): 3.

Tan, Haiyan, Kai Yang, Yuxin Li, Timothy I. Shaw, Yanyan Wang, Daniel Bastardo Blanco, Xusheng Wang, et al. 2017. “Integrative Proteomics and Phosphoproteomics Profiling Reveals Dynamic Signaling Networks and Bioenergetics Pathways Underlying T Cell Activation.” *Immunity* 46 (3): 488–503.

Tapia, Hugo, and Kevin A. Morano. 2010. “Hsp90 Nuclear Accumulation in Quiescence Is Linked to Chaperone Function and Spore Development in Yeast.” *Molecular Biology of the Cell* 21 (1): 63–72.

Tatchell, K. 1986. “RAS Genes and Growth Control in Saccharomyces Cerevisiae.” *Journal of Bacteriology* 166 (2): 364–67.

Temin, H. M. 1971. “Stimulation by Serum of Multiplication of Stationary Chicken Cells.” *Journal of Cellular Physiology* 78 (2): 161–70.

Tenen, Claudia C., and Iva Greenwald. 2019. “Cell Non-Autonomous Function of Daf-18/PTEN in the Somatic Gonad Coordinates Somatic Gonad and Germline Development in C. Elegans Dauer Larvae.” *Current Biology: CB* 29 (6): 1064–72.e8.

Tesnière, Catherine, Claire Brice, and Bruno Blondin. 2015. “Responses of Saccharomyces Cerevisiae to Nitrogen Starvation in Wine Alcoholic Fermentation.” *Applied Microbiology and Biotechnology* 99 (17): 7025–34.

Thevelein, Johan M., and Johannes H. de Winde. 1999. “Novel Sensing Mechanisms and Targets for the cAMP-Protein Kinase A Pathway in the Yeast Saccharomyces Cerevisiae.” *Molecular Microbiology*. https://doi.org/10.1046/j.1365-2958.1999.01538.x.

Tong, A. H., M. Evangelista, A. B. Parsons, H. Xu, G. D. Bader, N. Pagé, M. Robinson, et al. 2001. "Systematic Genetic Analysis with Ordered Arrays of Yeast Deletion Mutants." *Science* 294 (5550): 2364–68.

Tong, Amy Hin Yan, Guillaume Lesage, Gary D. Bader, Huiming Ding, Hong Xu, Xiaofeng Xin, James Young, et al. 2004. "Global Mapping of the Yeast Genetic Interaction Network." *Science* 303 (5659): 808–13.

Toulmay, Alexandre, and William A. Prinz. 2013. "Direct Imaging Reveals Stable, Micrometer-Scale Lipid Domains That Segregate Proteins in Live Cells." *The Journal of Cell Biology* 202 (1): 35–44.

Traven, Ana, Amrei Jänicke, Paul Harrison, Angavai Swaminathan, Torsten Seemann, and Traude H. Beilharz. 2012. "Transcriptional Profiling of a Yeast Colony Provides New Insight into the Heterogeneity of Multicellular Fungal Communities." *PloS One* 7 (9): e46243.

Tsukada, Miki, and Yoshinori Ohsumi. 1993. "Isolation and Characterization of Autophagy-Defective Mutants of Saccharomyces Cerevisiae." *FEBS Letters* 333 (1-2): 169–74.

Tsuruo, Takashi. 2008. "Faculty Opinions Recommendation of A Bistable Rb-E2F Switch Underlies the Restriction Point." *Faculty Opinions – Post-Publication Peer Review of the Biomedical Literature*. https://doi.org/10.3410/f.1108142.564136.

Tyler, Jessica K., and Jay E. Johnson. 2018. "The Role of Autophagy in the Regulation of Yeast Life Span." *Annals of the New York Academy of Sciences*, 31–43.

Unger, M. W., and L. H. Hartwell. 1976. "Control of Cell Division in Saccharomyces Cerevisiae by Methionyl-tRNA." *Proceedings of the National Academy of Sciences of the United States of America* 73 (5): 1664–68.

Valcourt, James R., Johanna M. S. Lemons, Erin M. Haley, Mina Kojima, Olukunle O. Demuren, and

Hilary A. Coller. 2012. “Staying Alive.” *Cell Cycle* 11 (9): 1680–96.

Valentin, Mayda, and Elizabeth Yang. 2008. “Autophagy Is Activated, but Is Not Required for the G0 Function of BCL-2 or BCL-xL.” *Cell Cycle* 7 (17): 2762–68.

Velthoven, Cindy T. J. van, and Thomas A. Rando. 2019. “Stem Cell Quiescence: Dynamism, Restraint, and Cellular Idling.” *Cell Stem Cell* 24 (2): 213–25.

Venkataram, Sandeep, Barbara Dunn, Yuping Li, Atish Agarwala, Jessica Chang, Emily R. Ebel, Kerry Geiler-Samerotte, et al. 2016. “Development of a Comprehensive Genotype-to-Fitness Map of Adaptation-Driving Mutations in Yeast.” *Cell* 166 (6): 1585–96.e22.

Verghese, Jacob, Jennifer Abrams, Yanyu Wang, and Kevin A. Morano. 2012. “Biology of the Heat Shock Response and Protein Chaperones: Budding Yeast (Saccharomyces Cerevisiae) as a Model System.” *Microbiology and Molecular Biology Reviews: MMBR* 76 (2): 115–58.

Villén, Judit, and Steven P. Gygi. 2008. “The SCX/IMAC Enrichment Approach for Global Phosphorylation Analysis by Mass Spectrometry.” *Nature Protocols* 3 (10): 1630–38.

Virgilio, Claudio de. 2012. “The Essence of Yeast Quiescence.” *FEMS Microbiology Reviews* 36 (2): 306–39.

Waliullah, Talukdar Muhammad, Akter M. S. T. Yeasmin, Atsuki Kaneko, Naoki Koike, Mashu Terasawa, Takaya Totsuka, and Takashi Ushimaru. 2017. “Rim15 and Sch9 Kinases Are Involved in Induction of Autophagic Degradation of Ribosomes in Budding Yeast.” *Bioscience, Biotechnology and Biochemistry*. https://doi.org/10.1080/09168451.2016.1234928.

Walter, David, Anja Matter, and Birthe Fahrenkrog. 2014. “Loss of Histone H3 Methylation at Lysine 4 Triggers Apoptosis in Saccharomyces Cerevisiae.” *PLoS Genetics* 10 (1): e1004095.

Wang, Chenhui, and Allan C. Spradling. 2020. “An Abundant Quiescent Stem Cell Population in

Drosophila Malpighian Tubules Protects Principal Cells from Kidney Stones." *eLife* 9 (March). https://doi.org/10.7554/eLife.54096.

Wang, Minghui, Yongzhong Zhao, and Bin Zhang. 2015. "Efficient Test and Visualization of Multi-Set Intersections." *Scientific Reports* 5 (November): 16923.

Wang, Xia, Kotaro Fujimaki, Geoffrey C. Mitchell, Jungeun Sarah Kwon, Kimiko Della Croce, Chris Langsdorf, Hao Helen Zhang, and Guang Yao. 2017. "Exit from Quiescence Displays a Memory of Cell Growth and Division." *Nature Communications* 8 (1): 321.

Wanke, Valeria, Elisabetta Cameroni, Aino Uotila, Manuele Piccolis, Jörg Urban, Robbie Loewith, and Claudio De Virgilio. 2008. "Caffeine Extends Yeast Lifespan by Targeting TORC1." *Molecular Microbiology* 69 (1): 277–85.

Wanke, Valeria, Ivo Pedruzzi, Elisabetta Cameroni, Frédérique Dubouloz, and Claudio De Virgilio. 2005. "Regulation of G0 Entry by the Pho80-Pho85 Cyclin-CDK Complex." *The EMBO Journal* 24 (24): 4271–78.

Wei, Min, Paola Fabrizio, Jia Hu, Huanying Ge, Chao Cheng, Lei Li, and Valter D. Longo. 2008. "Life Span Extension by Calorie Restriction Depends on Rim15 and Transcription Factors Downstream of Ras/PKA, Tor, and Sch9." *PLoS Genetics* 4 (1): 0139–49.

Werner-Washburne, M., Sushmita Roy, and George S. Davidson. 2012. "Aging and the Survival of Quiescent and Non-Quiescent Cells in Yeast Stationary-Phase Cultures." *Sub-Cellular Biochemistry* 57: 123–43.

Wilson, Wayne A., and Peter J. Roach. 2002. "Nutrient-Regulated Protein Kinases in Budding Yeast." *Cell* 111 (2): 155–58.

Woodward, J. R., and V. P. Cirillo. 1977. "Amino Acid Transport and Metabolism in Nitrogen-Starved Cells of Saccharomyces Cerevisiae." *Journal of Bacteriology* 130 (2): 714–23.

Wullschleger, Stephan, Robbie Loewith, and Michael N. Hall. 2006. “TOR Signaling in Growth and Metabolism.” *Cell* 124 (3): 471–84.

Yanagida, Mitsuhiro. 2009. “Cellular Quiescence: Are Controlling Genes Conserved?” *Trends in Cell Biology* 19 (12): 705–15.

Yanez, I., and M. O’Farrell. 1989. “Variation in the Length of the Lag Phase Following Serum Restimulation of Mouse 3T3 Cells.” *Cell Biology International Reports* 13 (5): 453–62.

Yang, Zhifen, Jiefei Geng, Wei-Lien Yen, Ke Wang, and Daniel J. Klionsky. 2010. “Positive or Negative Roles of Different Cyclin-Dependent Kinase Pho85-Cyclin Complexes Orchestrate Induction of Autophagy in Saccharomyces Cerevisiae.” *Molecular Cell* 38 (2): 250–64.

Yano, Shuya, Kiyoto Takehara, Hiroshi Tazawa, Hiroyuki Kishimoto, Yasuo Urata, Shunsuke Kagawa, Toshiyoshi Fujiwara, and Robert M. Hoffman. 2017. “Cell-Cycle-Dependent Drug-Resistant Quiescent Cancer Cells Induce Tumor Angiogenesis after Chemotherapy as Visualized by Real-Time FUCCI Imaging.” *Cell Cycle* 16 (5): 406–14.

Yao, Guang. 2014. “Modelling Mammalian Cellular Quiescence.” *Interface Focus* 4 (3): 20130074.

Yorimitsu, Tomohiro, Shadia Zaman, James R. Broach, and Daniel J. Klionsky. 2007. “Protein Kinase A and Sch9 Cooperatively Regulate Induction of Autophagy in Saccharomyces Cerevisiae.” *Molecular Biology of the Cell* 18 (10): 4180–89.

Young, Conor P., Cory Hillyer, Karsten Hokamp, Darren J. Fitzpatrick, Nikifor K. Konstantinov, Jacqueline S. Welty, Scott A. Ness, Margaret Werner-Washburne, Alastair B. Fleming, and Mary Ann Osley. 2017. “Distinct Histone Methylation and Transcription Profiles Are Established during the Development of Cellular Quiescence in Yeast.” *BMC Genomics* 18 (1): 107.

Yu, G., F. Li, Y. Qin, X. Bo, Y. Wu, and S. Wang. 2010. “GOSemSim: An R Package for Measuring Semantic Similarity among GO Terms and Gene Products.” *Bioinformatics*.

https://doi.org/10.1093/bioinformatics/btq064.

Yu, Guangchuang, Li-Gen Wang, Yanyan Han, and Qing-Yu He. 2012. “clusterProfiler: An R Package for Comparing Biological Themes among Gene Clusters.” *Omics: A Journal of Integrative Biology* 16 (5): 284–87.

Zakrajšek, Teja, Peter Raspor, and Polona Jamnik. 2011. “Saccharomyces Cerevisiae in the Stationary Phase as a Model Organism — Characterization at Cellular and Proteome Level.” *Journal of Proteomics*. https://doi.org/10.1016/j.jprot.2011.06.026.

Zetterberg, A., and O. Larsson. 1985. “Kinetic Analysis of Regulatory Events in G1 Leading to Proliferation or Quiescence of Swiss 3T3 Cells.” *Proceedings of the National Academy of Sciences of the United States of America* 82 (16): 5365–69.

Zhang, Bin, and Steve Horvath. 2005. “A General Framework for Weighted Gene Co-Expression Network Analysis.” *Statistical Applications in Genetics and Molecular Biology* 4 (August): Article17.

Zhang, Jinrui, Karla Martinez-Gomez, Elmar Heinzle, and Sebastian Aljoscha Wahl. 2019. “Metabolic Switches from Quiescence to Growth in Synchronized Saccharomyces Cerevisiae.” *Metabolomics: Official Journal of the Metabolomic Society* 15 (9): 121.

Zhang, Nianshu, and Lu Cao. 2017. “Starvation Signals in Yeast Are Integrated to Coordinate Metabolic Reprogramming and Stress Response to Ensure Longevity.” *Current Genetics* 63 (5): 839–43.

Ziv, Naomi, Bentley M. Shuster, Mark L. Siegal, and And David Gresham. 2017. “Resolving the Complex Genetic Basis of Phenotypic Variation and Variability of Cellular Growth.” *Genetics* 206 (3): 1645–57.